

FINITE ELEMENT MODELING OF STRESS EVOLUTION
IN QUENCHING PROCESS

A THESIS SUBMITTED TO
THE GRADUATE SCHOOL OF NATURAL AND APPLIED SCIENCES
OF
MIDDLE EAST TECHNICAL UNIVERSITY

BY

DORUK DOĞU

IN PARTIAL FULFILLMENT OF THE REQUIREMENTS
FOR
THE DEGREE OF MASTER OF SCIENCE
IN
METALLURGICAL AND MATERIALS ENGINEERING

DECEMBER 2005

Approval of the Graduate School of Natural and Applied Sciences

Prof. Dr. Canan Özgen
Director

I certify that this thesis satisfies all the requirements as a thesis for the degree of Master of Science.

Prof. Dr. Tayfur Öztürk
Head of Department

This is to certify that we have read this thesis and that in our opinion it is fully adequate, in scope and quality, as a thesis for the degree of Master of Science

Assoc.Prof. Dr. C.Hakan Gür
Supervisor

Examining Committee Members

Prof. Dr. Şakir Bor (METU,METE) _____

Assoc.Prof. Dr. C.Hakan Gür (METU,METE) _____

Prof. Dr. Tayfur Öztürk (METU,METE) _____

Prof. Dr. A. Erman Tekkaya (Atılım Unv.,MFGE) _____

Assoc. Prof. Dr. Cevdet Kaynak (METU,METE) _____

Name, Last name :

Signature :

I hereby declare that all information in this document has been obtained and presented in accordance with academic rules and ethical conduct. I also declare that, as required by these rules and conduct, I have fully cited and referenced all material and results that are not original to this work.

ABSTRACT

FINITE ELEMENT MODELING OF STRESS EVOLUTION IN QUENCHING PROCESS

Dođu, Doruk

M.S., Department of Metallurgical and Materials Engineering

Supervisor : Assoc. Prof. Dr. C. Hakan Gür

December 2005, 101 pages

In this thesis the finite element computer code QUEANA simulating the quenching of axisymmetric parts and determining the residual stress state was improved by adding pre- and post-processors. The code was further verified by additional numerical experiments and comparison of the results with commercial software “MARC”. The possible applications of this code are optimization of industrial quenching processes by controlling the evolution of internal stresses and dimensional changes.

Keywords: Quenching, Finite Element Modeling, Residual Stress

ÖZ

SU VERME İŞLEMİNDE OLUŞAN GERİLMELERİN SONLU ELEMAN YÖNTEMİYLE MODELLENMESİ

Doğu, Doruk

Yüksek Lisans, Metalurji va Malzeme Mühendisliği Bölümü

Tez Yöneticisi : Doç. Dr. C. Hakan Gür

Aralık 2005, 101 sayfa

Bu tezde, eksenel simetriye sahip çelik parçalara su verme işlemini sonlu eleman yöntemiyle modelleyen ve su verme işlemi sonrasındaki kalıntı gerilmeleri hesaplayan bir bilgisayar programı, "QUEANA", ön ve son işlemciler eklenerek geliştirildi. Program çeşitli numerik analizlerle ve ticari yazılım MARC'dan elde edilen sonuçlarla karşılaştırılarak doğrulandı. Bu program yardımıyla iç gerilmelerin oluşumu ve boyutsal değişimler kontrol altına alınarak endüstriyel su verme işlemleri optimize edilebilir.

Anahtar Kelimeler: Sonlu Eleman Modellemesi, Kalıntı Gerilme, Su Verme

ACKNOWLEDGMENTS

The author wishes to express his deepest gratitude to his supervisor Assoc. Prof. Dr. C. Hakan Gür for his guidance, advice, criticism, encouragements and insight throughout the research.

Author greatly thanks Mr. Caner Şimşir for his help on the usage of the computer program MARC, for his suggestion and helps.

The author would also like to thank Prof. Dr. Timur Doğu for his suggestions and comments.

The technical assistance of Ms.Serap G. Erkan, Mr. İ. Tolga Medeni and Mr. Fatih G. Şen are gratefully acknowledged.

The author also wishes to thank his family and friends for their support and encouragements.

TABLE OF CONTENTS

ABSTRACT	iv
ÖZ	v
ACKNOWLEDGMENTS	vi
TABLE OF CONTENTS	vii
LIST OF TABLES	x
LIST OF FIGURES	xi
CHAPTER	
1. INTRODUCTION	1
2. LITERATURE SURVEY	5
3. MODEL DESCRIPTION.....	14
3.1 Temperature Distribution Predictions.....	14
3.1.1 Finite Element Formulation of Heat Conduction.....	15
3.1.2 Surface Heat Transfer Stages in Quenching	18
3.2 Prediction of Microstructural Evolution	19

3.3	Predictions of Quench Stress Distribution	23
3.3.1	Elasto-Plastic Rate Equation	26
3.3.2	Thermo-Elasto-Plastic Stress-Strain Relations	28
3.3.3	Numerical Solution Procedures.....	29
3.3.4	Finite Element Modeling of Stress Computation.....	31
3.4	Description of the Program	36
3.5	Input Data for Numerical Analysis	39
3.5.1	Data for Temperature Calculations	39
3.5.2	Data for Stress Calculations	40
3.5.3	Data to Determine Transformed Amount of Phase.....	43
4.	IMPROVEMENT OF THE PROGRAM.....	48
4.1	Input Interface	48
4.2	Output Interface	48
5.	RESULTS AND DISCUSSION	57
5.1	Comparison for Verification	57
5.2	Monitoring the Evolution of Thermal Stresses During Rapid Cooling	62

5.3	Monitoring the Local Plastic Deformation	68
5.4	Monitoring the Evolution of Residual Stresses.....	72
5.4.1	Effect of Convective Heat Transfer Coefficient on Phase Transformations	72
5.4.2	Effect of Phase Transformation on Residual Stress Distribution	74
5.4.3	Investigating the Evolution of Internal Stresses and Phase Transformations	81
5.4.4	Monitoring the Local Plastic Deformation During Quenching.....	88
5.5	Effect of Meshing on the Results	91
6.	CONCLUSION.....	93
	REFERENCES.....	95

LIST OF TABLES

3.1	Temperature limits for phase transformations of steel.....	20
3.2	Thermal conductivity values of several steels	43
3.3	Heat capacity values of several steels	44
3.4	Latent Heat values for several steels.....	44
3.5	Elastic Modulus values of several steels.....	45
3.6	Yield strength values of several steels	46
3.7	Thermal expansion coefficient values of several steels	47
5.1	Input data for Ck45 steel.....	57
5.2	Convective heat transfer coefficients for 20°C and 60°C water quenching	69
5.3	Input data for different phases of C60 steel	75
5.4	Input data for C60 steel.....	91

LIST OF FIGURES

3.1	General structure of the program	38
4.1	QUEANA input interface step 1	49
4.2	QUEANA input interface step 2	50
4.3	QUEANA input interface step 3	51
4.4	QUEANA input interface step 4	52
4.5	QUEANA output interface (Results)	53
4.6	QUEANA output interface (Stress distribution graph).....	54
4.7	QUEANA output interface (Stress vs. time graph).....	55
4.8	QUEANA output interface (Cooling curve graph).....	56
5.1	QUEANA – MARC comparison (Tangential thermal stress) (680°C to 20°C, Ck45)	58
5.2	QUEANA – MARC comparison (Axial thermal stress) (680°C to 20°C, Ck45)	59
5.3	QUEANA – MARC comparison (Radial thermal stress) (680°C to 20°C, Ck45)	60

5.4	QUEANA – MARC comparison (Effective thermal stress) (680°C to 20°C, Ck45)	61
5.5	Cooling curve at the surface and at the center (680°C to 20°C, Ck45 cylinder, 30mm diameter)	63
5.6	Monitoring of tangential stress evolution during rapid cooling (680°C to 20°C, Ck45)	64
5.7	Monitoring of axial stress evolution during rapid cooling (680°C to 20°C, Ck45)	65
5.8	Monitoring of radial stress evolution during rapid cooling (680°C to 20°C, Ck45)	66
5.9	Monitoring of effective stress evolution during rapid cooling (680°C to 20°C, Ck45)	67
5.10	Monitoring of local plastic deformations (720°C to 60°C, C60 steel, 30mm diameter)	70
5.11	Monitoring of local plastic deformations (720°C to 20°C, C60 steel, 30mm diameter)	71
5.12	Phase distributions according to the convective heat transfer coefficient (830°C to 60°C, C60 steel)	73
5.13	Effect of phase transformation on the radial residual stress (830°C to 60°C, C60).....	77

5.14	Effect of phase transformation on the axial residual stress (830°C to 60°C, C60).....	78
5.15	Effect of phase transformation on the tangential residual stress (830°C to 60°C, C60).....	79
5.16	Effect of phase transformation on the effective residual stress (830°C to 60°C, C60).....	80
5.17	Variation of the radial component of internal stress along the radius during quenching (830°C to 60°C, C60 steel)	83
5.18	Variation of the axial component of internal stress along the radius during quenching (830°C to 60°C, C60 steel)	84
5.19	Variation of the tangential component of internal stress along the radius during quenching (830°C to 60°C, C60 steel)	85
5.20	Variation of the effective internal stress along the radius during quenching (830°C to 60°C, C60 steel)	86
5.21	Variation of the phase content along the radius during quenching (830°C to 60°C, C60 steel)	87
5.22	Change in effective stress and yield strength during quenching with phase transformation (830°C to 60°C, C60 steel, 30mm diameter) ...	89
5.23	Change in effective stress and yield strength during quenching without phase transformation (830°C to 60°C, C60 steel, 30mm diameter).....	90
5.24	Effect of meshing on the residual stresses (680°C to 20°C, C60)	92

CHAPTER 1

INTRODUCTION

Quenching is a widely used process in manufacturing to produce components with reliable service properties. Various mechanical properties can be achieved in steel parts by changing the cooling rate. This is one of the main reasons why steel is very widely used. Although heat treatment is a very important process in producing steel parts, it is also the one of the main reasons for rejected or reworked products. For eliminating the faulty production it would be very useful to have critical information about the affect of cooling rate on residual stresses and distortion in the parts. Residual stresses in any component can be determined by different measurement methods such as x-ray diffraction for surface residual stresses, but these procedures are hard, expensive, require experience, and have various limitations.

In quench hardening of steels microstructure, temperature, stress, and strain changes frequently. Quenching is a complicated pattern of thermo-mechanical couplings between different physical and mechanical events. Large temperature gradients occurring in the quenching process creates thermal stresses in the component. Thermo-mechanical properties at any point of the component vary with temperature and cooling rate and because of this the magnitude of thermal stresses at any point in the component changes with time.

After complete austenitization of the specimen, depending on the cooling rate at any location in the specimen, austenite will transform into ferrite, pearlite, bainite or martensite. At any time the amount of austenite transformed and the transformed phase in different parts of the specimen to will not be the same and will vary with

temperature and the cooling rates. Continuous cooling transformation (CCT) diagrams show how the phase transformations will occur according to the cooling procedures.

The stress field in a component will influence the evolution of microstructure. Solid state phase transformations result volumetric strain and transformation plasticity. Volumetric strain is the volume change with transformation in unit volume, and transformation plasticity is the strain produced by the interaction between the strains due to the phase transformations in the grains and the stress field that already exists. Also any stress in a volume affects the phase transformation in that volume. This is called stress induced transformation. During a quench process, because of all these mechanisms a continuously changing internal stress field occurs. If at any point of the component the yield strength is exceeded at a temperature, a non-uniform plastic flow occurs, and it causes a residual stress in the component. This residual stress can be either beneficial or destructive according to its magnitude and if it is tensile or compressive. If there is a compressive stress at the surface of the specimen this is a very preferable stress state, but if there is a tensile stress at the surface, there will be serious problems with the fatigue properties of the component.

Residual stresses may also result from the previously applied processes like metal working and machining. If the steel that is heat treated applied to different processes before heat treatment the results of the heat treatment may change. If there is a residual stress on the part before the heat treatment some changes may occur in the shape and size of the part during the quenching process, because of this, process schedule must be arranged so that the part should not have any stress in it before the heat treatment. In the quenching process, the shape of the part usually distorts, so it is a risk to machine the part to close tolerances before quench hardening. On the other hand, machining a part after quench hardening is very hard, and because of the local heating effects there may be a loss of hardness during machining or distortion due to the disturbance of the existing residual stress state or even cracking. The process schedule must be arranged to have the desired properties, by considering all these factors.

Residual stresses are elastic stresses existing in a material in uniform temperature and without any external forces, which are in a self equilibrium condition. All materials, components, parts and structures have residual stresses on them. There are a great variety of residual stresses due to the production techniques and process schedules which are applied during manufacturing. Residual stresses in a material are in an equilibrium, means, total force and total moment of forces acting on any plane in the component must be zero.

Residual stresses are classified into three groups. First class of residual stresses is homogeneous in several grains in the material, and in equilibrium over the bulk material. In a component containing this kind of residual stress, dimensions of the interfaces that are in equilibrium will change. Second class of residual stresses is homogeneous in a grain or in a part of the grain, and in equilibrium over some small number of grains. If this equilibrium is disturbed then the dimensions of the bulk material may change. Third class of residual stresses has no homogeneity in any atomic distances and in equilibrium over small parts of a grain. These stresses are located around lattice defects in the material. If the equilibrium is disturbed in a component containing this kind of residual stress, no macroscopic dimensional changes will occur.

Good process controls are very beneficial and cost effective because variability of materials and process parameters affects the properties of the parts manufactured. Avoidance of crack initiation, achievement of sufficient hardenability, microstructural control to get improved material properties, achievement of a specific hardness distribution, reduction of residual stresses and distortion should be closely controlled to improve the effects of quench hardening. These objectives are traditionally controlled and optimized by use of experience or trial and error method. Processes can not be optimized perfectly until some methods are developed to predict critical size ranges depending on the composition, grain size of the austenite, geometry of the manufactured part, and the quenching procedures. To predict the final dimensions and residual stresses, complete stress-strain behavior must be

examined. So, it would be very beneficial to simulate the quenching process by numerical methods before the production starts.

To simulate a quench process temperature field, phase transformations, mechanical properties of the material at different temperatures must be considered. The properties of a material that is being heat treated at any instant of time depend on temperature and phase content. Firstly, the temperature distribution must be determined as a function of geometry and time. Temperature distribution is affected by the quench conditions, thermal conductivity of the material, heat capacity and latent heat due to phase transformations. Then, a model that gives volume fractions of phases as a function of time must be developed. Finally, to describe the stress-strain behavior during heat treatment thermo-elasto-plastic approach is used.

In this thesis, the computer code “QUEANA” was improved by adding post and pre-processors. By the help of this program, dimensional effects during quenching and quench parameters can be controlled, and a desired microstructure and residual stress distribution can be achieved for optimum service performance, and the process schedule can be optimized.

CHAPTER 2

LITERATURE SURVEY

The earliest attempts to calculate hardening stresses were based on available methods to calculate thermal stresses. The material was assumed to be fully plastic and not being able to sustain any stresses until the surface had reached a temperature low enough to become elastic. The temperature differences in the material at that moment multiplied by the thermal expansion coefficient was then used to calculate the residual stresses that exist after the body had attained on uniform temperature. Scott measured the expansion in three regions during cooling of a steel [1]. The calculated thermal expansion coefficients in relevant temperature intervals were then used to calculate stresses in cylinders, and the cooling rate was neglected. In the second half of 1920's, theoretical attempts to obtain internal stresses during quenching have been made by Maurer [2, 3]. He did not separate, however, the plastic portion from the elastic one in steel, and also did not consider stresses induced in plastic portion. Later, Treppschuh [4] treated quenching of steel cylinders undergoing pearlite transformation. In these studies, residual stresses for a circular disk were calculated from a known temperature history, assuming linearly elastic material.

Attempts to solve the problem of residual stresses in heat-treated cylinders appeared in a work by Weiner and Huddleston [5]. They considered circular cylinders, either solid or hollow, and assumed the material to be elastic-perfectly plastic, obeying Tresca's yield condition. They considered a phase transformation by assuming that the transformation occurred at a critical temperature rather than over a temperature range. Later, Landau and Zwicky improved this approach by using a temperature dependent von Mises' yield condition and allowed compressibility [6]. They also

assumed a temperature distribution approximating that of a phase transformation and applied numerical integration.

The earliest comprehensive development of finite element thermal analysis was made by Nickell and Wilson [7], based upon the functional used by Gurtin [8]. Alternative forms of this functional have derived by some authors [9, 10]. These yield identical definitions of the finite element representations for linear thermal analysis. The solution difficulties due to the nonlinear boundary conditions [11-12] and due to temperature dependence of conductivity were also studied.

Finite element analysis of a hollow cylinder with a non-steady state temperature distribution was examined by Inoue et al. [14]. Toshioka developed Maurer's approach to give such predictions and to include martensite and bainite transformations [15]. A maximum shear stress criterion was used. But, he used approximate expressions of physical significance and neglected the temperature dependencies of thermal expansion coefficients, Young's modulus and Poisson's ratio. Ueda and Yakamakawa presented an analytical method for general elastic-plastic thermal stress problems as related to FEM [16].

Sakai presented a calculation of stress in a cylindrical body during non-martensitic transformations [17]. The calculation was based on elastic-plastic theory and the total strain was calculated by a non-linear integral equation through successive integrations. Plastic strain is calculated by total strain theory and linear hardening stress-strain diagrams. Young's modulus and the stress-strain diagrams are taken as temperature dependent.

Inoue and Tanaka measured the radial, circumferential and biaxial residual stress components in plain carbon steels quenched [18, 19]. The experimental results, which were obtained using the Sach's boring-out method, were compared with the corresponding data obtained by the use of an elasto-plastic mathematical method. They included consideration of the thermal and transformation strains as well as the variation of yield stress and work hardening coefficient with temperature. Inoue et al.

calculated the temperature field by solving the basic equation of thermal conduction including the heat of transformation [20, 21]. They look care of the progress of the phase transformation and the specific volume changes by regarding the coefficient of thermal expansion as a function of temperature and cooling rate. The coefficient of thermal expansion is derived from dilatation-temperature curves at several cooling rates. A finite-element formulation is then used to calculate the stresses during and after quenching. The stress strain relation is expressed as a linear strain hardening relation where the yield strength and strain hardening parameter depend on temperature. Subsequently, Inoue and Raniecki examined the effect of cooling rate on the residual stress distribution in a cylinder that had been quenched from one end to form a mixed pearlite and martensite structure by refining Inoue's model [22, 23]. They used equations for the pearlite transformation based on Cahn's theory for transformation kinetics. The volume dilatation in absence of stresses is assumed to be a linear function of the specific volumes and the weight fractions of phases. To account for the influence of phase transformation on the plastic properties the non-isothermal plasticity theory is generalized by introducing thermal- hardening parameters. Variational principles and bounding inequalities associated with the fundamental rate-problem are considered.

Burnett presented a finite element calculation of the residual stress field in heat-treated, case-hardened cylinders [24]. Then, Burnett and Padovan concluded that a non-cyclic heat treatment process may lead to cyclic plasticity and that kinematic hardening yields a better model than isotropic hardening [25].

Ishikawa analyzed the stress distributions in a heat-treated solid cylinder using the method of successive elastic solutions [26]. This procedure is restricted to a cylindrical geometry and a material whose properties can be described by a simple temperature dependence.

Wolfstieg has carried out calculations of hardening stresses for a cylinder on an analog computer. This work has been continued by Yu using finite element method [27]. He calculated residual stresses in rotationally-symmetric bodies considering

temperature, phase transformation and the elasto-plastic problems. Account was taken to the temperature dependence of the heat transfer, heat conductivity, heat capacity, yield stress and dilatation. The phase transformation was carried out with the model by Tzitzelkov, who used TTT diagram instead of CCT diagram to simulate the phase transformation [28]. Yu et al. have made an extensive study on the generation of thermal stress during the quenching of steel cylinders of various diameters into different quench media [29-32].

Rammersdorfer et al. have incorporated both transformation plasticity and kinematic hardening into thermal stress calculation [33]. They used ADINA to evaluate the residual stress field for a thermo-elasto-plastic material during quenching. A pseudo-plasticity effect was considered for the dilatational strain due to the phase transformation. However, heat source and heat generation due to deformation of body were not included. The transformation which releases latent heat was simulated by a modified temperature dependence of the specific heat.

Fujio mainly concerned with the calculation of stresses by the finite element technique in carburized gears, studied the generation of thermal stresses in water quenched cylinder of the same composition and similar dimensions to those used by Inoue and Tanaka [34]. However, he used an average surface heat transfer coefficient while Inoue and Tanaka took into account the very marked differences in the rate of heat removal that occur during the various stages of the quench. His work did not include latent heat of transformation, detailed consideration of the kinetics of the various transformations as well as kinematic hardening.

Sjöström examined the specimens that were close in composition and diameter to those used by Inoue and Fujio, and also investigated the effect of changes in radius of the cylinder on the stress generation process [35]. His model included the effect of stress on the transformation strain as well as mixed proportions of isotropic and kinematic hardening. He obtained information about the relationships between stress and temperature at the surface of a material that was through hardened during water quenching. Denis and her co-workers have studied the interactions between

transformation and stress generation during the quenching of a steel cylinder, which produced fully martensite. They have found that transformation plasticity had a marked effect on the residual stress distribution [36-38]. Ishikawa et al. improved their previous approach to evaluate the thermo-elastic stresses of low carbon steel during phase transformations into the modified coefficient of thermal expansion [39].

The various interactions between temperature, phase transformation and stress-strain were investigated and a constitutive model was presented by Sjöström. He has examined the effect of the degree of memory of deformation in the earlier stages of the quench on the subsequent stress generation process. A parameter varied between 1 and 0, defining the amount of memory loss was used to adjust the rate of change to the work hardening parameter [40].

Denis et al. studied the effect of the internal stress on the kinetics of the transformation and the relationship between this effect and the generation of thermal stress and strain [41-43]. They reviewed the main effects of stress on phase transformation; metallurgical interactions and mechanical interactions (i.e., transformation plasticity). Leblond et al. discussed the kinetics of anisothermal structural transformations and the influence of the transformations on transformation plasticity [44]. They proposed models incorporating the existence of a temperature dependent equilibrium proportion of the phases, and then, extended this model by including the possibility of isothermal kinetics of the Johnson-Mehl type as well as the influence of austenite grain size.

Fernandes et al. proposed a mathematical model coupling phase transformations with temperature field predictions at each instant during the cooling process [45]. They applied this model to the pearlitic transformation of eutectoid plain-carbon steel, and the effect of stress on the kinetics of the same transformation was considered. Raniecki presented a phenomenological model which is capable of estimating both the overall stress-strains induced by quenching, and the mean stresses in each metallurgical phase [46].

Inoue and Wang have predicted constitutive relations for a time-dependent inelastic material within the framework of continuum thermodynamics and of the heat conduction equation and transformation kinetics for processes involving phase transformations [47]. Kamamoto et al. predicted residual stresses and distortion caused due to quenching in a large low-alloy steel shaft by developing a finite element code, based on Inoue's and Ueda's models [48]. They discussed the effects of transformational behavior on residual stresses and distortion by using the CCT diagrams. Fa-rong and Shang-li analyzed the transient temperature and internal stress fields in a cylindrical steel specimen during quenching using Adina/Adinat by considering only martensitic transformation [49].

Schröder examined the effect of parameters on residual stresses [50]. For this aim, different steel types (with and without transformation) were quenched under the variation of cylinder diameter and quenching conditions. Later, Graja, performed numerical and experimental studies to investigate the influence of continuous and discontinuous heat treatment methods on the thermal and transformation residual stresses and distortion of plain-carbon and low-alloy steels [51].

Inoue et al. developed a finite element code for 3D and 2D simulation of various heat treatment processes based on the thermo-mechanical theory [52]. Coupled equations of heat conduction, inelastic stresses and kinetics of phase transformations were derived as well as the diffusion equation during carburization, followed by finite element formulation. Buchmayr and Kirkaldy presented a finite element model for the similar calculations [53]. Their microstructural model was based on fundamentals of thermodynamics and kinetics taking into account alloying and synergistic effects. Das et al. presented a comprehensive methodology based on finite element analysis for the prediction of quench related macro- and micro-residual stresses [54]. They enhanced a general purpose finite element code to account for the micro-residual stress effects by including the tracking of relative fractions of various phases using the theory of transformation kinetics and the computation of additional strains due to volumetric dilatation and transformation plasticity. Majorek et al. studied the

influence of surface heat transfer conditions on the development of residual stresses and distortions in martensitically hardened steels [55].

Oddy et al. [56] have further generalized Greenwood and Johnson's work to tri-axial stress state and partial phase transformations. Sawamiphakdi and Kroop have used ABAQUS to model Greenwood and Johnson's expression for transformation plasticity [57].

Ju has made a metallo-thermo-mechanical simulation of quenching and tempering of steels by considering the interaction among phase transformations [58]. Wang has computationally and experimentally studied the quenching of carbon steels [59]. He has made an investigation of the quenching of SAE 1080 steel cylinders to determine the validity of the model. His model was simulated by using finite element method and, calculated temperature dependent material properties and elastic-plastic stresses including phase transformations of austenite-pearlite and austenite-martensite.

Cheng simulated CCT-diagram of C45 steel from its TTT-diagram by mathematical transformation. On the basis of a non-linear surface heat-transfer coefficient, he calculated the temperature field, the volume fraction of austenite, pearlite, bainite, martensite, and the residual stresses using the finite-element technique [60].

Hamouda employed finite element model to investigate the residual stress state and the variation of internal stresses in St 50 steel quenched from 600°C to 0°C [61]. He first made thermal analysis to obtain the cooling curves for the core and surface of the models, and then he made a full structural analysis to predict the stress state.

Pacheco et al. proposed a constitutive model to describe the thermo-mechanical behavior related to the quenching process considering the austenite–martensite phase transformation. This anisothermal model was formulated within the framework of continuum mechanics and the thermodynamics of irreversible processes. The proposed general formulation was applied to the progressive induction hardening of steel cylinders. The numerical experiments were carried out neglecting energy

equation thermo-mechanical coupling terms associated with internal and thermal couplings [62]. He also analyzed the importance of the energy equation thermo-mechanical coupling terms due to internal and thermal couplings [63]. He considered three different models. The first one was an uncoupled model in the sense that these terms were neglected, corresponding to the rigid body energy equation. In second model, these couplings were represented through the incorporation of a source term in the energy equation associated with the latent heat released during the austenite–martensite phase transformation. Finally, the third model considered all thermo-mechanical coupling terms of the proposed model.

A finite element technique has been used to predict the residual and thermal stresses which occur during water quenching of solid stainless-steel spherical balls [64]. The variations of residual stresses at different positions and cross-sections, e.g. the radial, axial and tangential directions, have been examined. Also, the influence of heat transfer coefficient, the initial temperature and the hardening assumption on residual stress results has been investigated.

Ferguson discussed an optimization method to derive the phase transformation kinetics parameters from dilatometry experiments. A discussion of a method based on the lattice parameters of individual phases and a method based on a lever rule for building the bridge between phase transformations and dilatometry strains was offered. The determination of kinetics parameters using an optimization algorithm was implemented into a commercial heat treatment simulation software package, DANTE[®] [65].

The effect of austenite-martensite phase transformation during quenching in the determination of residual stresses was analyzed by Savi, comparing two different models: complete thermo-elasto-plastic model with austenite-martensite phase transformation and without phase transformation. The finite element method was employed for spatial discretization together with a constitutive model that represents the thermo-mechanical behavior of the quenching process, and found that if phase transformation is neglected great differences occur [66].

Reti developed a general multi-phase decomposition model designated to the phenomenological description of simultaneous reactions taking place under isothermal and non-isothermal conditions, and examined the phase transformations during cooling of steels after austenitization [67].

CHAPTER 3

MODEL DESCRIPTION

This chapter summarizes the models for the temperature distributions in an infinitely long cylindrical specimen, for the prediction of microstructural evolution and for the prediction of quench stresses, which were previously developed [68].

3.1. Temperature Distribution Predictions

Quenching is an unsteady non-linear heat transfer problem. Estimation of temperature distribution as a function of position and temperature is the essential first step for the prediction of quench stresses in a specimen. Quenching is an unsteady heat conduction problem with an internal heat source due to latent heat effect associated with the phase transformations. The general transient three dimensional heat conduction equation with a finite heat source term $\partial S/\partial t$, can be written as

$$\rho c \frac{\partial T}{\partial t} = \lambda \left(\frac{\partial^2 T}{\partial x^2} + \frac{\partial^2 T}{\partial y^2} + \frac{\partial^2 T}{\partial z^2} \right) + \frac{\partial S}{\partial t} \quad (3.1)$$

In this equation ρ is the density, c is the heat capacity and λ is the thermal conductivity of the specimen. In writing this heat conduction equation the energy change due to adiabatic expansion and the energy change due to plastic flow are neglected basing on the literature arguments that their order of magnitudes are less than 1 % of the heat generation and the accumulation terms [40]. The heat source term, which is due to the heat release or absorbed due to phase transformation reactions, can be expressed as [69]

$$\frac{\partial S}{\partial t} = \Delta H \rho \frac{\partial V}{\partial t}. \quad (3.2)$$

Here, $\rho \frac{\partial V}{\partial t}$ is the rate of change of phase fraction (mass) with respect to time and ΔH is the heat of phase transformation per unit mass of steel specimen. For a cylindrical specimen Equation 3.1 is reduced to a parabolic partial differential equation,

$$\rho c \frac{\partial T}{\partial t} = \lambda \left(\frac{\partial^2}{\partial r^2} + \frac{1}{r} \frac{\partial}{\partial r} + \frac{\partial^2}{\partial z^2} \right) T + \frac{\partial S}{\partial t}. \quad (3.3)$$

The following flux boundary conditions at the surfaces of the specimen and the initial conditions were written for the heat conduction equation:

$$-\frac{dq(T)}{dt} = \lambda \left[\left(\frac{\partial T}{\partial r} \right) l_r + \left(\frac{\partial T}{\partial z} \right) l_z \right] = -h_c (T_s - T_m) \quad (3.4)$$

$$T(r, z, t) \Big|_{t=0} = T_{initial} \quad (3.5)$$

In this equation $\frac{dq(T)}{dt}$ is the rate of heat flux at the surface of the specimen, T_s and T_m are the surface and the quenching medium temperatures, h_c is the convective heat transfer coefficient, and l_r and l_z are the direction cosines at the surface, respectively.

3.1.1. Finite Element Formulation of Heat Conduction

In this formulation the central strip of the cylinder was divided into m number of elements interconnected at n number of nodes. At the initial times of the quench, a steep temperature gradient is expected near the surface. Considering this, the mesh was refined near the surface. An isoparametric quadrilateral ring-element was chosen for the formulation of the element matrix equations. Integration of the shape

functions and/or their derivatives are needed in the derivation of elemental equations. By writing the shape functions in terms of local coordinate system, these integrals were evaluated.

The following approximation was made for the temperature field.

$$T = \sum_{i=1}^n N_i T_i \quad (3.6)$$

Equation 3.6 may be substituted into the conduction equation (Equation 3.3) and weighted and integrated residual may be equated to zero to obtain the equations for T_i values at n nodes. Modification of these equations by the use of Green's theorem leads to the following equation.

$$\begin{aligned} & - \iiint \lambda \left(\frac{\partial N_i}{\partial r} \sum_1^4 \frac{\partial N_j}{\partial r} + \frac{\partial N_i}{\partial z} \sum_1^4 \frac{\partial N_j}{\partial z} \right) T_j dV + \iiint N_i \frac{\partial S_i}{\partial t} dV - \\ & \iiint N_i \rho c \sum_1^4 N_j \frac{\partial T_j}{\partial t} dV + \frac{\lambda}{r} \iint N_i \left(\sum_1^4 \frac{\partial N_j}{\partial r} l_r + \sum_1^4 \frac{\partial N_j}{\partial z} l_z \right) T_j dA = 0 \quad (3.7) \end{aligned}$$

There are n such equations. The last integral in Equation 3.7 arises only in the boundary nodes and may be evaluated using the boundary condition (Equation 3.4). For an infinitely long cylinder, the derivatives with respect to z become zero. Equation 3.7 can be expressed in matrix notation as,

$$[H]\{T\} + [C]\left\{\frac{dT}{dt}\right\} + \{Q\} = 0 \quad (3.8)$$

where $[H]$ is the thermal conductivity vector and also includes the convective heat flux contributions at the surface nodes.

$$[H] = \iiint \lambda r \left[\frac{\partial N_i}{\partial r} \frac{\partial N_i^T}{\partial r} + \frac{\partial N_i}{\partial z} \frac{\partial N_i^T}{\partial z} \right] dV + \iint h_c N_i N_i^T dA \quad (3.9)$$

In Equation 3.8, $[C]$ and $\{Q\}$ correspond to the heat capacity matrix and to the externally supplied nodal heat fluxes vector which includes both heat generation due to phase transformation at any node and the time dependent convective heat transfer at the surface nodes, respectively.

$$[C] = r \iiint \rho c N_i N_i^T dV \quad (3.10)$$

$$\{Q\} = - \iiint r \frac{\partial S_i}{\partial t} N_i dV - \iint h_c N_i T_m dA \quad (3.11)$$

The terms containing the surface integral in Equations 3.9 and 3.11 correspond to the surface convection heat transfer and those terms should be calculated only for elements that have boundaries to the surfaces of the specimen.

Due to the temperature dependence of $[H]$, $[C]$ and $\{Q\}$, this is a non-linear transient heat transfer problem. For such problems, the use of finite elements in time involving a weighted residual formulation of Equation 3.8 is recommended [70]. The numerical solution of this equation was obtained following a weighted residual approach for discrete approximation in time. This approach involves the approximation of $\{T\}_{t+\Delta t}$ from the known value of $\{T\}_t$ and the forcing vector $\{Q\}_t$ acting in the interval of time.

$$\{T\}_{t+\Delta t} = \frac{([C] - \Delta t(1-\theta)[H])\{T\}_t - \{Q\}_t \Delta t}{[C] + \Delta t\theta[H]} \quad (3.12)$$

In this work implicit algorithm with $\theta = 2/3$ (Galerkin scheme) is used.

During the numerical procedure, calculations are continued until the error norm (Equation 3.13) becomes less than a certain convergence limit e . In this calculation, the differences of temperature between successive iterations ($T_i - T_{i-1}$) have to be evaluated at each node where total number of nodes is n .

$$\sqrt{\sum_{j=1}^n \frac{(T_i - T_{i-1})^2}{(T_{i-1})^2}} \leq e \quad (3.13)$$

The time stepping of the algorithm is quite critical for better convergence and for the run-time of the program. If the temperature changes of the specimen are fast, short time step lengths and if the temperature changes are slow, longer time steps should be chosen. To achieve this, a self-adaptive scheme for the selection of time steps is recommended. In this adaptive procedure, the norm of the temperature differences is calculated at each step and compared with a predetermined value of ΔT_{\min} . If the calculated norm is greater than the predetermined value, then Δt is decreased by a factor, and if the opposite is the case, Δt is increased.

3.1.2. Surface Heat Transfer Stages in Quenching

The surface heat transfer rate has a significant influence on the stress generation and distortion. Consequently, correct estimation of the convective heat transfer coefficients are extremely important. At the first stage of quenching, intense boiling of the liquid which is adjacent to the surface is expected. At this stage, heat transfer coefficients are rather high. After a short time of contact, vapor covers the surface as a continuous film (vapor blanket stage) during which heat transfer coefficients become very low due to the heat transfer resistance of this vapor blanket. As the temperature of the surface was decreased, a third stage of boiling starts at which the vapor blanket breaks down and gas bubbles are formed on the surface (nucleate boiling). In this stage, heat transfer coefficients are higher. The temperature at which the boiling mechanism was changed from the vapor blanket stage to nucleate boiling stage is called Leidenfrost temperature. With a further decrease of the surface temperature of the specimen, formation of bubbles decreases until the temperature of

the surface becomes equal to the boiling temperature of the liquid. This causes a decrease in surface heat transfer coefficients. Finally a convective heat transfer stage to the liquid starts [71]. Besides these changes in the boiling regime during the quench period, shape, size, chemical composition and state of the specimen's surface etc. also effects the heat transfer rates. Consequently, instead of using prediction correlations for the estimation of the surface heat transfer coefficients, experimentally determined values are usually used. Temperature dependent heat transfer coefficients are needed to estimate the real heat transfer rates at different stages. Experimental heat transfer coefficients reported for nickel cylinders immersed in water are used in calculations [55]. In some applications, oils are used as the quench medium, especially if the required rate of cooling is low.

3.2. Prediction of Microstructural Evolution

Variations in temperature distribution during the quench, strongly influence the microstructure and phase distributions within the specimen. During cooling from austenitization temperature, transformation of austenite to ferrite, pearlite, bainite or martensite is expected at any point in the specimen, at certain temperatures. These changes in the microstructure strongly influence the mechanical properties of steels. Changes in volume during the quench cause volumetric strains. Also, due to the interaction between the stresses generated by the microstructure transformations of individual grains (due to transformation plasticity); strains are produced within the specimen. These phase transformations in the microstructure also cause heat effects due to the latent heat of phase transformations. Such effects contribute to the heat conduction equation as a source term.

For the prediction of the changes in the microstructure during the cooling period, CCT diagrams or IT diagrams may be used. For the CCT diagrams, exact temperature histories are needed to draw the cooling curves. Another undesired property of this approach is that two different thermal histories with the same parameter may yield similar results [72]. Temperatures at which transformations

occur between the phases are estimated using the empirical correlations given in the literature. A summary of these correlations is given in Table 3.1.

With a decrease in temperature, up to ferrite start temperature at a certain point within the specimen, nucleation of ferrite starts. This nucleation step was then followed by a phase growth period. This takes place following a diffusion process with movement of atomic species at the interface of the eutectic structure. The nucleation rate is reported to be function of the amount of supercooling below the ferrite start temperature Ae_3 [73]. The grain size of the austenite is also an important parameter. The nucleation rate determines the rate of increase of the volume fraction of the ferrite in the specimen. Similarly, nucleation of austenite to pearlite and to bainite starts at eutectoid temperature and bainite start temperature, respectively. However, an incubation period, which depends upon the temperature, should pass before the start of formation of pearlite or bainite by the decomposition of austenite. The additivity method proposed by Scheil [74] is recommended for the estimation of the incubation period. According to this method, nucleation was considered to be over if the summation term S , which is defined by Equation 3.14, is equal to unity [75, 76, 77]. The cooling curve at a certain point can be assumed to be composed of a series of small isothermal time steps. This summation is taken over the isothermal time steps i , Δt_i being the length of time step and τ_i being the beginning time for the isothermal transformation.

Table 3.1. Temperature limits for phase transformations of steel

TRANSFORMATION	START TEMPERATURE, (°C)	REFERENCE
Ferrite start temperature	$Ae_3 = 912 - 203C^{1/2} + 15.2Ni + 44.7Si - 104V + 31.5Mo + 13.1W - 30Mn - 11Cr - 20Cu + 700P + 400Al + 120As + 400Ti$	[78, 79]
Eutectoid temperature	$Ae_1 = 723 - 10.7Mn - 16.9Ni + 29Si + 16.9Cr + 290As + 6.4W$	[80]
Bainite start temperature	$B_s = 656 - 58C - 35Mn - 75Si - 15Ni - 34Cr - 41Mo$	[81]
Martensite start temperature	$M_s = 561 - 474C - 33Mn - 17Ni - 17Cr - 21Mo$	[80, 81]

$$S = \int_0^t \frac{dt}{\tau_i} = \sum_{i=1}^j \frac{\Delta t_i}{\tau_i} = 1 \quad (3.14)$$

An exponential decrease in the nucleation rate is expected to decrease exponentially with respect to time, however the phase growth rate was generally considered as constant (Avrami equation). The relation between the transformed volume fraction of V_k , initial volume fraction of austenite before the transformation V_γ and the quenching time may be expressed as,

$$V_k = V_\gamma \left(1 - \exp(-b_k t^{n_k}) \right) \quad (3.15)$$

Here, b_k and n_k are two constants specific for phase k and these are temperature dependent. The following equation was then derived [68] for the transformed volume fraction, at time $t + \Delta t$.

$$V_{k(t+\Delta t)} = V_{k(t+\Delta t)}^* \left(V_{\gamma(t)} + V_{k(t)} \right) V_{\max} \quad (3.16)$$

Here V_{max} is the maximum amount of volume fraction of the new phase and $V_{k(t+\Delta t)}^*$ is defined as the fictitious transformed volume fraction depending upon a fictitious time τ defined by Equation 3.18.

$$V_{k(t+\Delta t)}^* = 1 - \exp\left(-b_k (\tau + \Delta t)^{n_k}\right) \quad (3.17)$$

$$\tau = n_k \sqrt[n_k]{-\frac{\ln(1 - V_{k(t)})}{b_k}} \quad (3.18)$$

This calculation procedure requires the numerical values for V_{max} , n_k and b_k . By use of the Fe-C phase equilibrium diagram, the value of V_{max} may be calculated using the lever rule for pre-eutectoid transformations. For this calculation information about the equilibrium amount of transformation products (V_{eq}) (amount of ferrite for hypoeutectoid steels or amount of cementite for hypereutectoid steels) just above the eutectoid temperature Ae_1 is needed. The maximum amount of pre-eutectoid constituent is equal to V_{eq} and to zero, for $T \leq Ae_1$ and for $T > Ae_3$, respectively. Using the lever rule, for $Ae_1 < T < Ae_3$, V_{max} may be estimated from $V_{max} = V_{eq} ((Ae_3 - T) / (Ae_3 - Ae_1))$. In the cases of transformations to pearlite and bainite V_{max} may be assumed as one.

The constants of Avrami equation, namely n_k and b_k for phase k are computed from the following equations

$$n_k = \frac{\log \frac{\ln(1 - V_s)}{\ln(1 - V_f)}}{\log \frac{t_s}{t_f}} \quad (3.19)$$

$$b_k = -\frac{\ln(1 - V_s)}{t_s^{n_k}} \quad (3.20)$$

In these equations t_s and t_f correspond to the time values at which transformation to phase k starts and finishes at a given temperature and $V_s=0.01$ and $V_f=0.99$ are the corresponding volume fractions. In the work of Tzitzelkov [28], the polynomial relations were recommended for the estimation of these constants.

$$\log b = a_0 + a_1T + a_2T^2 + a_3T^3 \quad (3.21)$$

$$n = c_0 + c_1T + c_2T^2 + c_3T^3 \quad (3.22)$$

For the temperature range in which bainitic and pearlitic transformations occur at the same time, the evaluation of the parameters b and n is not possible [73]. If pearlite is still formed at the bainite start temperature B_s , continuation of the transformation of the existing pearlite/austenite interface was assumed to yield bainite.

At temperatures below the martensite start temperature M_s , martensite forms without significantly influenced by the cooling rate. The growth stage of martensite is so fast that the rate of volume transformation was essentially controlled by nucleation [82]. For low carbon steel M_s was reported to be about 500 °C. With an increase in carbon content a decrease in M_s is reported. In steels containing more than 0.4% C, some austenite is reported to be retained after quenching and this is considered as a factor improving the toughness of steels [82]. For the estimation of the amount of martensite formed below M_s the following equation proposed in the literature may be used [83]. Here, V_γ is the volume fraction of austenite available at M_s .

$$V_m = V_\gamma (1 - \exp(-0.011(M_s - T))) \quad (3.23)$$

3.3. Predictions of Quench Stress Distribution

Temperature profiles developed in the specimen and the volume variations cause residual stresses. In order to predict the internal stress distributions, temperature, physical properties and mechanical properties have to be known at any time and at

any point within the specimen. The following properties are needed to characterize the elastic stress-strain relations and the material behavior during quenching [68]:

- i- A yield condition corresponding to the start of plastic flow.
- ii- A flow rule for the relation between the plastic strain increments and the current stresses and the stress increments subsequent to yielding.
- iii- A hardening rule for the yield surface changes as a result of plastic flow.

The stress field σ_{ij} , the strain field ε_{ij} and the displacement field u_i has to be determined within a given domain V having a boundary A. For a general static problem, the following relations should be satisfied between the stresses and the forces (F_i is the body force):

$$\sigma_{ji,j} + F_i = 0 \quad \text{on} \quad V \quad (3.24)$$

$$\sigma_{ji}n_j = T_i \quad \text{on} \quad A \quad (3.25)$$

In the quench problem, besides these equations, appropriate consecutive equations relating stresses and strains are needed.

For an infinitely long axisymmetrical cylinder, all stress derivatives with respect to z and θ directions disappear and the stress equilibrium relation becomes,

$$\frac{d\sigma_r}{dr} + \frac{\sigma_r - \sigma_\theta}{r} = 0 \quad . \quad (3.26)$$

A constant axial strain was considered. Other assumptions made in the analysis are that, the displacement u_r was not a function of z and there were no displacements depending on θ (no torsion). For this case, the strain vector was shown to reduce to

$$\{\varepsilon_r \quad \varepsilon_\theta \quad \varepsilon_z\} = \left\{ \frac{du_r}{dr} \quad \frac{u_r}{r} \quad \frac{du_z}{dz} \right\} \quad (3.27)$$

With an assumption that steel behave like a thermo-elasto-plastic material, the total strain rate of the steel during quenching was expressed in terms of elastic, thermal, transformation, plastic and transformational plasticity strain terms.

$$\frac{d\varepsilon_{ij}}{dt} = \frac{d\varepsilon_{ij}^{el}}{dt} + \delta_{ij} \frac{d\varepsilon_{ij}^{th}}{dt} + \delta_{ij} \frac{d\varepsilon_{ij}^{tr}}{dt} + \frac{d\varepsilon_{ij}^{pl}}{dt} + \frac{d\varepsilon_{ij}^{tp}}{dt} \quad (3.28)$$

In this analysis constitutive equations for the effect of temperature on Poisson's ratio, Young modulus, yield stress, plastic hardening coefficient and thermal expansion coefficient are needed.

The rate of change of the elastic strain with respect to time (which appear in Equation 3.28) is defined as,

$$\frac{d\varepsilon_{ij}^{el}}{dt} = \frac{1}{E} \left[-\frac{dE}{dt} \frac{((1+\nu)\sigma_{ij} - \delta_{ij}\nu\sigma_{mm})}{E} + \frac{d\nu}{dt} (\sigma_{ij} - \delta_{ij}\sigma_{mm}) + (1+\nu) \frac{d\sigma_{ij}}{dt} - \delta_{ij}\nu \frac{d\sigma_{mm}}{dt} \right] \quad (3.29)$$

In this equation E and ν are elastic modulus and Poisson's ratio and they are dependent on the temperature and the phase composition.

By taking the thermal strain as zero for austenite at 0 °C, the summation of thermal strain rate and transformation strain rate, which appear in Equation 3.28, was formulated as,

$$\frac{d\varepsilon_{ij}^{th}}{dt} + \frac{d\varepsilon_{ij}^{tr}}{dt} = \sum_{k=1}^p \left[\frac{dV_k}{dt} \int_0^T \alpha_k dT + V_k \alpha_k \frac{dT}{dt} \right] + \sum_{k=1}^{p-1} \frac{dV_k}{dt} \varepsilon_k^{tr} \quad (3.30)$$

In this equation α_k and ε_k'' are the temperature dependent thermal expansion coefficient of phase k and the expansion associated with the transformation from austenite into the phase k, respectively.

3.3.1. Elasto-Plastic Rate Equation

In the formulation of elasto-plastic rate equations for small strain deformations the following assumptions were usually made [84]:

1. An initial yield condition defining the elastic limit of the material exists;
2. Loading surfaces that define the limits of elastic and plastic behavior beyond initial yielding exists;
3. The relations between the plastic strain rates and corresponding stress states are linear;
4. Materials are isotropic;
5. Hydrostatic pressure has negligible effect on the yield behavior of metal.
6. Yielding is insensitive to rate of deformation.

For the quenching problem, a relation between the yield function ϕ , state of stress $F(\sigma_{ij})$ and variable flow stress σ_f was defined as

$$\phi = F(\sigma_{ij}) - (\sigma_f(T, V_k, \varepsilon^p))^2 \quad (3.31)$$

Here, effective plastic strain ε^p is a strain hardening parameter. The stresses must remain on the yield surface for plastic deformations. The plastic consistency condition was then obtained by the differentiation of yield function.

$$\frac{d\phi}{dt} = \frac{\partial F}{\partial \sigma_{ij}} \frac{d\sigma_{ij}}{dt} - 2\sigma_f \left[\frac{\partial \sigma_f}{\partial T} \frac{dT}{dt} + \sum_{k=1}^p \frac{\partial \sigma_f}{\partial V_k} \frac{dV_k}{dt} + \frac{\partial \sigma_f}{\partial \varepsilon^p} \frac{d\varepsilon^p}{dt} \right] = 0 \quad (3.32)$$

The scalar function of stress $F(\sigma_{ij})$ was written as

$$F(\sigma_{ij}) = \frac{3}{2} \left(\sigma_{ij} - \frac{1}{3} \delta_{ij} \sigma_{mm} \right) \left(\sigma_{ij} - \frac{1}{3} \delta_{ij} \sigma_{mm} \right) \quad (3.33)$$

Here, σ_{ij} is the Cauchy stress tensor. From the Prandtl-Reuss flow rule, which states that the plastic strain is in the direction of the outward normal to the surface represented by $F(\sigma_{ij})$ in stress space, the following equations were derived [68].

$$\frac{d\varepsilon_{ij}^p}{dt} = d\lambda \frac{\partial \phi}{\partial \sigma_{ij}} = d\lambda \frac{\partial F}{\partial \sigma_{ij}} \quad (3.34)$$

where $d\lambda$ is the plastic (Lagrange) multiplier. The plastic consistency equation given by Equation 3.32 was then became as

$$\frac{\partial F}{\partial \sigma_{ij}} \frac{d\sigma_{ij}}{dt} - 2\sigma_f \left[\frac{\partial \sigma_f}{\partial t} \frac{dT}{dt} + \sum_{k=1}^p \frac{\partial \sigma_f}{\partial V_k} \frac{dV_k}{dt} \right] - 2\sigma_f \left(Hd\lambda \sqrt{\frac{2}{3} \frac{\partial F}{\partial \sigma_{ij}} \frac{\partial F}{\partial \sigma_{ij}}} \right) = 0 \quad (3.35)$$

Both yield stress and elastic modulus change depend upon temperature. Consequently, for the same plastic strain, plastic stresses are different at different temperatures. During quenching phase transformations take place and the plastic deformation accumulated in the austenite phase is lost. Consequently, a new strain hardening parameter κ is defined. For austenite, κ is equal to the effective plastic strain.

After various modifications, this equation took the following form.

$$\frac{\partial F}{\partial \sigma_{ij}} \frac{d\sigma_{ij}}{dt} + A_1 - A_2 d\lambda = 0 \quad (3.36)$$

where,

$$A_1 = -2\sigma_f \left(\sum_{k=1}^p V_k \left(\frac{dY_k}{dt} + \frac{dH_k}{dt} \kappa_k \right) + H_\gamma \kappa_\gamma \frac{dV_\gamma}{dt} \right) \quad (3.37)$$

$$A_2 = 2\sigma_f \sum_{k=1}^p V_k H_k \sqrt{\frac{2}{3} \frac{\partial F}{\partial \sigma_{ij}} \frac{\partial F}{\partial \sigma_{ij}}} \quad (3.38)$$

Here, H and Y define the instantaneous values of incremental secant modulus (strain hardening constant) and yield stress, respectively.

3.3.2. Thermo-Elasto-Plastic Stress-Strain Relations

The initial strain increments $d\varepsilon^o/dt$ within the specimen are caused due to temperature change and phase transformations during quenching. By using the Hook's law and the Equations 3.28 and 3.34 and further modifications, an explicit relation between the stress changes and imposed strain changes was obtained.

$$\frac{d\sigma_{ij}}{dt} = [D_{ep}] \left(\frac{d\varepsilon_{ij}}{dt} - \frac{d\varepsilon_{ij}^o}{dt} \right) \quad (3.39)$$

Here, $[D_{ep}]$ is the elasto-plastic matrix. If the instantaneous value of $d\lambda$ becomes negative, it is taken as zero. A similar analysis gave an equation for the consistent tangent modular matrix Q .

$$\frac{d\sigma_{ij}}{dt} = Q \left(\frac{d\varepsilon_{ij}}{dt} - \frac{d\varepsilon_{ij}^o}{dt} - d\lambda \frac{\partial F}{\partial \sigma_{ij}} \right) \quad (3.40)$$

$$Q = [D_e] \left[1 + \Delta\lambda [D_e] \frac{\partial^2 F}{\partial \sigma_{ij}^2} \right]^{-1} \quad (3.41)$$

By setting $\Delta\lambda$ to zero in this equation, Q becomes equal to the elastic constitutive matrix. Further derivations gave the following equations.

$$[D_e] = \frac{E}{(1+\nu)(1-2\nu)} \begin{bmatrix} 1-\nu & \nu & \nu \\ \nu & 1-\nu & \nu \\ \nu & \nu & 1-\nu \end{bmatrix} \quad (3.42)$$

$$[D_{ep}] = [C]^{-1} \quad (3.43)$$

$$C_{ij} = \frac{p}{E} + \frac{1}{A_2} \frac{\partial F}{\partial \sigma_i} \frac{\partial F}{\partial \sigma_j} \quad (3.44)$$

Here $p=1$ for $i=j$ and $p=\nu$ for $i \neq j$.

3.3.3. Numerical Solution Procedures

The external forces caused by temperature gradients and volume changes during quenching are applied in increments at each step, in the forward-Euler integration scheme used. The strains and stresses are computed within each element using the relations between strains and displacement rates. Then, stresses are computed using the elasto-plastic stress-strain rate law. The total strain is decomposed into the plastic and elastic components. Increments of plastic strain and stress are determined and the procedure is repeated until the history of response is obtained.

A summary of the integration scheme is given below:

1. In the first computational cycle, all stress and strain values are zero and the constitutive matrix $[D]$ is equal to the elastic constitutive matrix $[D_e]$ and the first incremental load is calculated from the temperature gradients and phase transformations within the given Δt .

2. For the sampling points yielding $\phi < 0$ (for the current $\{\sigma_{i-1}\}$), $[D]_{i-1} = [D_e]_{i-1}$. Plastic deformation is indicated otherwise and for that case, $[D_{ep}]_{i-1}$ was evaluated for the Gauss points where plastic deformation occurs.

3. In the third step elemental stiffness matrices are evaluated.

4. Structure displacement rates, displacement increments $\{\Delta a\}_i$ and strain increments $\{\Delta \varepsilon\}_i$ are then solved at the Gauss points.

5. Effective stress value is calculated by adding the stress increments evaluated from (assuming elastic deformation)

$$\{\Delta \sigma_i\} = [D]_i (\{\Delta \varepsilon_i\} - \{\Delta \varepsilon^o\}_i) \quad (3.45)$$

to the existing stress values. Then, it is checked if this value is greater than the yield stress. If a Gauss point is found to be in the elastic range calculations are continued from step 9.

6. If a Gauss point is in the plastic regime the portion of the stress greater than the yield stress should be reduced to the yield surface [85].

7. The solution is then updated.

$$\{a\}_i = \{a\}_{i-1} + \{\Delta a\}_i \quad (3.46)$$

$$\{\sigma\}_i = \{\sigma\}_{i-1} + \{\Delta \sigma\}_i \quad (3.47)$$

8. In order to prevent progressive drift corrective loads are introduced.

9. The displacements are then updated using Equation 3.46, the next load increment is applied and calculations are continued by returning to step 2.

In order to reduce the integration errors due to large strain deformations the strain increment vector may be partitioned into β sub increments:

$$\{\sigma_{n+1}\} = \{\sigma_n\} + \frac{1}{\beta} \sum_1^{\beta} [D_{ep}] \{\Delta\varepsilon\} \quad (3.48)$$

It is important to determine whether the stresses exceed yield criterion or not for each integration point. The equivalent stress at each point is compared with the yield stress. Also, if a change occurs from elastic to plastic state at a point, evaluation of the portion of the stress increment that causes elastic deformation is needed.

3.3.4. Finite Element Modeling of Stress Computation

The values for each element are determined using the temperature values and the microstructure evaluated at corresponding nodal points, and then, they are used in stress calculations. In the temperature calculations, the central section of the cylindrical specimen is divided into m rectangular-strain vector quadrilateral axisymmetric elements. These elements are interconnected at n number of nodes. It is assumed that all elements have a linear displacement field. An approximation is done on the elemental level by replacing rate vector with a kinematically complete distribution given by

$$\left\{ \frac{du}{dt} \right\} = [N] \left\{ \frac{da}{dt} \right\} \quad (3.49)$$

$\{da/dt\}$ involves nodal displacement rates associated with the element and $[N]$ is the interpolation (shape) function matrix

Linear displacements give rise to constant strains. Therefore, the state of strain rate in a given element can be represented symbolically by

$$\left\{ \frac{d\varepsilon}{dt} \right\} = \begin{bmatrix} \frac{\partial}{\partial r} & \frac{1}{r} & 0 \\ 0 & 0 & \frac{\partial}{\partial z} \end{bmatrix} \left\{ \frac{du}{dt} \right\} = [B] \left\{ \frac{da}{dt} \right\} \quad (3.50)$$

where, $\{da/dt\}$ is a eight-vector whose components are the displacement rates at each of the nodes, and $[B]$ is a 3x8 matrix whose elements depend on the geometry of the element. In the integration calculations the actual coordinate system (r,z) is transformed into the natural coordinate system (s,t). Chain rule is used for this transformation. The initial strain vector due to initial stresses is defined as

$$\left\{ \frac{d\varepsilon^o}{dt} \right\} = \left\{ \frac{d\varepsilon_r^o}{dt} \frac{d\varepsilon_\theta^o}{dt} \frac{d\varepsilon_z^o}{dt} \right\}^T = \frac{d}{dt} \begin{bmatrix} \frac{1}{E} (\sigma_r - \nu(\sigma_z + \sigma_\theta)) + \varepsilon_r^{th} + \varepsilon_r^{tr} + \varepsilon_r^{pl} \\ \frac{1}{E} (\sigma_\theta - \nu(\sigma_r + \sigma_z)) + \varepsilon_\theta^{th} + \varepsilon_\theta^{tr} + \varepsilon_\theta^{pl} \\ \frac{1}{E} (\sigma_z - \nu(\sigma_r + \sigma_\theta)) + \varepsilon_z^{th} + \varepsilon_z^{tr} + \varepsilon_z^{pl} \end{bmatrix} \quad (3.51)$$

The $i = r, \theta, z$ components of this vector are calculated from.

$$\frac{d\varepsilon_i^o}{dt} = -\frac{1}{E^2} \frac{dE}{dt} [\sigma_i - \nu(3\sigma_{mm} - \sigma_i)] - \frac{1}{E} \frac{d\nu}{dt} (3\sigma_{mm} - \sigma_i) + \frac{A_1}{A_2} \frac{\partial F}{\partial \sigma_i} + \frac{d\varepsilon_i^{th}}{dt} + \frac{d\varepsilon_i^{tr}}{dt} \quad (3.52)$$

With the assumption that elements are connected only at their nodes and considering that any external loads are replaced by concentrated loads at the nodes, the following element load rate vector caused by initial strains was written as

$$\left\{ \frac{df^o}{dt} \right\} = [B]^T [D] \left\{ \frac{d\varepsilon^o}{dt} \right\} V^e \quad (3.53)$$

Here, $[D]$ is the symmetric standard tangent modular (elemental constitutive) matrix. The element equation and the element tangent stiffness matrix, with V^e being the volume of the element, are

$$[K]^e \left\{ \frac{da}{dt} \right\}^e = \left\{ \frac{df^o}{dt} \right\} \quad (3.54)$$

$$[K]^e = [B]^T [D] [B] V^e \quad (3.55)$$

The assemblage procedure is based on the requirement of compatibility at the element nodes. At the nodal points where elements are connected, the values of the unknown variables must be same of all elements joining at this node. The assembly of equation is done in the usual manner to form the complete strip elements. As a result the complete structural equation is obtained,

$$[K]^e \left\{ \frac{da}{dt} \right\} = \left\{ \frac{df}{dt} \right\} \quad (3.56)$$

In which $\{df / dt\}$ is the resultant load rate vector obtained by assembling the elemental initial load rate $\{df^o / dt\}$ and the external load rate $\{df^{ext} / dt\}$ vectors.

The tangent modulus formulation determines the stiffness matrix using the stress and deformation state, and plastic zone at the beginning of a step. Such an approach leads to problems of load imbalance, in the sense that calculated stress distributions do not equilibrate applied loads. The simplest corrective procedure for reducing the amount of drifting to tolerable levels introduced the introduction of an equilibrium connection term that may be added as a load vector at regular intervals in the incremental procedure. Thus, the $\{df / dt\}$ term in equation (3.84) is replaced by $\{dR / dt\}$ which contain a residual correction term. In the first iteration of a given load increment is

$$\left\{ \frac{dR}{dt} \right\} = \left\{ \frac{df}{dt} \right\} \quad (3.57)$$

Starting from the second iteration

$$\left\{ \frac{dR}{dt} \right\} = \frac{\{f\} - \{g\}}{\Delta t} \quad (3.58)$$

where $\{g\}$ is the load vector calculated by using the stress values computed at the end of the iteration and for each element is calculated using

$$\{g\} = \int [B]^T \{\sigma\} dV \quad (3.59)$$

Axial displacements at the bottom-line nodes are zero. For that reason, the corresponding rows and columns in the matrix equations are deleted.

Axial displacement of nodal points on the upper line are equal to each other, i.e., both ends that are perpendicular to the axis to remain plane after deformation because of the continuity of deformation.

The nodal points on the upper and bottom lines, which are under each other, have the same radial displacements.

The external nodal forces have no radial components, as there is no shear present the outer surface is unloaded,

Also, the z-components of the external forces have to sum up to zero. These natural boundary conditions can be represented such that the net force acting on a cross-section is zero.

This is equivalent to the statement that boundary condition is satisfied over the surface as a whole but not at individual points on the surface. This approximation allows the use of infinitely long body model that considers only the generation of stress and strain in sections well away from the ends.

The reduced and symmetric form of tangent stiffness matrix is as follows,

$$\begin{bmatrix} [K1] & [K2] \\ [K2]^T & [K5] \end{bmatrix} \begin{Bmatrix} \left\{ \frac{da_A}{dt} \right\} \\ \left\{ \frac{da_B}{dt} \right\} \end{Bmatrix} = \begin{Bmatrix} \left\{ \frac{df_A^o}{dt} \right\} \\ 0.5 \left(\left\{ \frac{df_B^o}{dt} \right\} + \left\{ \frac{df_D^o}{dt} \right\} \right) \{1\} \end{Bmatrix} \quad (3.60)$$

Equation (3.60) can be symbolized in the overall matrix equation from as,

$$[K]^{red} \begin{Bmatrix} da \\ dt \end{Bmatrix}^{red} = \begin{Bmatrix} df \\ dt \end{Bmatrix}^{red} \quad (3.61)$$

The overall matrix equations are solved by Gauss-elimination method. The results are tested by an overall convergence criterion. The iteration is considered complete when the ratios of the changes in nodal forces to the square of the force vector falls below a certain value.

$$\sum_{k=1}^n \frac{\left(\left\{ f^{red} \right\} - \left\{ g^{red} \right\} \right)^2}{\left\{ f^{red} \right\}^2} \leq Enorm \quad (3.62)$$

The tolerance on the unbalanced forces in combination with the load increment dictates the number of iterations for convergence. Choosing the tolerance too high would reduce the number of iterations. However, this could be only done after checking other factors. The thermal gradients determine the incremental loading experienced by the cylinder. Valid stress result can be obtained by using temperature gradients within a given maximum temperature difference at the surface of the

cylinder. These gradients are the most severe at the beginning of the quenching and very small time steps are required. Too large thermal gradient causes excessive iterations and does not allow calculated plastic stresses to be properly brought back down to the yield surface after each iteration sequence. The ratio of equivalent stress to yield stress is an indication of the stress back down to the yield surface. If this ratio is near 1, this means that the technique is bringing the plastic stresses back to yield surface for elements where plastic flow prevailed [24]. On the other hand, to check out the elastic portion of the program the sum of the radial (σ_r) and tangential stresses (σ_θ) is used. This summation must be equal to σ_z . However, this equality is valid for the elements that are deformed in the elastic region only. When the $\sigma_z / (\sigma_r + \sigma_\theta)$ ratio is very close to one, this gives confidence for calculation of elastic stresses.

3.4. Description of the Program

This program, consisting of eighteen subroutines, simulates the quench process of axisymmetric parts. The flowchart of the program is given in Figure 3.1. At each time step the program calculates the radial profiles of temperature, volume fraction of phases, and internal stresses. It stops calculations when the temperature of the whole specimen gets equal to the temperature of the quench medium, and then, gives the final residual stress state in the specimen. The program has been written in Fortran [68], and in this thesis pre- and post-processors written in Visual Basic are added to make the program user friendly.

Subroutine MAIN

- i- Opens the input and output card files;
- ii- Determines starting points for arrays that will be used during calculation of temperature and stress, in the global array constructed by dynamic dimensioning method;
- iii- Calls INFORM to read and write input data; controls the workspace for dynamically dimensioning array;

- iv- Calls MACRO so start and control the calculations

Subroutine INFORM

- i- Initializes matrices and arrays;
- ii- Reads necessary input data;
- iii- Calls GENER for automatic mesh generation, coding of all nodal points to define boundary conditions for temperature and stress calculations.
- iv- Reads all mesh data and codes for boundary conditions if mesh generation is user defined.
- v- Calculates half-band width for the construction of global stiffness matrix for the solution of heat transfer problem
- vi- Writes initial data defining the program to the output card file.

Subroutine MACRO

- i- Starts time step in the quenching process.
- ii- Starts iteration
 - Initializes the array and the matrix of global system of equations
 - Calls STIFTEM to construct the global stiffness matrix equations for determining temperature distribution considering the phase transformation effects (PHASE)
 - Calls SOLVER to solve the global system of equations, which are arranged in banded-symmetric form, for nodal temperatures by Gauss elimination method
 - Calls CONVTEM to check the convergence of the solution and time step length
 - If solution is not converged, updates the nodal temperatures and restarts this step.
- iii- Calculates elemental temperatures and volume fraction of phases by averaging the nodal values of the element.
- iv- Calls STIFSIG to calculate internal stress and strains.
- v- Calls OUTPUT to write the results if desired and restart from step ii.

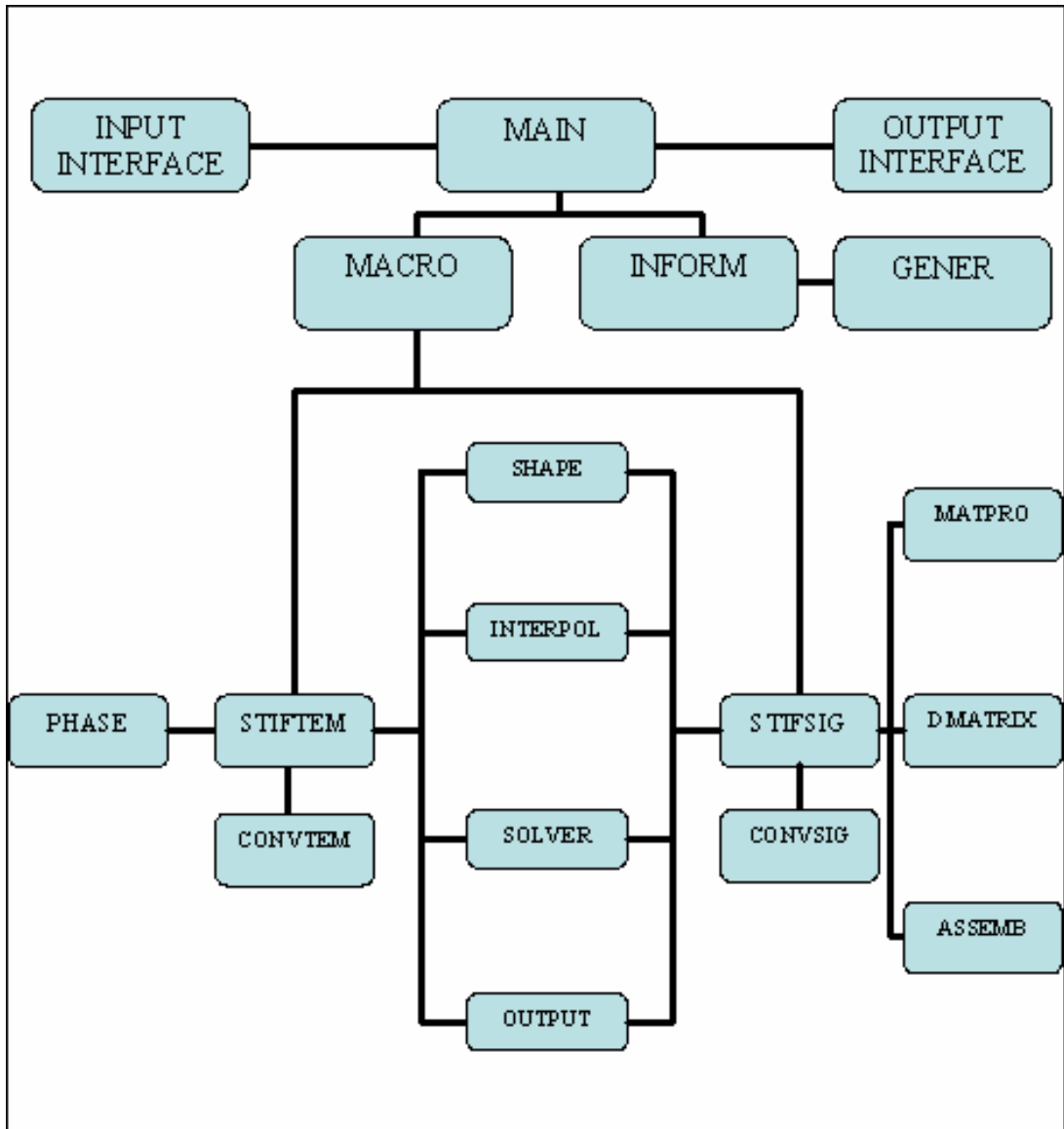


Figure 3.1. General structure of the program

3.5. Input Data for Numerical Analysis

3.5.1. Data for Temperature Calculations

The temperature dependent values of thermal conductivity and heat capacity of the steel, the surface heat transfer coefficient of the quenchant, and latent heats of phase transformations are needed to predict the temperature field.

Thermal conductivity is a function of microstructure, so it may change considerably during the quenching process. The lowest conductivity of austenite is between 15 and 26 W/m°C in the temperature range 25 – 850 °C. Other phases have higher conductivity values in a range of 25 – 40 W/m°C. Conductivity of phases that are in equilibrium in low temperatures usually decreases as the temperature increases. A simple weighted mean of conductivities of constituents is a satisfactory method to obtain the thermal conductivity of duplex structures [35]. Some values of thermal conductivities of various phases for different steels are tabulated in Table 3.2.

Heat capacity is the multiplication of density and specific heat per unit volume. Specific heat is affected from both temperature and microstructure. It has extremely high values around temperatures phase transformation occurs. The values of these high peaks are not known exactly since there are contradictory values in the literature. Composition of low-alloy steels does not affect the specific heat considerably; temperature and microstructure are much more important variables. Some values of heat capacities of various phases for different steels are tabulated in Table 3.3.

Surface heat transfer coefficients can be used to control the generation of stresses and distortion in the specimen. It is used to describe the heat flow from the surface of the specimen into the quench medium. Heat flow from specimen to medium is described as

$$q = h \cdot A(T_s - T_m) \quad (3.63)$$

where h is the surface heat transfer coefficient, A is the surface area of the specimen, T_s is the temperature of the surface and T_m is the temperature of the quench bath. Surface heat transfer coefficient is very sensitive to small changes in the quench bath conditions, the state of the specimen surface, size and shape of the specimen, and varies very much during the quench process that is a big problem during the calculations. This problem forces experimental measurements of temperature at the surface and center of the specimen to use as boundary conditions during temperature profile calculations. Also surface heat transfer coefficient is determined from the experimental temperatures that are close to the surface. On the other hand, to make the thermal stress calculations more practical, data that can be used in a wide range of situations are required. So, surface heat transfer or heat flux rate data that are characteristic of specific surface-quench medium combinations for particular temperatures are preferred to cooling curves of a specific specimen.

Latent heat is also added into the heat flow equation. Latent heat is the heat released in the material when a phase change occurs. Some values of latent heats of various phases for different steels are tabulated in Table 3.4.

3.5.2. Data for Stress Calculations

Temperature gradient at nodal points and temperature dependent mechanical properties (Poisson's ratio, yield strength, strain hardening coefficient, thermal expansion coefficient and transformation strains) of the steel are needed for stress calculations.

For low alloy steels, composition and microstructure do not have a significant effect on elastic modulus. However, austenite shows a slightly lower value of elastic modulus than other phases at the same composition and temperature. The rates of thermal loading during quenching are of the same order as those used during the static determination of elastic modulus [86]. So, the statically determined data can be used in calculations of thermal stresses in a quench process. Some values of elastic modulus of different phases of different steels are tabulated in Table 3.5.

Poisson's ratio is usually taken as 0.3 and is nearly equal for all phases in steels. As the temperature increases from room temperature to austenitization temperatures, the value increases from about 0.28 to 0.31.

The yield strength of austenite increases from 20 MPa to 190 MPa as the temperature falls from the austenitization temperature to martensite start temperature. Also yield strengths close to 190 MPa increase more rapidly as the temperature is reduced. Some values of yield strength of different phases of different steels are tabulated in Table 3.6. It is difficult to surely predict the effect of composition on yield stress with the limited amount of data available. In general, the overall is affected by parameters representing the grain size, the phase boundaries and the contiguity of the constituents. The functional behavior of the model is very different from real but, if the overall yield stress function fits the experimental observations well, then this can describe all the possible situations in quenching.

As the temperature falls from 800 to 400°C work hardening coefficient increases. Sjöström has used values for SIS 2511 (0.58%C) between 10^3 MPa and $3.1 \cdot 10^3$ MPa for austenite, $20 \cdot 10^3$ and $60 \cdot 10^3$ for ferrite, $1 \cdot 10^3$ and $16 \cdot 10^3$ for pearlite, and $104 \cdot 10^3$ and $118 \cdot 10^3$ for martensite. Some authors have assumed a direct relation between elastic modulus and strain hardening coefficient such as Inoue and Tanaka [77].

Expansion coefficients of various phases are needed to determine the thermal strain. Increased temperature increases the thermal expansion coefficient, the addition of carbon commonly lowers the coefficient of expansion at all temperatures, the rate of increased expansion coefficient versus temperature has a marked tendency to increase C-content it generally increases at a decreasing rate with rising temperature [86]. It is difficult to distinguish thermal expansion coefficients of ferrite, pearlite, and bainite and martensite from each other from the obtained dilatation curves. Some values of thermal expansion coefficient of different phases of different steels are tabulated in Table 3.7. Sjöström has found no effect of carbon on this property, and alloying additions have little effect [35]. Most of the available data for the austenite

down to martensite start temperature show that the thermal expansion coefficient is constant at values at a range of $20 \cdot 10^{-6}$ and $23 \cdot 10^{-6}/^{\circ}\text{C}$. Sjöström suggested that the thermal expansion coefficient of martensite in plain-carbon steels increases from $10 \cdot 10^{-6}$ to $21 \cdot 10^{-6}$ as carbon content increases from 0 to 0.9 percent. Except carbon content the thermal expansion coefficient of martensite is not significantly affected by alloy additions.

In addition to the thermal strains, phase transformations also produce volume changes. This change varies for different phase transformations and also dependent on the temperature at which the transformation takes place. This effect is because of; the parent austenitic phase has a higher expansion coefficient than that of the product phases. To overcome this problem most data are used at a standard reference temperature, 0°C . It is usually to treat transformation plasticity strain, for example, the enhanced strain induced as a consequence of the presence of a stress during the change in phase, as an entity distinct from that produced under stress-free conditions. Several theoretical expressions have been used to obtain values of the transformations plasticity and a limited amount of experimental data are available, although there is a general agreement that the plastic strain is proportional to the applied stress and the proportionality constant is known in a limited number of cases [71].

A linear volume fractioning model is used to deal with continuous phase transformations. In the calculation of the overall values of elastic modulus, Poisson's ratio, yield strength and strain hardening coefficient the following equation was used by considering the values obtained in simple tension test.

$$X = \sum_{k=1}^n V_k X_k \quad (3.64)$$

3.5.3. Data to Determine Transformed Amount of Phase

On the TTT-diagram of C60, certain points are represented, for example, temperature and corresponding values of time for both transformation start (1%) and finish (%99) curves. These values are inputs for the program. Any value different from the input data is calculated by the program by linear interpolation. The constants in the Avrami equation (n, b) are calculated in the program at certain temperatures using the transformation start and finish curves for each phase present in the TTT diagram.

Table 3.2. Thermal conductivity values of several steels (W/m°C)

Steel	T(°C)	Austenite	Ferrite	Pearlite	Bainite	Martensite
Ck45	0	15.00	49.00	49.00	-	43.10
	300	18.00	41.70	41.70	-	36.70
	600	21.70	34.30	34.30	-	30.10
	900	25.10	37.00	27.00	-	-
S45 C	-	29.13	-	35.20	-	39.93
SIS 2511	0	10.50	58.20	38.20	33.60	24.50
	200	17.30	54.50	40.00	36.40	25.50
	400	20.00	50.00	36.40	31.80	26.40
	600	22.70	45.40	31.80	24.50	-
	800	25.50	-	-	-	-
SCM 3	-	29.55	-	-	-	52.32
Cr Mo V	20	-	-	-	44.40	-
	200	24.40	-	-	42.60	-
	600	24.40	-	-	41.90	-
	800	26.70	-	-	-	-
	1000	27.90	-	-	-	-

Table 3.3. Heat capacity values of several steels (MJ/m³°C)

Steel	T(°C)	Austenite	Ferrite, Pearlite, Bainite	Martensite
St 37	0	3.18	3.52	3.52
	300	3.60	3.85	3.85
	600	3.98	4.27	4.27
	900	4.40	4.60	4.60
S45 C	-	5.12	4.93	4.89
Ck 45	0	4.15	3.78	3.76
	300	4.40	4.46	4.45
	600	4.67	5.09	5.07
	900	4.90	5.74	-
St 50	-	-	4.53	-
SIS 2511	0	2.54	3.10	3.10
	200	2.89	3.63	3.63
	400	3.31	4.14	4.14
	600	3.65	4.84	4.84
	800	4.00	-	-
16 Mn Cr 5	0	-	3.52	3.52
	300	3.14	3.85	3.85
	600	3.56	4.27	4.27
	900	3.98	4.60	4.60

Table 3.4. Latent heat values for several steels (MJ/m³)

Steel	Aus.→Ferr.	Aus.→Pear.	Aus.→Bain.	Aus.→Mart.
St37, Ck45	623	623	623	623
S45 C	-	171	-	614
SIS2511	590	590	590	590

Table 3.5. Elastic modulus values of several steels (GPa)

Steel	T(°C)	Austenite	Ferrite, Pearlite	Bainite	Martensite
St37	0	200	210	210	210
	300	170	190	190	190
	600	140	155	155	-
	900	60	100	-	-
Ck45	0	200	210	210	210
	300	175	193	193	193
	600	150	165	165	-
	900	124	120	-	-
SIS2511	0	195	220	-	210
	200	185	200	-	200
	400	155	180	-	180
	600	115	150	-	-
	850	50	90	-	-

Table 3.6. Yield strength values of several steels (MPa)

Steel	T(°C)	Austenite	Ferrite	Pearlite	Bainite	Martensite
St37	0	50	260	260	300	1200
	300	40	200	200	240	1080
	600	30	40	40	40	880
	900	20	20	20	-	-
Ck45	0	190	360	360	440	1600
	300	110	230	230	330	1480
	600	30	140	140	140	1260
	900	20	30	30	30	-
SIS2511	0	45	395	460	-	1300
	200	80	305	415	-	1100
	400	85	220	365	-	-
	600	65	135	315	-	-
	850	30	-	-	-	-
30 Cr Mo Ni V 4 11	0	300	400	400	700	1200
	300	175	300	300	550	1000
	600	50	100	100	150	600
	900	30	40	40	50	-
16 Mn Cr 5	0	-	300	300	620	1260
	300	42	220	220	500	1140
	600	34	50	50	50	930
	900	26	30	30	-	-

Table 3.7. Thermal expansion coefficient values of several steels ($\mu/\text{°C}$)

Steel	Phase	α
St37	Austenite	21.0
	Ferrite + Pearlite, Bainite, Martensite	13.0
Ck45	Austenite	21.0
	Ferrite + Pearlite, Bainite	14.0
	Martensite	13.0
S45 C	Austenite	20.8
	Pearlite	15.2
	Martensite	11.4
AISI 1080	Austenite	22.5
	Ferrite	14.5
	Pearlite	15.5
30 Cr Mo Ni V 4 11	Austenite	19.5
	Ferrite + Pearlite, Bainite, Martensite	15.0
SIS 2511	Austenite	22.0
	Ferrite, Pearlite, Bainite, Martensite	11.0 – 25.0
16 Mn Cr 5	Austenite	21.0
	Ferrite + Pearlite, Bainite	13.0
	Martensite	12.0
Cr-Mo-V	Austenite	21.0 – 25.0
	Bainite	11.0

CHAPTER 4

IMPROVEMENT OF THE PROGRAM

To make the program user friendly a user interface was developed. It lets the user to input the data to the program easily by and see the outputs in an interface that also draws graphs. Both the INPUT and OUTPUT Interfaces are programmed in Visual Basic.

4.1 INPUT Interface

- i- Gets the data from the user by a user friendly windows based structure. (Figure 4.1 – 4.4)
- ii- Writes them into an input card that is used by the program itself.

4.2 OUTPUT Interface

- i- Shows the output data to the user (Figure 4.5).
- ii- Draws graphically the stress distribution in the specimen (Figure 4.6).
- iii- Draws stress vs. time graphs (Figure 4.7).
- iv- Draws cooling curve graphics for nodal points (Figure 4.8).
- v- Exports results to excel

QUEANA Input Step1

Name: c60 ph 30mm 830-60

Total Number of Elements in the Finite Element Mesh: 10

Total Number of Nodal Points in the Finite Element Mesh: 22

Phase Transformation: Yes No

Number of Gauss Integration Points: 4

Nodal Degree of Freedom for Temperature Calculations: 1

Nodal Degree of Freedom for Stress Calculations: 2

Number of Nodes per Element: 4

Choice of Time Stepping: Constant time step size User defines step size

Do You Want Stress Calculations: Yes No

Mesh Generation: Automatic User Defined

Mesh Refinement Near Surface: Constant element size Finer mesh near surface

Number of Time Steps Having This Time Increment: []

Time Increment: []

Number of Time Steps: []

Number of Time Steps Having This Time Increment: []

Buttons: EXIT, Next Step -->, SAVE DATA, LOAD DATA, LOAD SAVED OUTPUT

Figure 4.1. QUEANA input interface step 1

QUEANA Input Step2

Initial Temperature of the Specimen	830.0	Transformation start temperature for bainite	540.0
Temperature of the quench bath	60.0	Transformation finish temperature for bainite	300.0
Transformation start temperature for pearlite	750.0	Transformation start temperature for martensite	300.0
Transformation start temperature for ferrite	720.0	Transformation finish temperature for martensite	90.0

Thermal Conductivities and Heat Capacities for Different Temperatures

Temperature	Convective Heat Transfer Coefficient	Temperature	Thermal Conductivity	Heat Capacity
000.00000	40.00000E+2	Austenite	015.00000	41.5000E+5
0100.0000	40.00000E+2	Ferrite	018.00000	44.0000E+5
0200.0000	40.00000E+2	Pearlite	021.70000	46.7000E+5
0300.0000	40.00000E+2	Bainite	025.10000	49.0000E+5
0400.0000	40.00000E+2	Martensite	025.10000	49.0000E+5
0500.0000	40.00000E+2		025.10000	49.0000E+5
0600.0000	40.00000E+2		025.10000	49.0000E+5
0700.0000	40.00000E+2		025.10000	49.0000E+5
0800.0000	40.00000E+2		025.10000	49.0000E+5
0900.0000	40.00000E+2	TTT-Diagram Data	025.10000	49.0000E+5

EXIT

<-- Previous Step

Next Step -->

SAVE DATA

LOAD DATA

LOAD SAVED OUTPUT

Figure 4.2. QUEANA input interface step 2

QUEANA Input Step3

Enter the Enthalpy Values for Each Type of Phase Transformation Respectively

Austenite to:	Ferrite	0000.0060
	Pearlite	0000.0060
	Bainite	0000.0060
	Martensite	0000.0145

Enter the Strain Values for Each Type of Phase Transformation Respectively

Austenite to:	Ferrite	0000.0060
	Pearlite	0000.0060
	Bainite	0000.0060
	Martensite	0000.0145

Number of Divisions in r-axis:

Number of Divisions in z-axis:

Diameter of the Cylinder:

Diameter of the Hole (If Hollow Cylinder):

Height of the Cylinder:

Time Step Size (time increment):

Height of the elements:

Factor for the Change in Time Increment:

Time Step Factor:

Maximum Time Increment Allowed:

Minimum Time Increment Allowed:

Maximum Temperature Change Allowed at Nodal Points:

Maximum % Temperature Change Allowed at Nodal Points:

Convergence Limit for Temperature Calculations:

Acceleration Coefficient:

Time Discretization Factor:

Convergence Limit for Stress Calculation:

Buttons: EXIT, <-- Previous Step, Next Step -->, SAVE DATA, LOAD DATA, LOAD SAVED OUTPUT

Figure 4.3. QUEANA input interface step 3

QUEANA Input Step4

Austenite
 Ferrite
 Pearlite
 Bainite
 Martensite

Temperature	Elastic Modulus	Poisson's Ratio	Yield Stress	Strain Hardening Coefficient	Thermal Expansion Coefficient
00.0	0200.0E+3	0.29	0220.0E+0	01.000E+3	021.700E-6
300.	0175.0E+3	0.31	0130.0E+0	16.000E+3	021.700E-6
600.	0150.0E+3	0.33	0035.0E+0	10.000E+3	021.700E-6
900.	0124.0E+3	0.35	0035.0E+0	00.500E+3	021.700E-6
900.	0124.0E+3	0.35	0035.0E+0	00.500E+3	021.700E-6
900.	0124.0E+3	0.35	0035.0E+0	00.500E+3	021.700E-6
900.	0124.0E+3	0.35	0035.0E+0	00.500E+3	021.700E-6
900.	0124.0E+3	0.35	0035.0E+0	00.500E+3	021.700E-6
900.	0124.0E+3	0.35	0035.0E+0	00.500E+3	021.700E-6

Figure 4.4. QUEANA input interface step 4

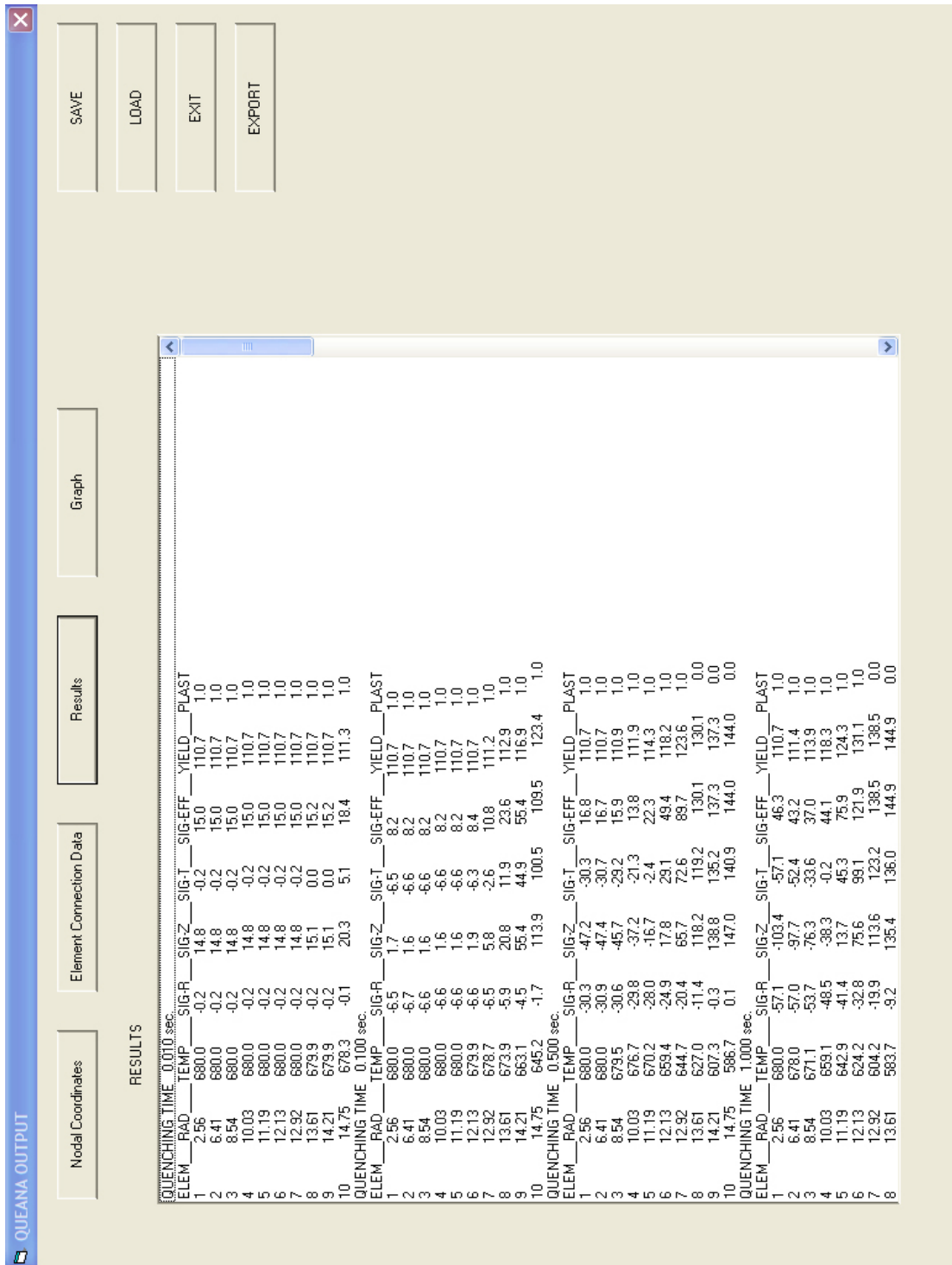


Figure 4.5. QUEANA output interface (Results)

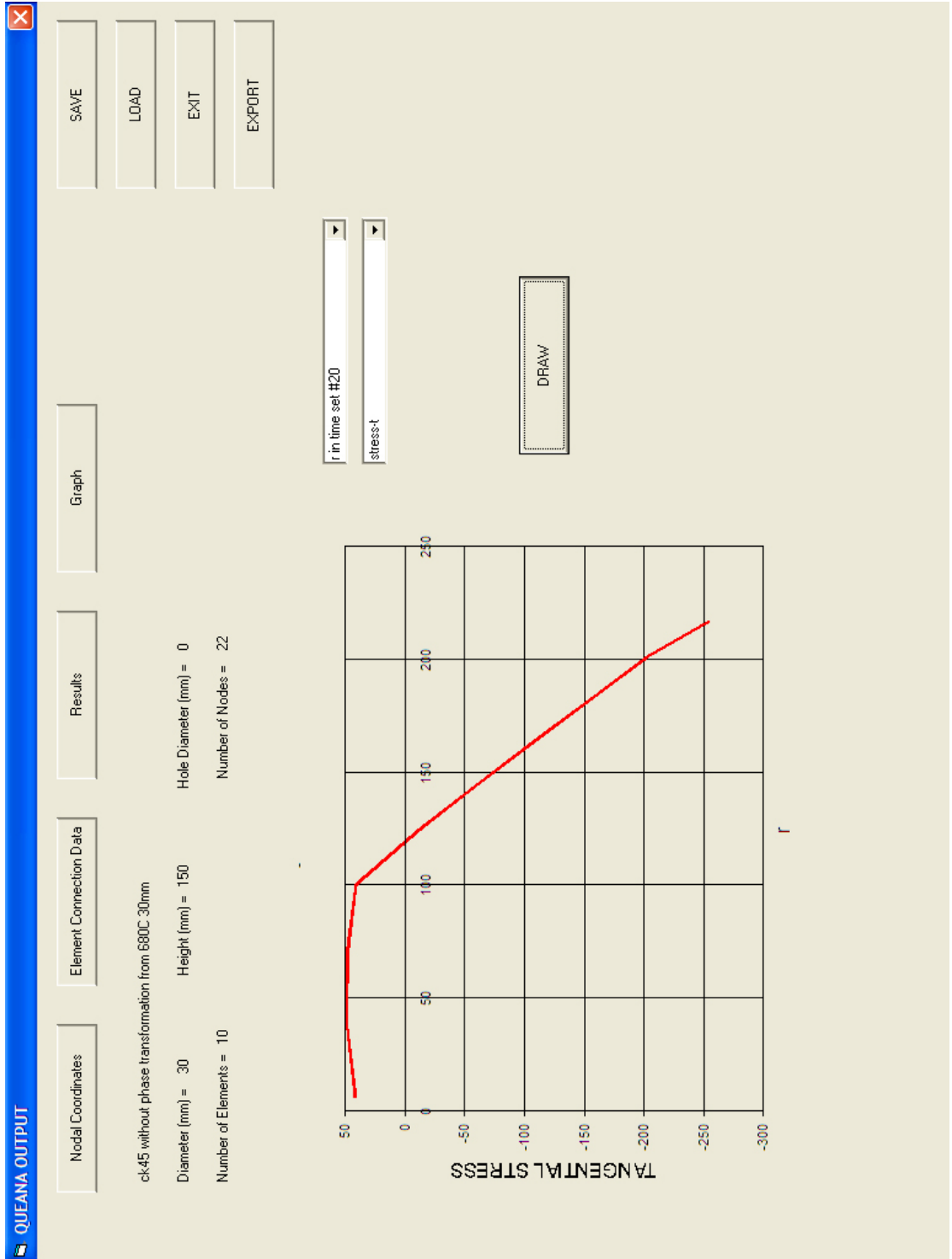


Figure 4.6. QUEANA output interface (Stress distribution graph)

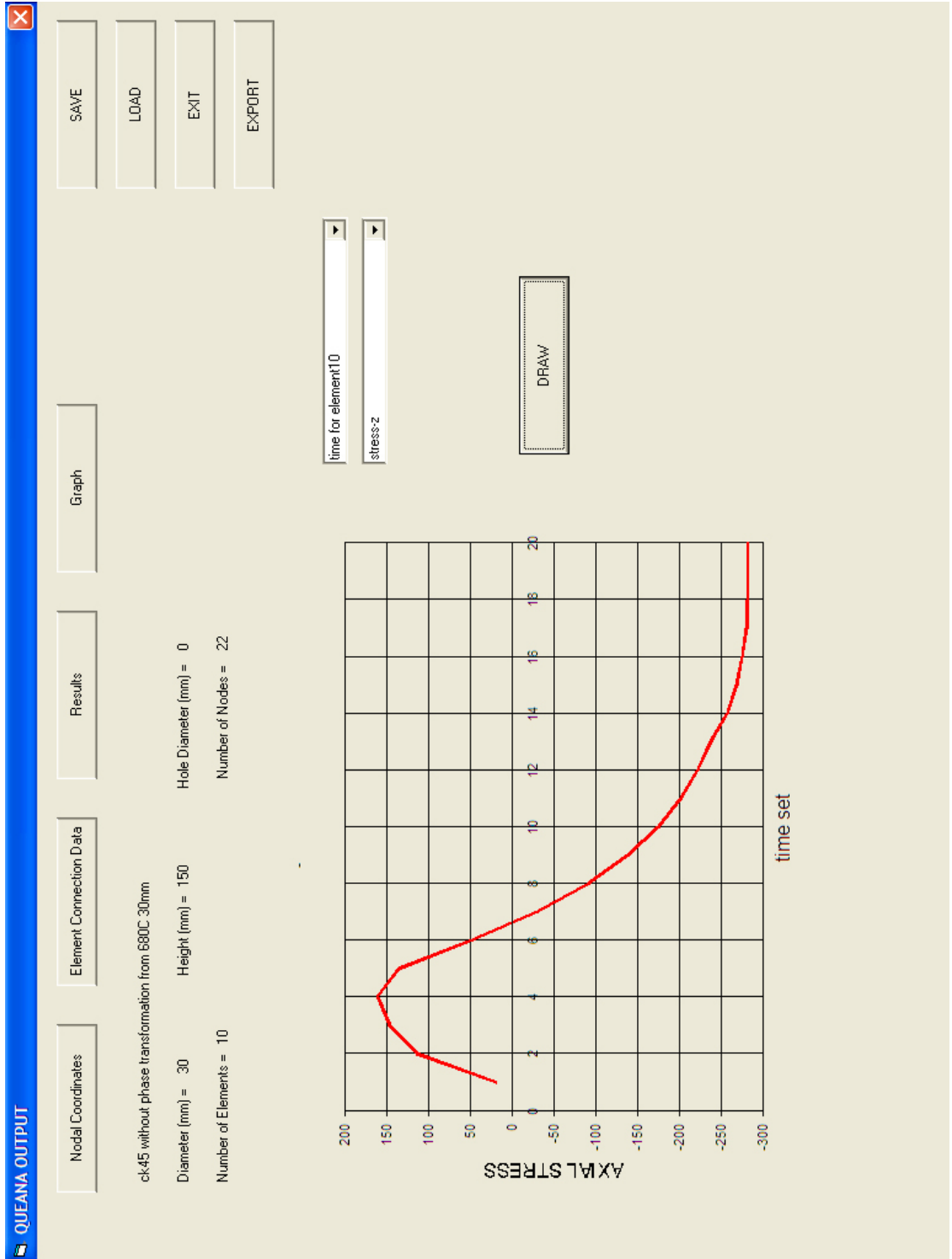


Figure 4.7. QUEANA output interface (Stress vs. time graph)

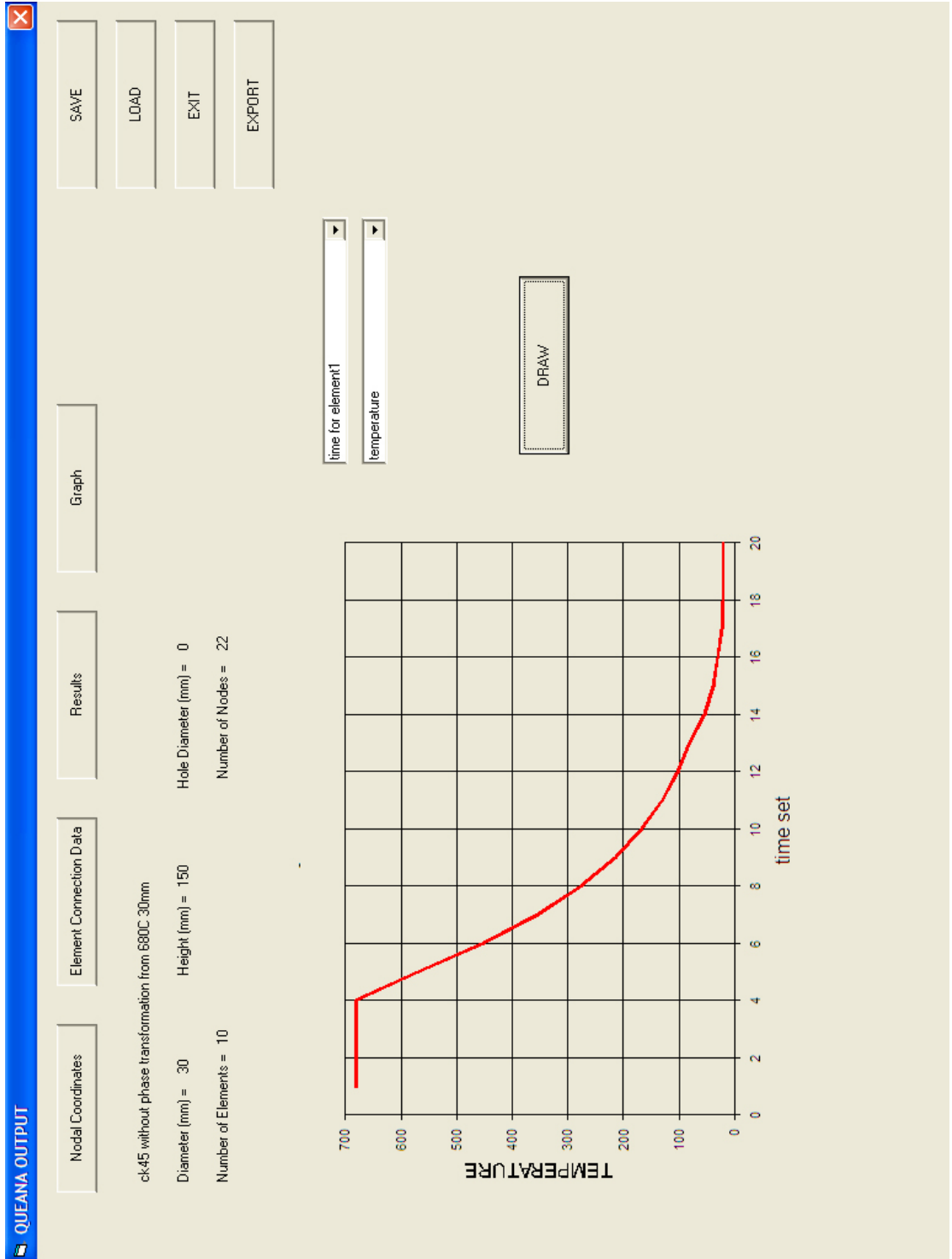


Figure 4.8. QUEANA output interface (Cooling curve graph)

CHAPTER 5

RESULTS AND DISCUSSION

5.1. Comparisons For Verification

Results of QUEANA were verified by the results taken from finite element code MARC. Ck45 steel at a diameter of 30mm was rapidly cooled from 680°C into 20°C water. The input data used in the calculations are given in Table 5.1.

Table 5.1. Input data for Ck45 steel

T(°C)	E(GPa)	ν	σ_y (MPa)	α ($\mu/\text{°C}$)	λ (J/ms °C)	C_p (MJ/m ³ °C)
0	210	0.28	360	14	49.0	3.78
300	193	0.30	230	14	41.7	4.46
600	165	0.31	140	14	34.3	5.09
900	120	0.33	30	14	27.0	5.74

The results for Ck45 steel with 30mm diameter are given in Figure 5.1 – 5.4. The results of QUEANA and MARC show a very good agreement. Tangential, radial and effective thermal stresses are almost the same in MARC and QUEANA, and axial thermal stress shows a very similar behavior. The difference for the axial thermal stresses can be explained as follows. In QUEANA specimens are assumed to be infinitely long and calculations are made in 1 dimension, in MARC simulations, a specimen with 300mm height was used and 3-D calculations were performed.

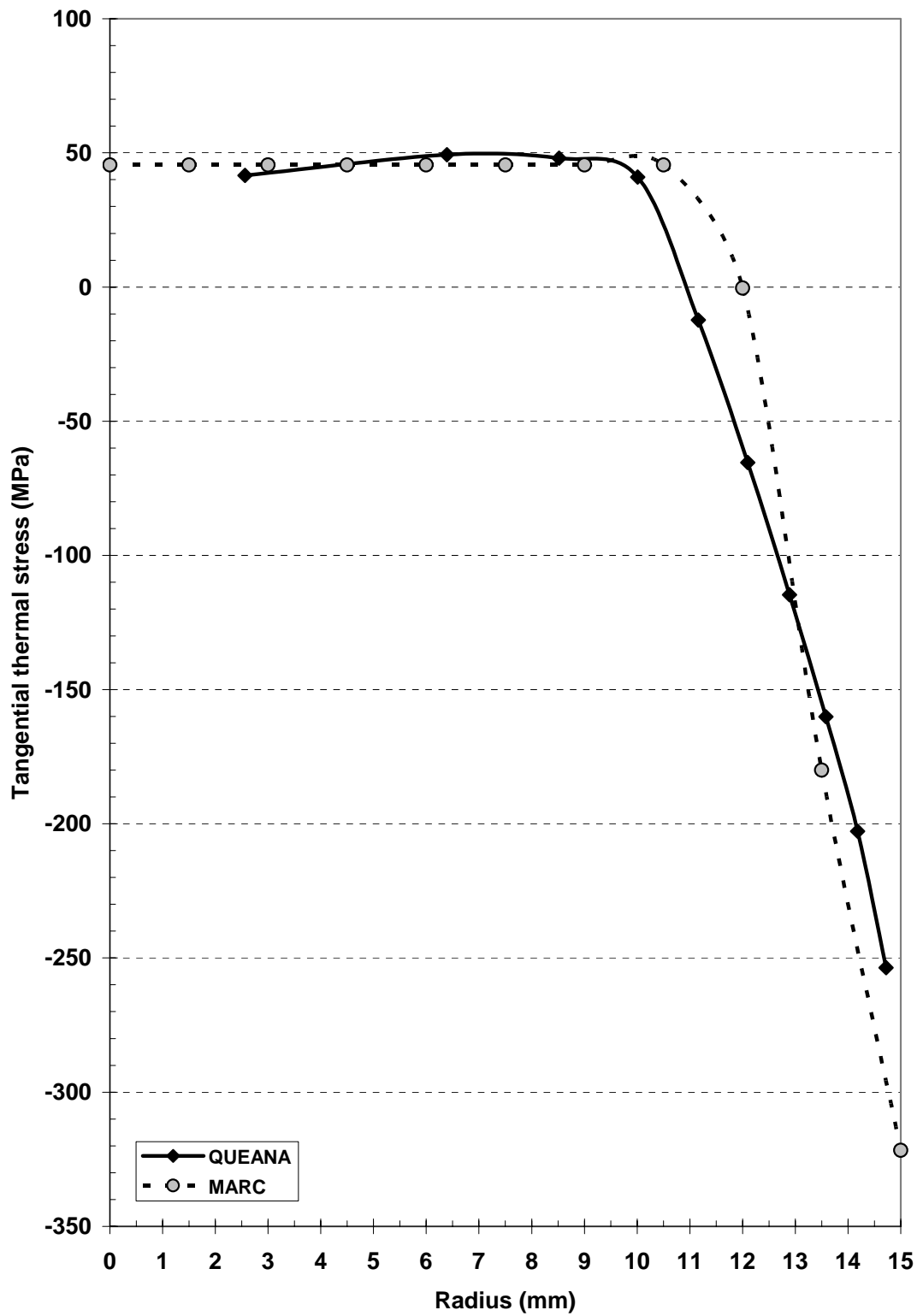


Figure 5.1. QUEANA – MARC comparison (Tangential thermal stress)
(680°C to 20°C, Ck45)

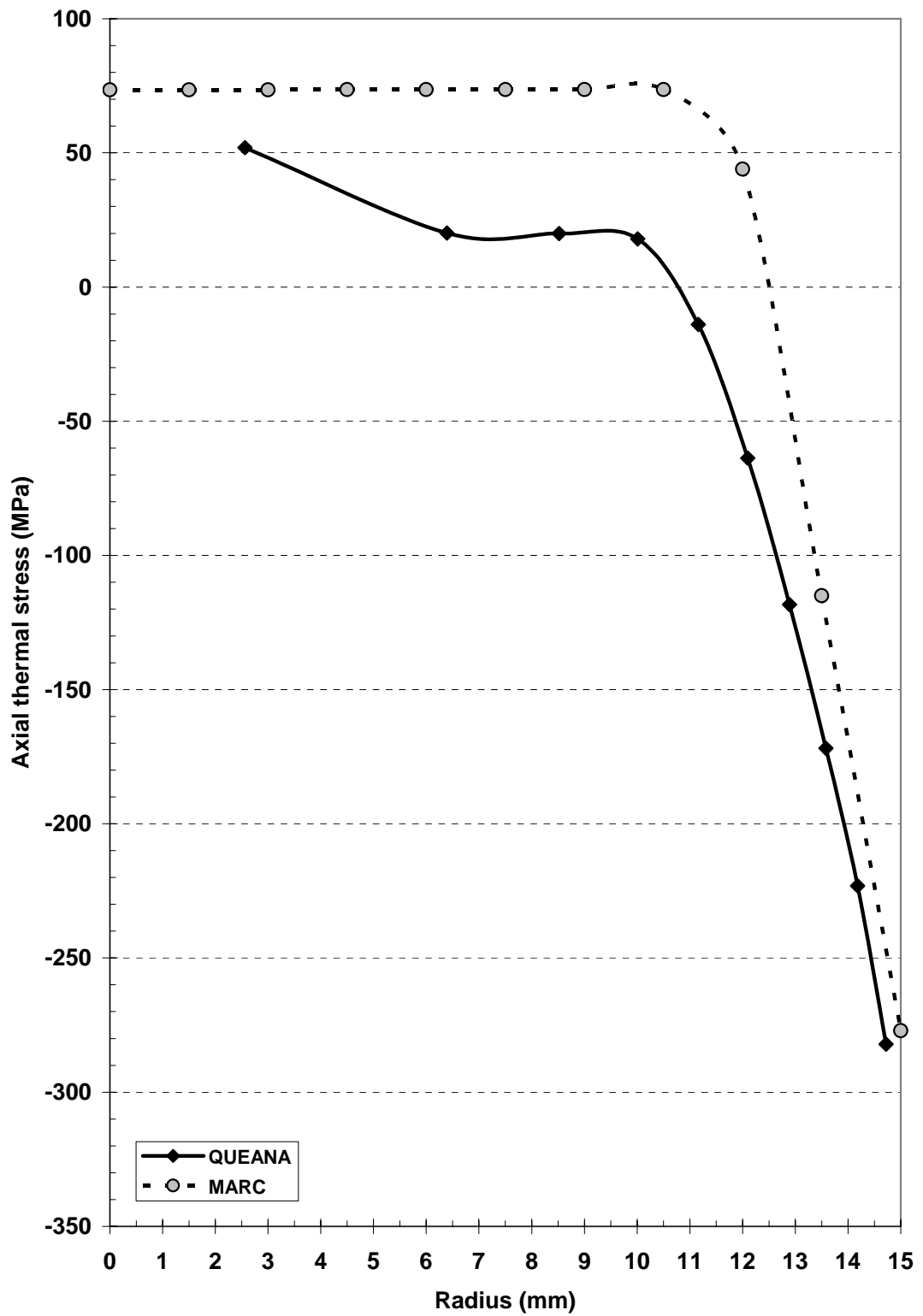


Figure 5.2. QUEANA – MARC comparison (Axial thermal stress)
(680°C to 20°C, Ck45)

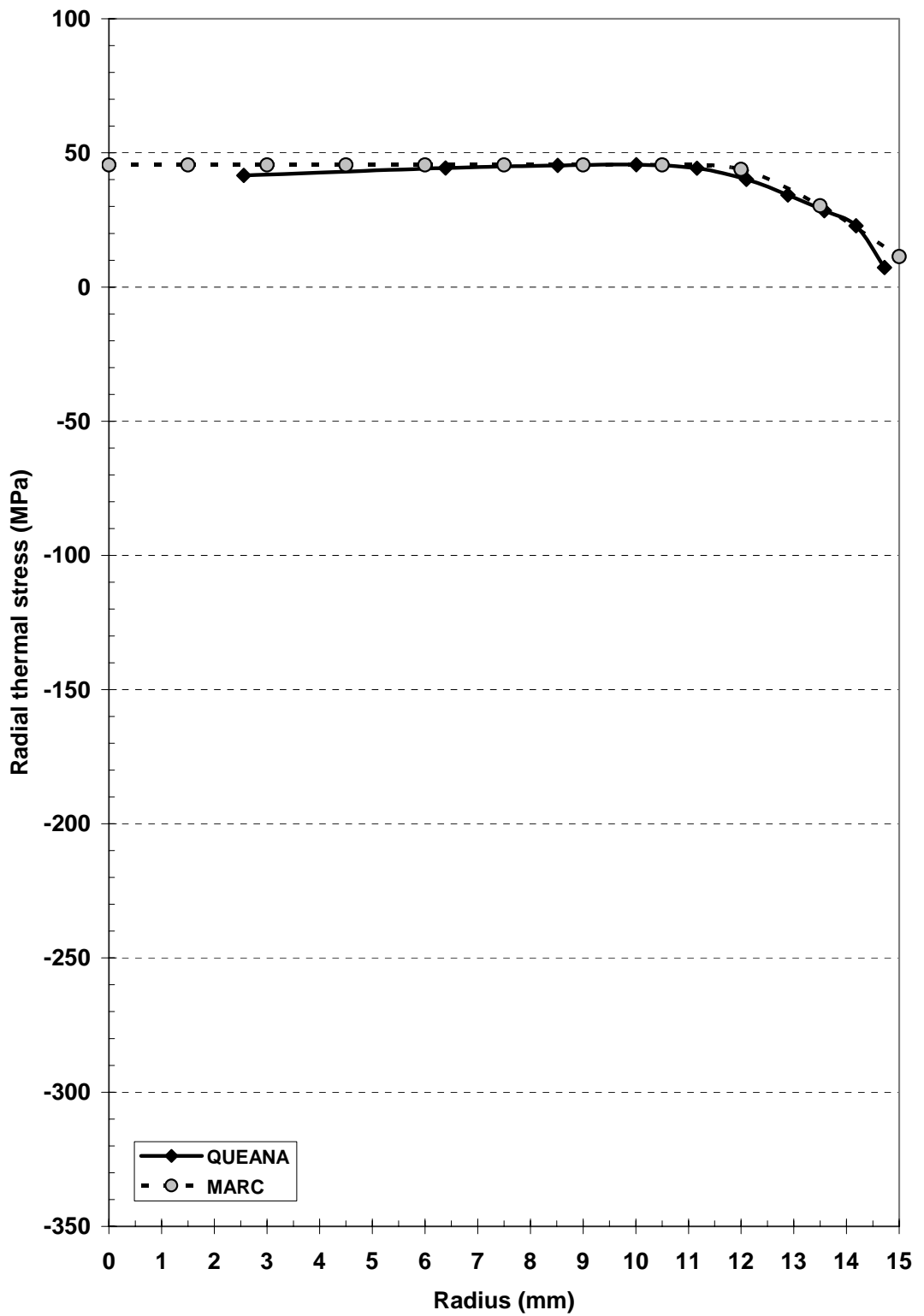


Figure 5.3. QUEANA – MARC comparison (Radial thermal stress)
(680°C to 20°C, Ck45)

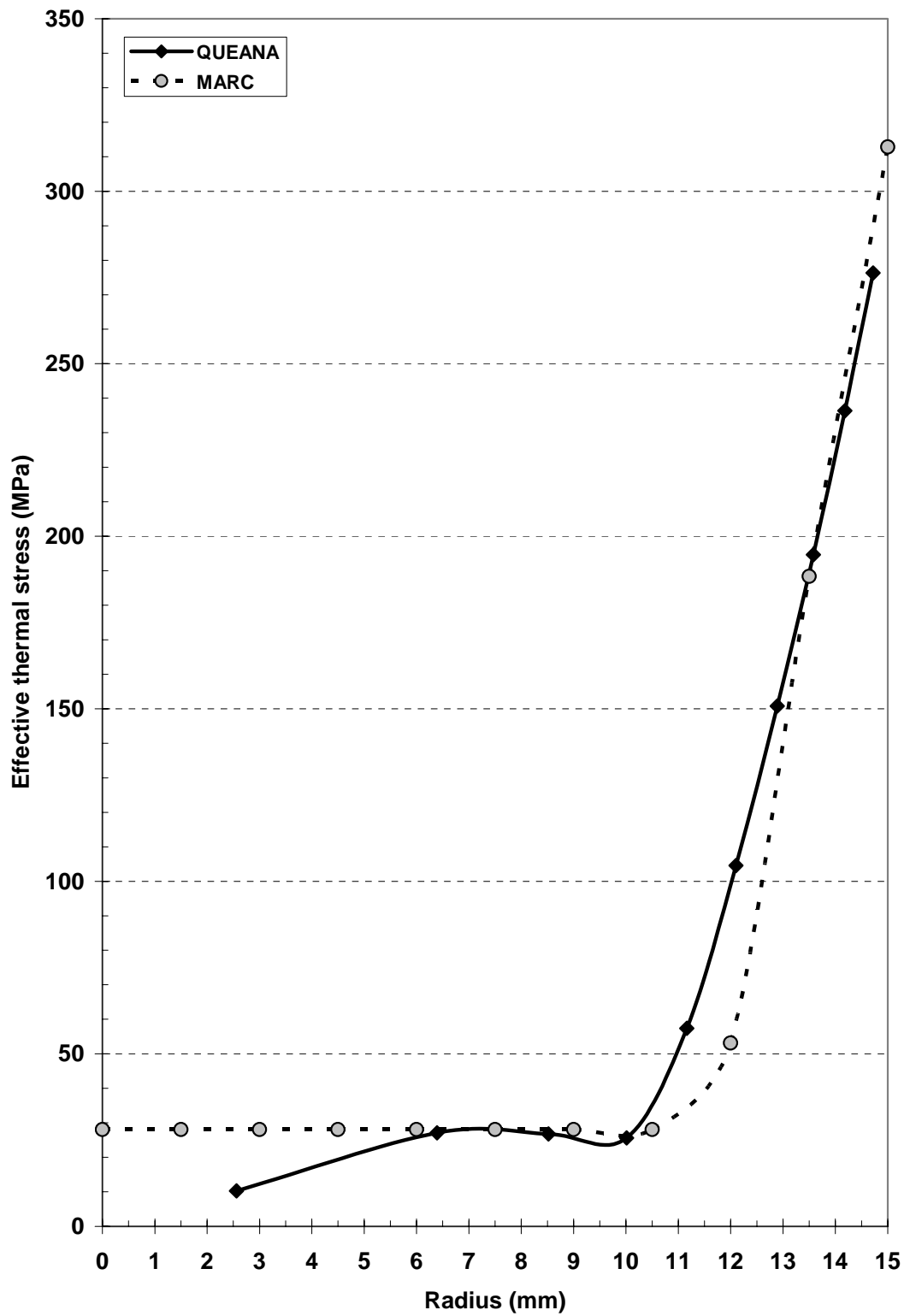


Figure 5.4. QUEANA – MARC comparison (Effective thermal stress)
(680°C to 20°C, Ck45)

5.2. Monitoring The Evolution Of Thermal Stresses During Rapid Cooling

The change in the thermal stress distributions during rapid cooling was analyzed for Ck45 cylinder with 30mm diameter. Figure 5.5 shows the cooling curves at the surface and at the center of the cylinder. Surface cools faster than the core, and cooling rate is higher at the beginning of the process. As the temperature decreases cooling rate also decreases, and therefore temperature gradient decreases.

Stresses are caused by the volume changes in the specimen. When temperature decreases the volume decreases since surface cools faster than the core, a temperature gradient occurs which create a difference in the volumes. Because of these volumetric changes, thermal stresses occur in the specimen. If the effective stress reaches yield stress, plastic deformation occurs. These plastic deformations cause change in the volumes, and this is the reason for residual stresses. As the cooling continues, and the temperature gradient decreases, these volume changes create a stress in the opposite direction of the stresses at the beginning.

The results are summarized in Figure 5.6 - 5.9. At the initial stages of quenching tangential and axial stresses are compressive in the core and tensile at the surface. However, after a certain time this situation reverses, and at the end of the cooling, the final tangential and axial thermal stresses become tensile in the core and compressive at the surface. The time for this transition is around 5 seconds. In the case of the radial stresses, they equal to zero at the surface at any time. At the other points of the specimen it is compressive at the initial stages of the cooling, and after some time they turn out to become tensile. The effective stress in the core increases more than that at the surface during the initial stages of the rapid cooling. Then, it starts to decrease and goes to zero at the surface. At later stages of cooling it again starts to increase while at the core it is still decreasing. At the end of the cooling the final effective stress at the surface is higher than that in the core.

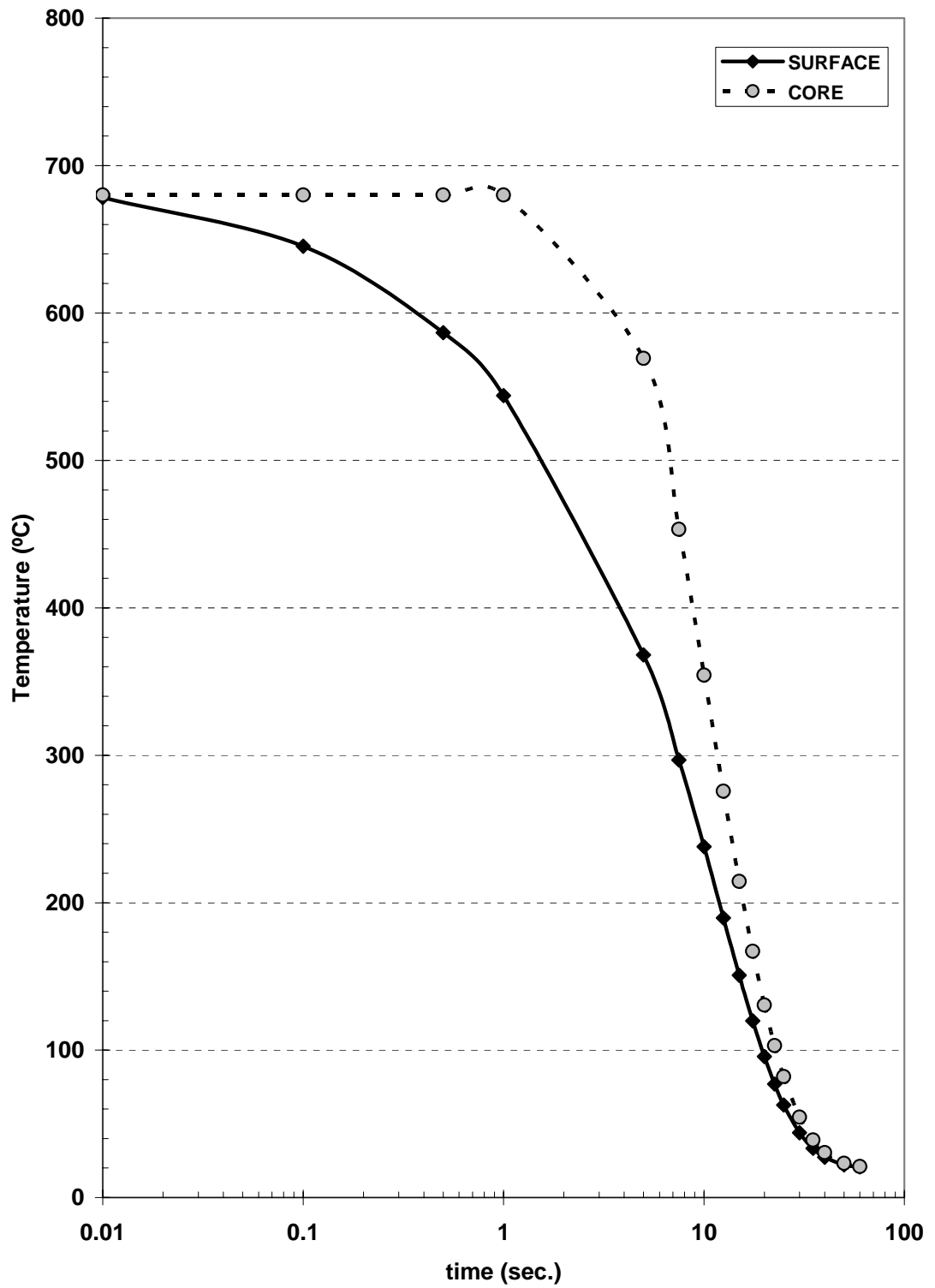


Figure 5.5. Cooling curve at the surface and at the center (680°C to 20°C, Ck45 cylinder, 30mm diameter)

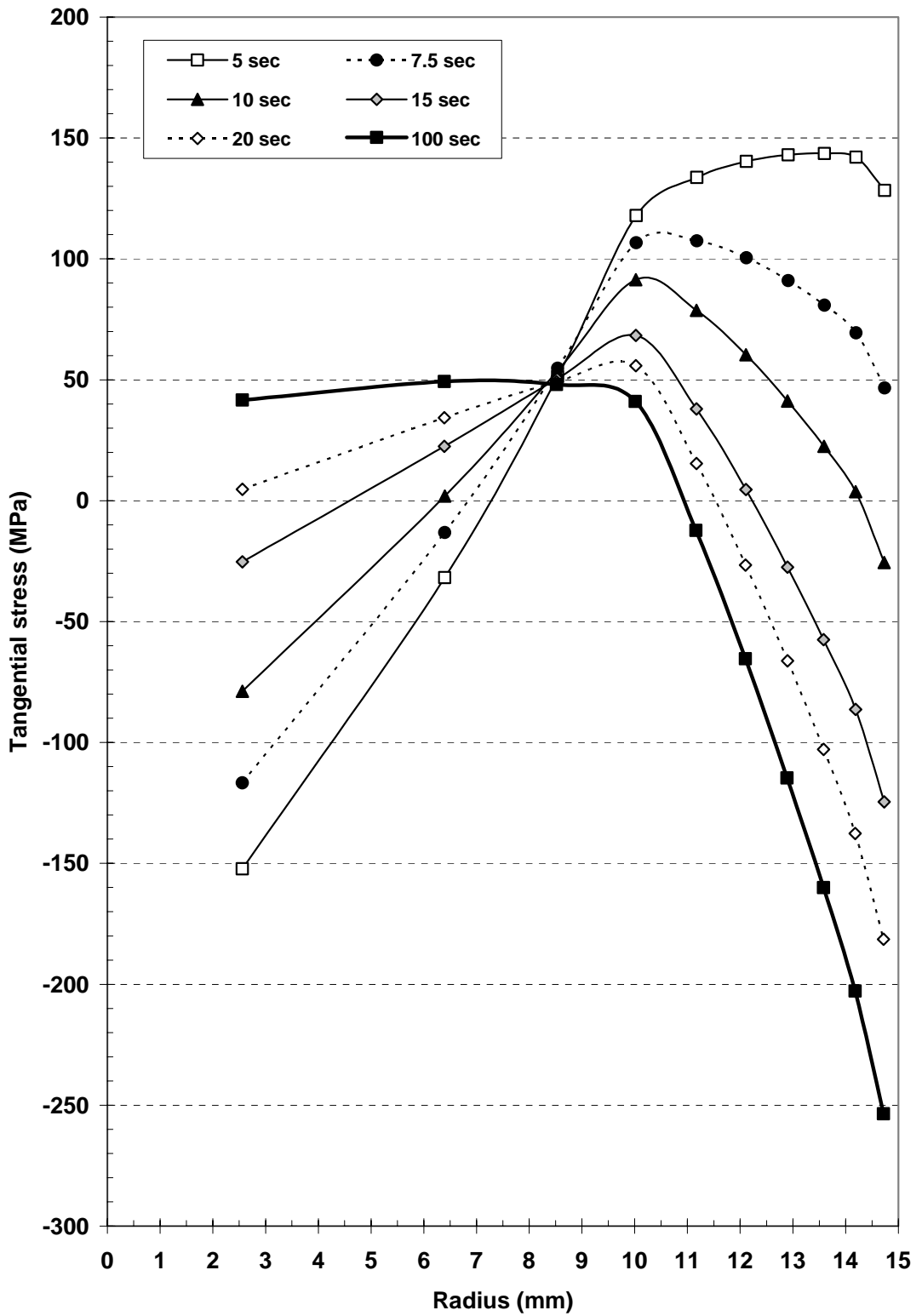


Figure 5.6. Monitoring of tangential stress evolution during rapid cooling (680°C to 20°C, Ck45)

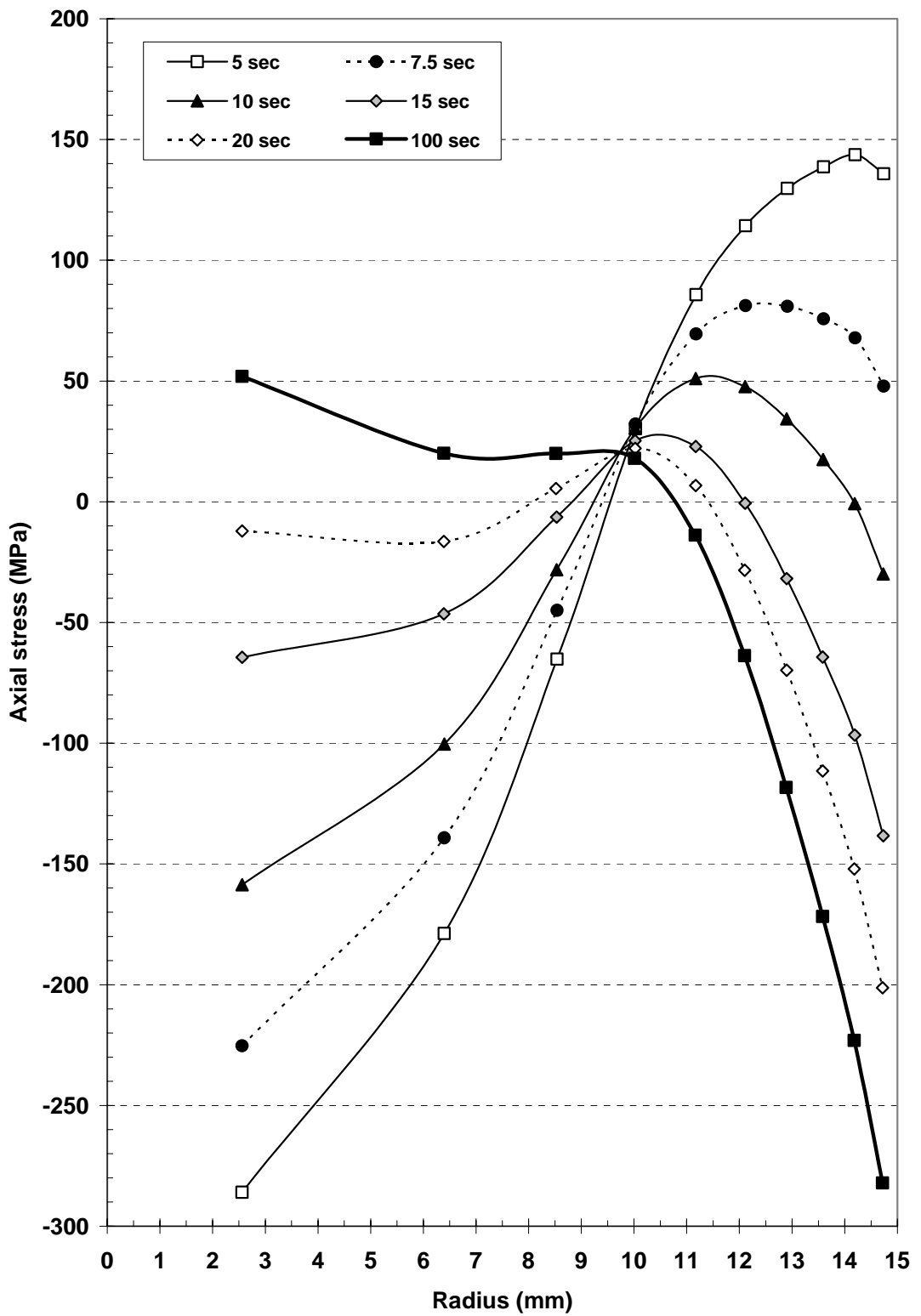


Figure 5.7. Monitoring of axial stress evolution during rapid cooling (680°C to 20°C, Ck45)

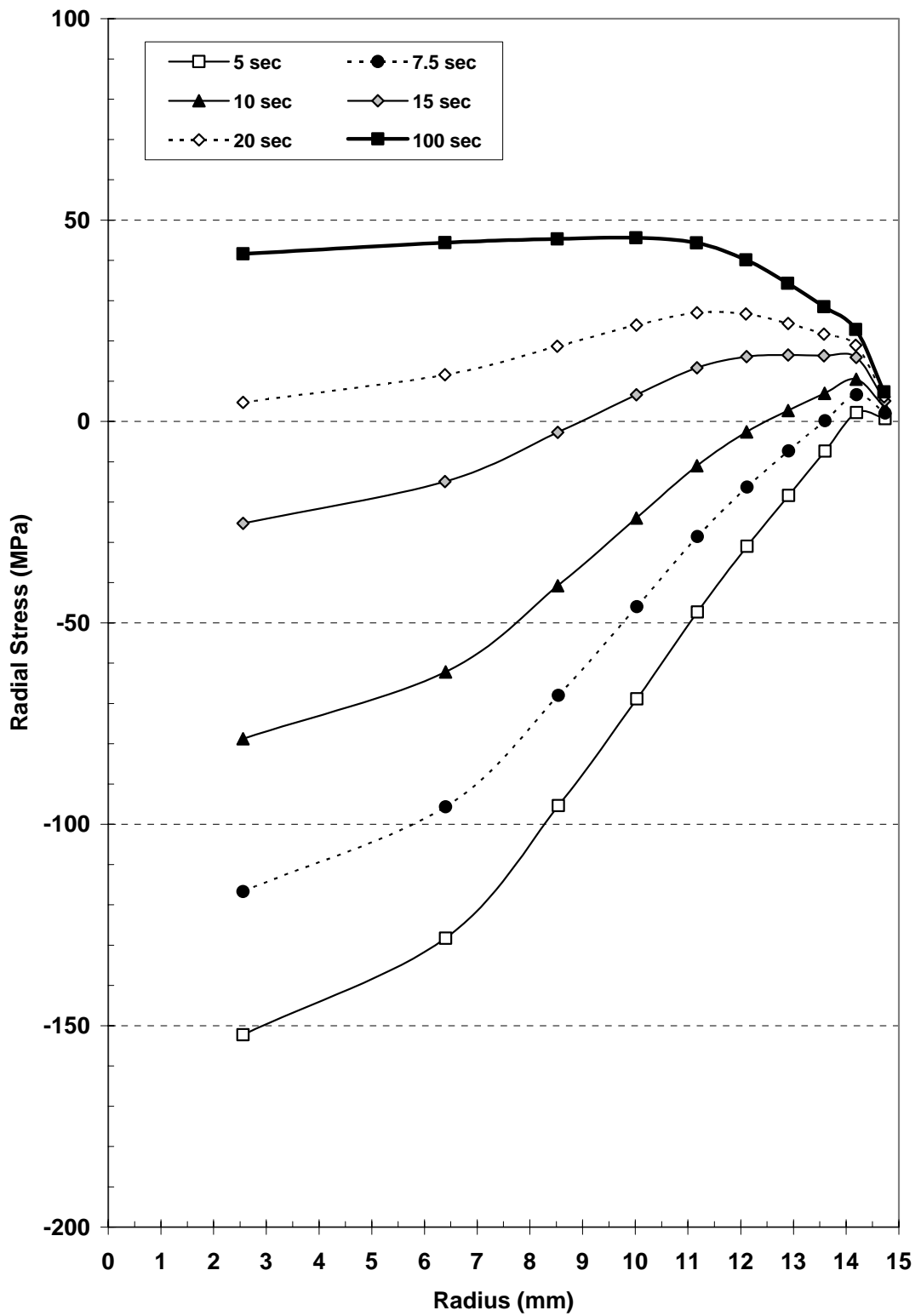


Figure 5.8. Monitoring of radial stress evolution during rapid cooling (680°C to 20°C, Ck45)

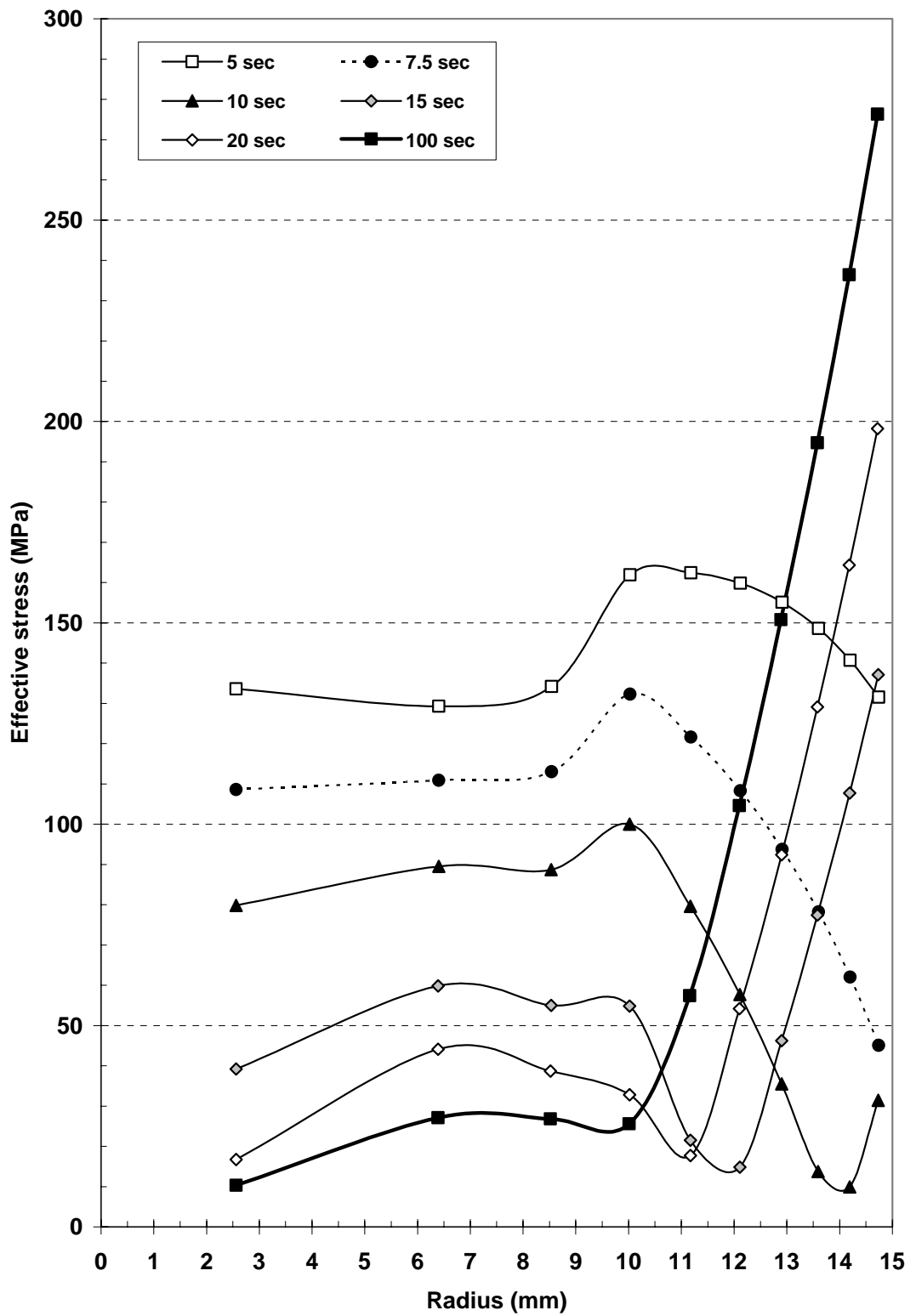


Figure 5.9. Monitoring of effective stress evolution during rapid cooling (680°C to 20°C, Ck45)

5.3. Monitoring the Local Plastic Deformation

By the help of QUEANA local plastic deformations can also be monitored. For investigating the local plastic deformations, C60 steel with 30 mm diameter is rapidly cooled from 720°C to 60°C and 20°C. Variation of the heat transfer coefficient with respect to the temperature is given in Table 5.2. To investigate the local plastic deformation effective stresses and yield strength should be monitored at the same time. If effective stress at any point reaches yield stress, local plastic deformation occurs.

Figure 5.10 shows the comparison of the variations of effective stress and yield strength at the surface and at the center with respect to time for cooling to 60°C. At the center local plastic deformation starts at 3 seconds and lasts for almost 2 seconds. After 5 seconds from the start of the cooling plastic deformation stops at the center since effective stress decreases, while yield strength increases. At 10th seconds effective stress again starts to increase but it converges to a maximum of around 100 MPa. Since yield strength is more than 100 MPa after 3 seconds from the start of the process and converges to a maximum of around 400 MPa, no plastic deformation is seen at the center after 5th second.

At the surface plastic deformation starts very early, at around 0.5 seconds. After 3.5 seconds there is a drop in the effective stress which stops the plastic deformation. Between 30-35 seconds effective stress again reaches the yield strength which yields local plastic deformation, but after 35th seconds effective stress can not increase as the yield strength so plastic deformation at the surface stops at that point.

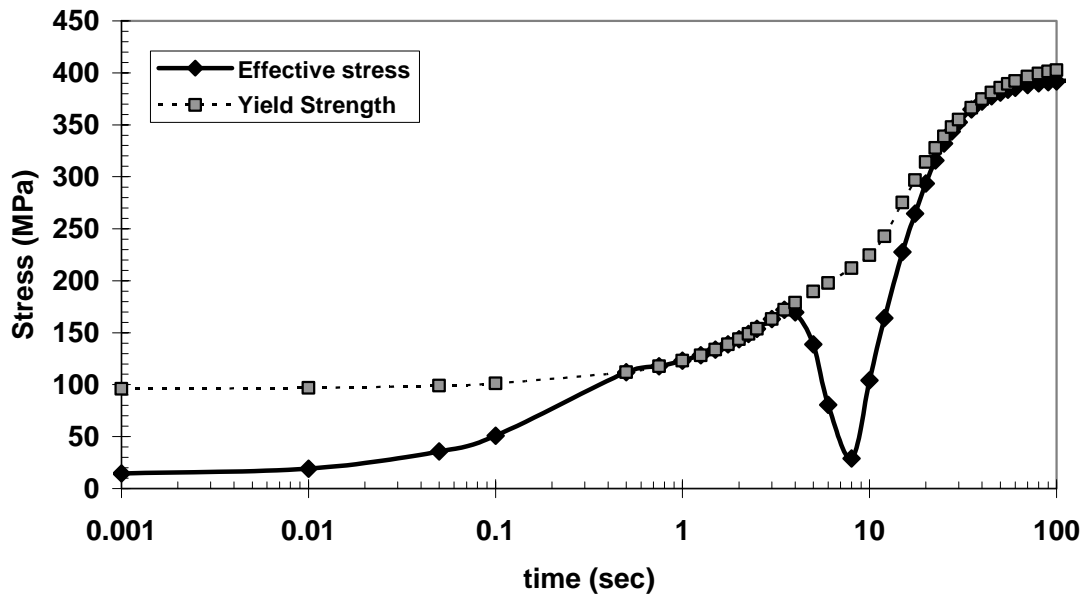
Effective stress and yield strength change for cooling to 20°C is given in Figure 5.11. At the center effective stress reaches the yield strength after 0.5 seconds. Local plastic deformation starts at that time at the center and continues until 3rd second where a decrease in effective stress is observed until 5th second from. After that point effective stress at the center increases and converges to 250 MPa which is much lower than the yield strength and does not allow plastic deformation to occur.

At the surface, plastic deformation starts just after 0.1 second from the start of the rapid cooling process. Between 1.25 seconds and 5 seconds a drop in effective stress is observed and plastic deformation is not seen in this interval. At 5 seconds effective stress again reaches the yield strength, which yields local plastic deformation at the surface, and this continues until the end of the process.

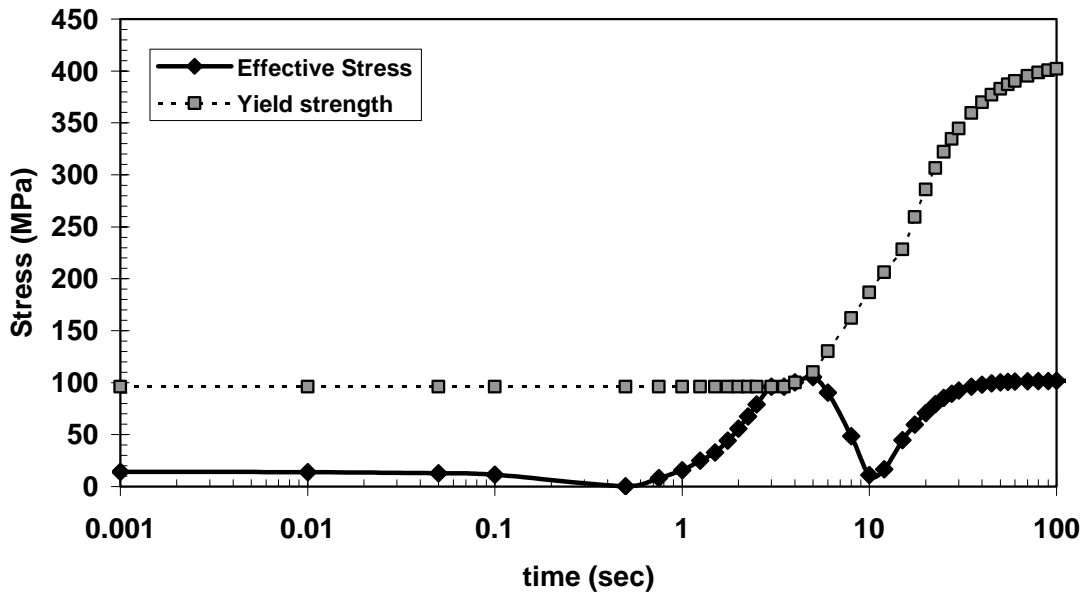
Plastic deformation was not occurring at the surface in the later stages of the process for cooling to 60°C other than cooling to 20°C. Also at the center, for cooling to 20°C, have higher effective stress values than cooling to 60°C. These differences are because of the difference in the temperature gradients in the specimen. Because of the lower cooling medium temperature and higher convective heat transfer coefficients in quenching to 20°C there occurs higher temperature gradients in the specimen, which yields higher amount of effective stress in the specimen. This causes plastic deformations continue at the surface until the end of the process for cooling to 20°C, while it stops at 35th second for cooling to 60°C, and higher effective stress values at the center for cooling to 20°C.

Table 5.2. Convective heat transfer coefficients for 20°C and 60°C water quenching

20°C		60°C	
Temperature (°C)	h_c (J/m ² s°C)	Temperature (°C)	h_c (J/m ² s°C)
0	4350.0	0	135.3
200	8207.1	200	2029.2
400	11961.7	400	2840.9
430	13491.7	445	3291.2
500	12500.0	500	3422.0
560	10206.2	570	2610.9
600	7793.0	600	2157.0
700	2507.0	800	430.3
800	437.1	900	135.2
900	135.3	-	-

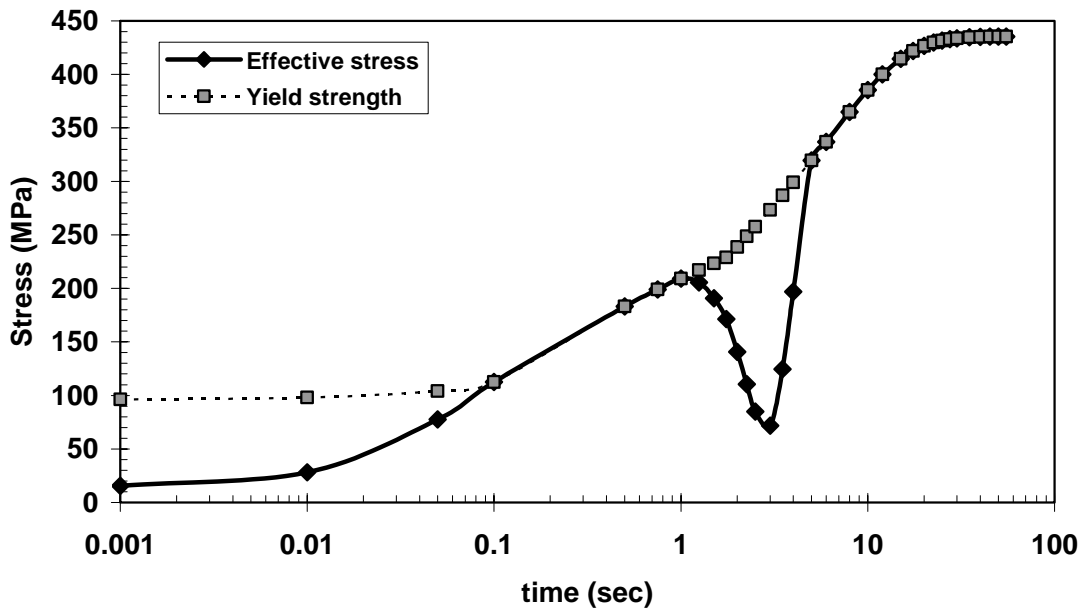


(a)

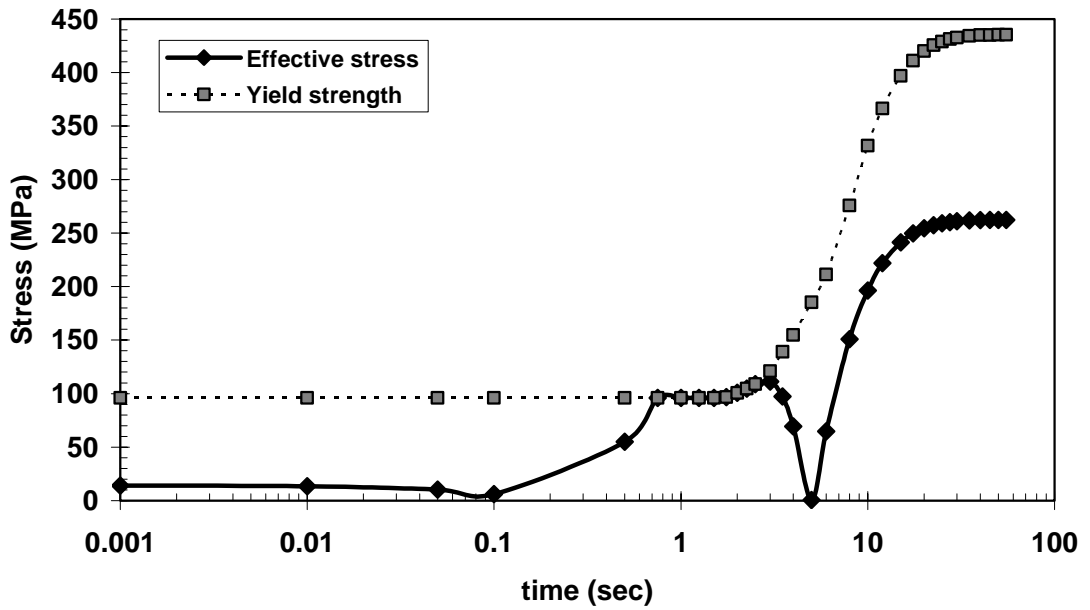


(b)

Figure 5.10. Monitoring of local plastic deformations
(720°C to 60°C, C60 steel, 30mm diameter)
a) Surface, b) Center



(a)



(b)

Figure 5.11. Monitoring of local plastic deformations
(720°C to 20°C, C60 steel, 30mm diameter)
a) Surface, b) Center

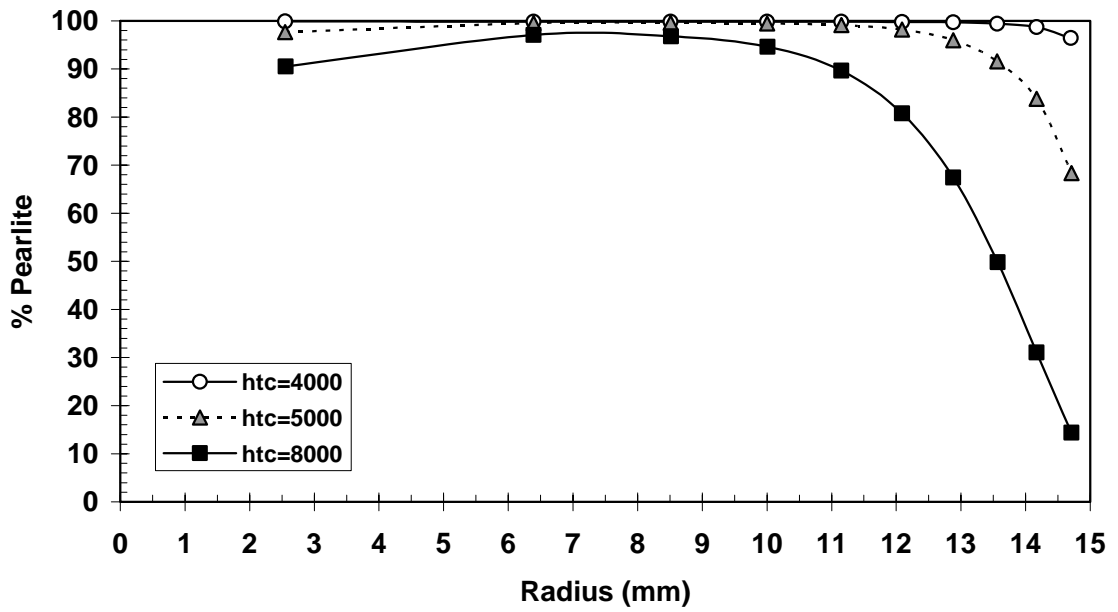
5.4. Monitoring The Evolution of Residual Stresses

5.4.1. Effect of Convective Heat Transfer Coefficient on Phase Transformations

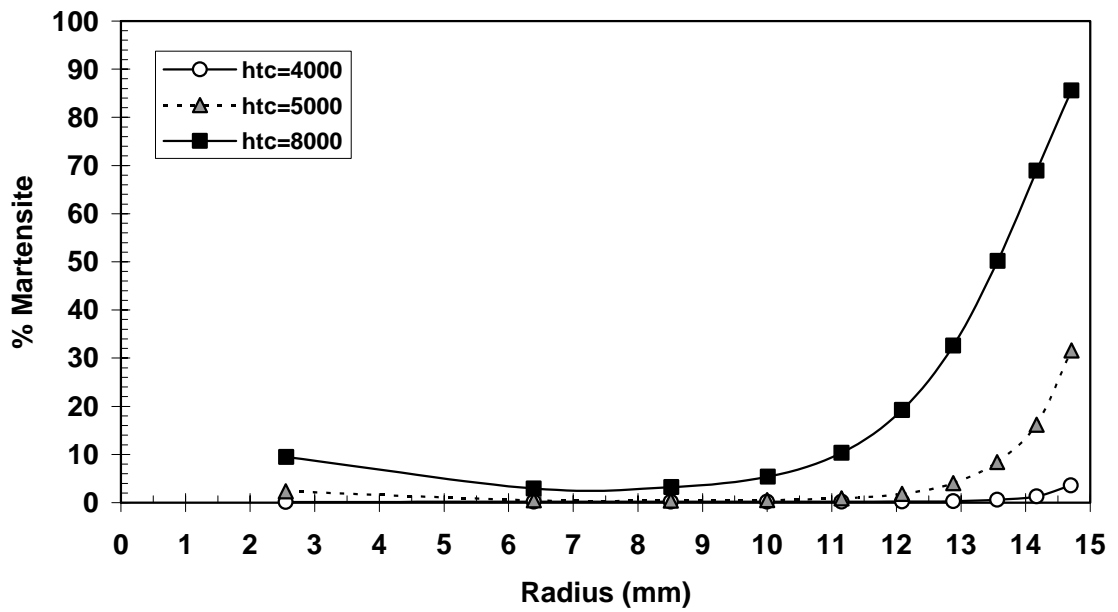
The severity of quenching, i.e., the convective heat transfer coefficient (h_c), is a very important parameter affecting the residual stresses and phase transformations. Value of heat transfer coefficient is very sensitive to the condition of quench bath and specimen geometry. C60 steel with 30 mm diameter quenched from 830°C to 60°C was used for this investigation. Three runs were carried out, in which the convective heat transfer coefficient was kept constant and taken as 4000, 5000 and 8000 J/m²s°C.

Figure 5.12 shows the amount of pearlite and martensite at the end of the process for different convective heat transfer coefficients. When the convective heat transfer coefficient increases, specimen will cool faster, and possibility of martensite transformation will increase. As expected, if the heat transfer coefficient is taken 4000 J/m²s°C very few martensite forms in the specimen. However, for 8000 J/m²s°C the surface consists of 85% martensite, and the core mostly pearlite. For 8000 J/m²s°C austenite at the surface transforms relatively earlier since it forms martensite. Martensite and pearlite has a higher conductivity than austenite, and this result in a faster cooling at the center besides the effect of higher temperature gradient. This faster cooling of the center causes the center to have some more amount of martensite than at around 6 mm from the center.

The convective heat transfer coefficient is the most critical physical property in quench analysis. It highly affects the phase transformations and residual stresses in the specimen during quenching. It must be studied closely to detect the correct values of convective heat transfer coefficient to obtain better results.



(a)



(b)

Figure 5.12. Phase distributions according to the convective heat transfer coefficient
(830°C to 60°C, C60 steel)
a) %Pearlite, b) %Martensite

5.4.2. Effect of Phase Transformation on Residual Stress Distribution

In order to differentiate the influences of thermal and phase transformation stresses on the formation of final residual stress state, two runs were performed considering the quenching of C60 steel bar of 30 mm diameter from 830°C to 60°C:

- a) The exact case, i.e. there occurs phase transformations and most of the specimen transforms into pearlite,
- b) Hypothetical case, assuming there is no phase transformation and representing the influence of thermal stresses only.

The input data used in exact case are given in Table 5.3. For the hypothetical case data for pearlite was used. The convective heat transfer coefficient was taken constant as 4000J/m²s°C.

Figures 5.13 to 5.16 show the distributions of the radial, axial, tangential components of residual stress and effective stress along the radius for two different cases. It is seen that these two cases doesn't have too much difference, because in the exact case most of the specimen transforms into pearlite, and hypothetical case is assumed to be always pearlitic. Since phase transformation occurs in early stages of quenching and the final phases are almost the same, the effect of phase transformation is minimum.

Austenite has a face centered cubic structure which is denser than all the other phases. During the transformation of austenite to other phases an expansion occurs. This expansion is largest for the austenite to martensite transformation since martensite has a much less density than all other phases. It is seen in Figure 5.13 that radial residual stress at the center is higher for the exact case than the hypothetical case, and lower at the surface. This is because of the small amount of martensite formed at the surface of the specimen.

Figure 5.14 shows the axial residual stress distribution in the specimens. There is just a little difference in the axial stress distribution of two cases. For the hypothetical case axial stress is relatively less tensile at the center and a less compressive at the

surface. At around 13 mm from the center value axial residual stress of the hypothetical case slightly exceeds the exact case. Beginning from that point to the surface martensite is seen considerably. This shows how phase transformations affect the stress distributions.

Table 5.3. Input data for different phases of C60 steel

Austenite

T(°C)	E(GPa)	ν	σ_y (MPa)	H(GPa)	$\alpha(\mu/^\circ\text{C})$	λ (J/ms °C)	C_p (MJ/m ³ °C)
0	200	0.29	220	1000	21.7	15.0	4.15
300	175	0.31	130	16000	21.7	18.0	4.40
600	150	0.33	35	10000	21.7	21.7	4.67
900	124	0.35	35	500	21.7	25.1	4.90

Pearlite, Bainite, Ferrite

T(°C)	E(GPa)	ν	σ_y (MPa)	H(GPa)	$\alpha(\mu/^\circ\text{C})$	λ (J/ms °C)	C_p (MJ/m ³ °C)
0	210	0.28	450	1000	15.3	49.0	3.78
300	193	0.30	230	16000	15.3	41.7	4.46
600	165	0.31	140	10000	15.3	34.3	5.09
900	120	0.33	30	500	15.3	27.0	5.74

Martensite

T(°C)	E(GPa)	ν	σ_y (MPa)	H(GPa)	$\alpha(\mu/^\circ\text{C})$	λ (J/ms °C)	C_p (MJ/m ³ °C)
0	200	0.28	1750	1000	13	43.1	3.76
300	185	0.30	1550	16000	13	36.7	4.45
600	168	0.31	1350	10000	13	30.1	5.07

Tangential residual stresses occur in the specimens during quenching are shown in Figure 5.15. The difference between the tangential stresses of two cases is slightly higher than the axial stresses, but still they are similar. Just as in axial stresses exact case has more tensile tangential stress at the center and more compressive at the surface, caused by the volume expansion during phase transformation.

Figure 5.16 shows the effective residual stress distributions for the exact case and the hypothetical case. Hypothetical case has higher effective stress than the exact case at the center, and lower at the surface. Effective stress distribution for both cases show a similar behavior, but the affect of phase transformation can still be observed clearly. For the case of no phase transformations effective stress is same at the points near the surface, but for the exact case there is an increase in effective stress when closing to the surface. This is caused by the small amount of martensite formed at the surface of the specimen. Other points are also affected from the martensite formation at the surface, but main reason of the difference at the other points is the austenite to pearlite phase transformation strains and the austenite present at the initial stages of the process for the exact case, where for the hypothetical case there is no phase transformations and the specimen is assumed to be 100% pearlitic during all the process, stresses are generated just because of the shrinkage due to cooling.

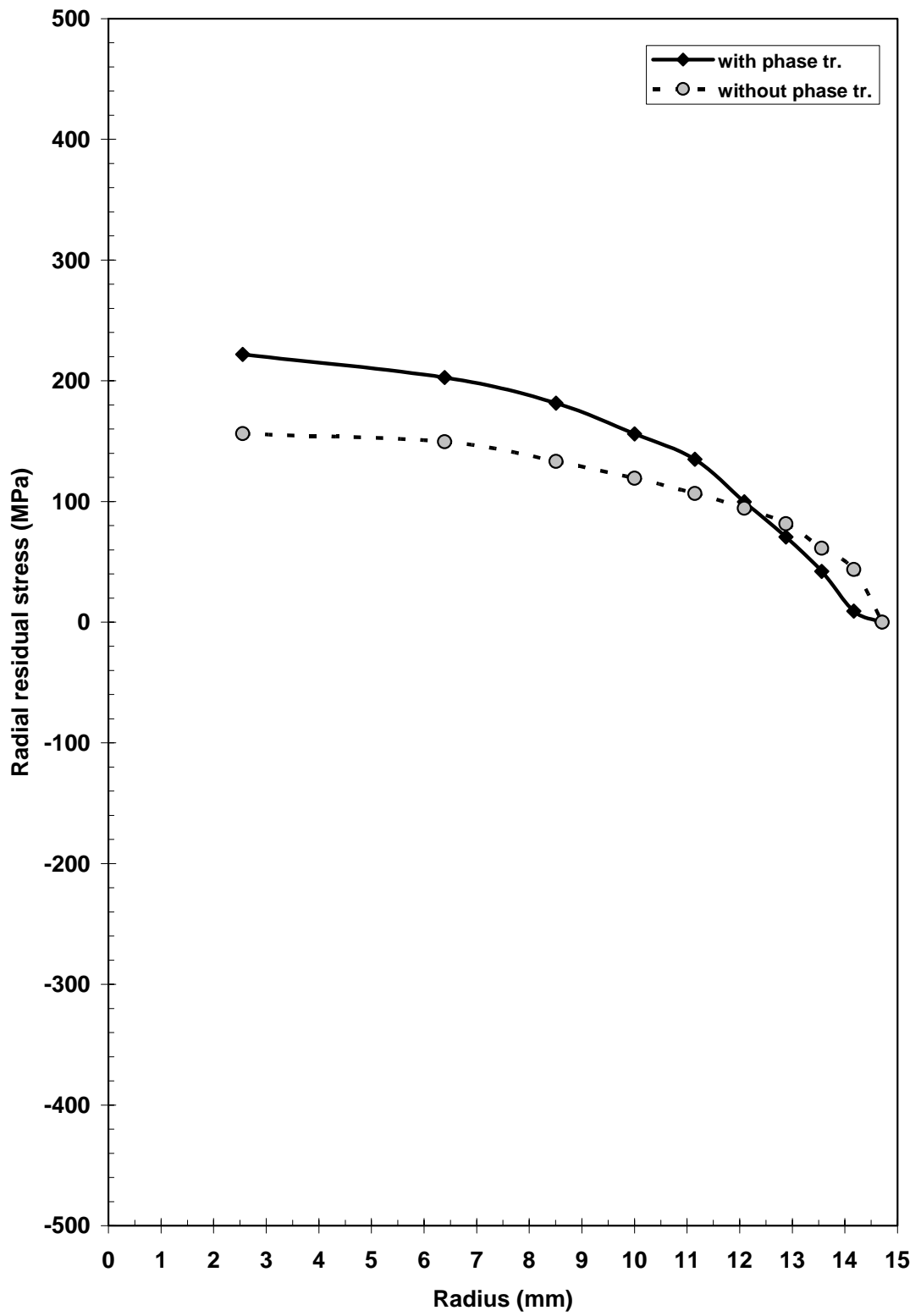


Figure 5.13. Effect of phase transformation on the radial residual stress (830°C to 60°C, C60)

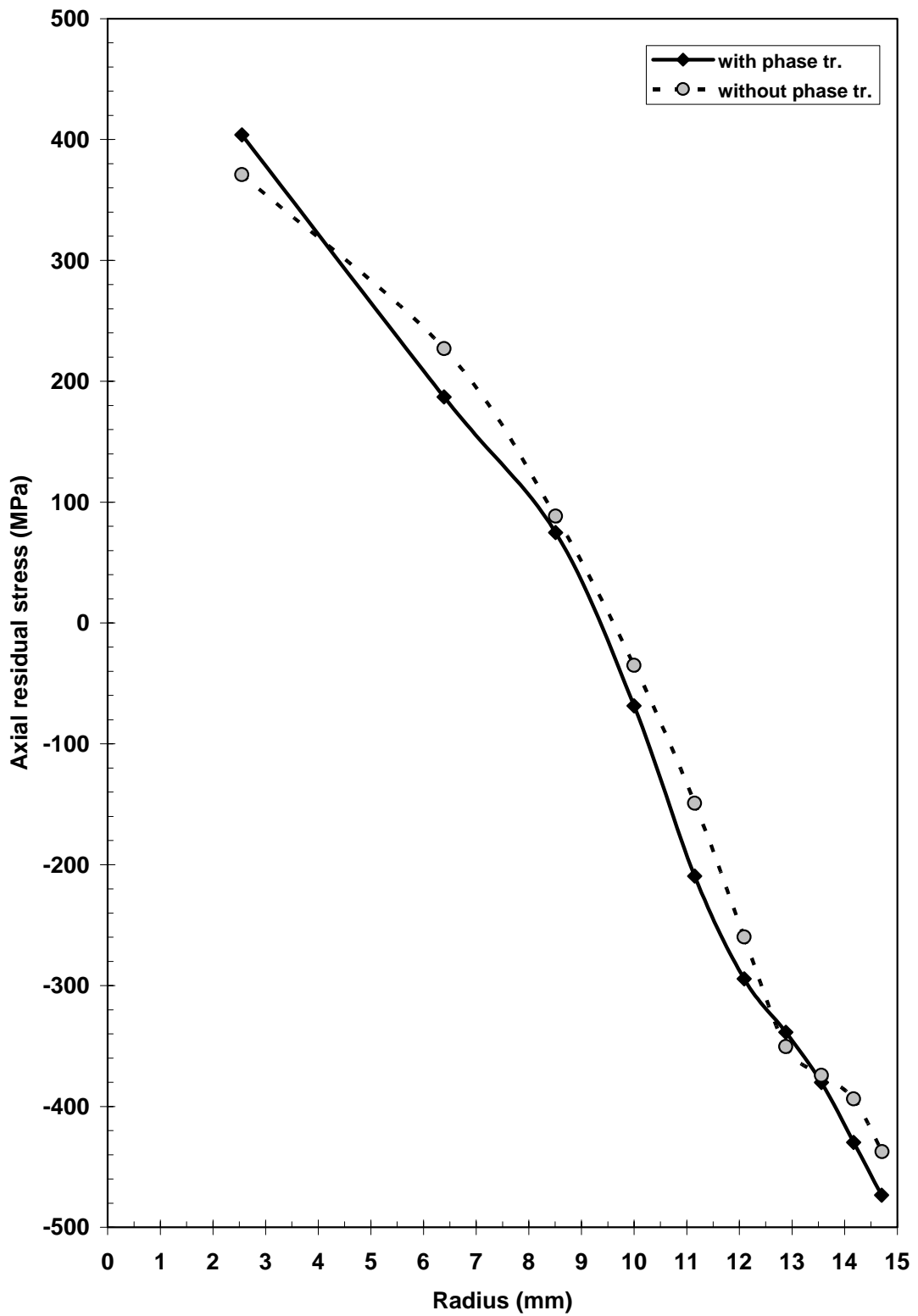


Figure 5.14. Effect of phase transformation on the axial residual stress (830°C to 60°C, C60)

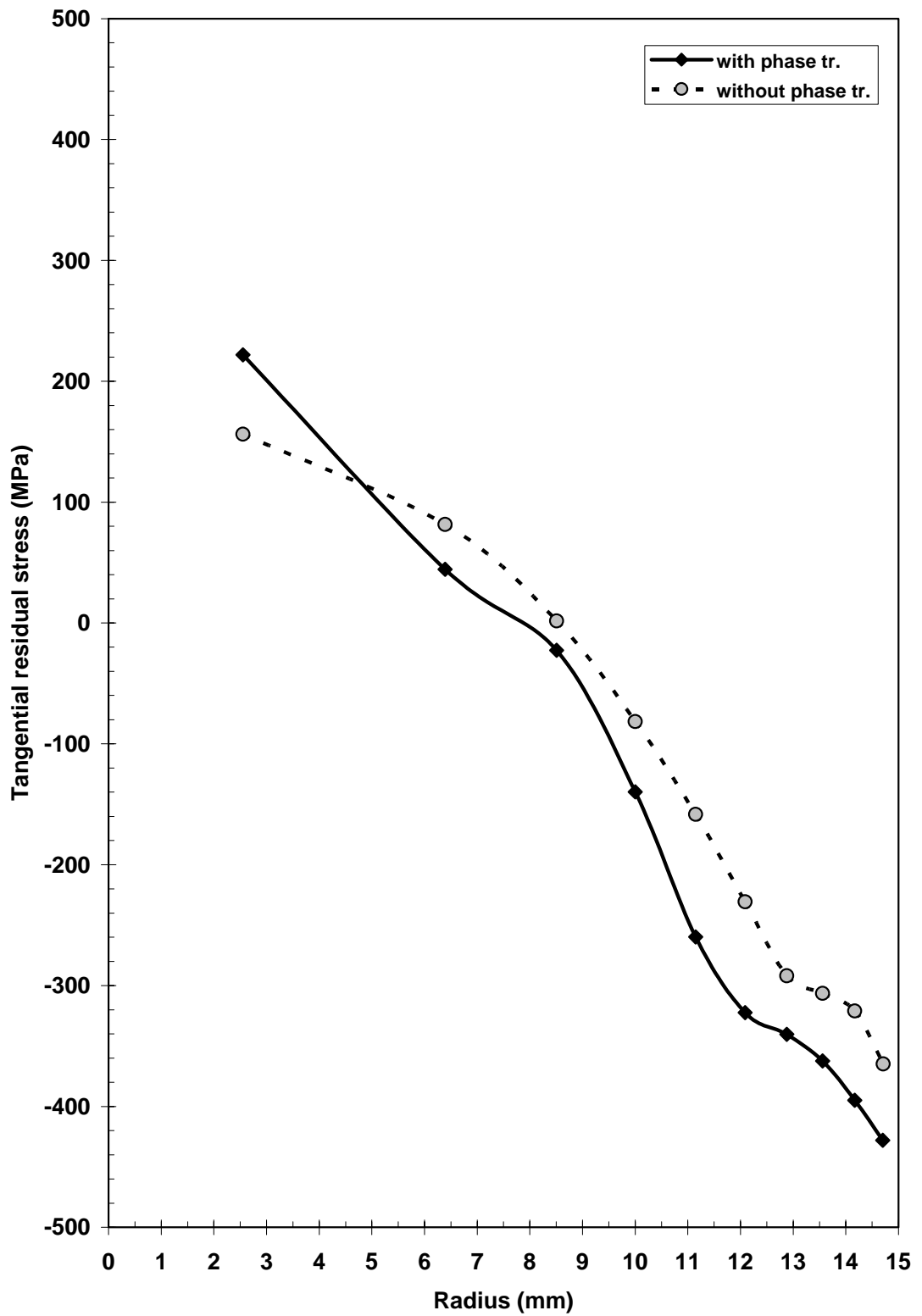


Figure 5.15. Effect of phase transformation on the tangential residual stress (830°C to 60°C, C60)

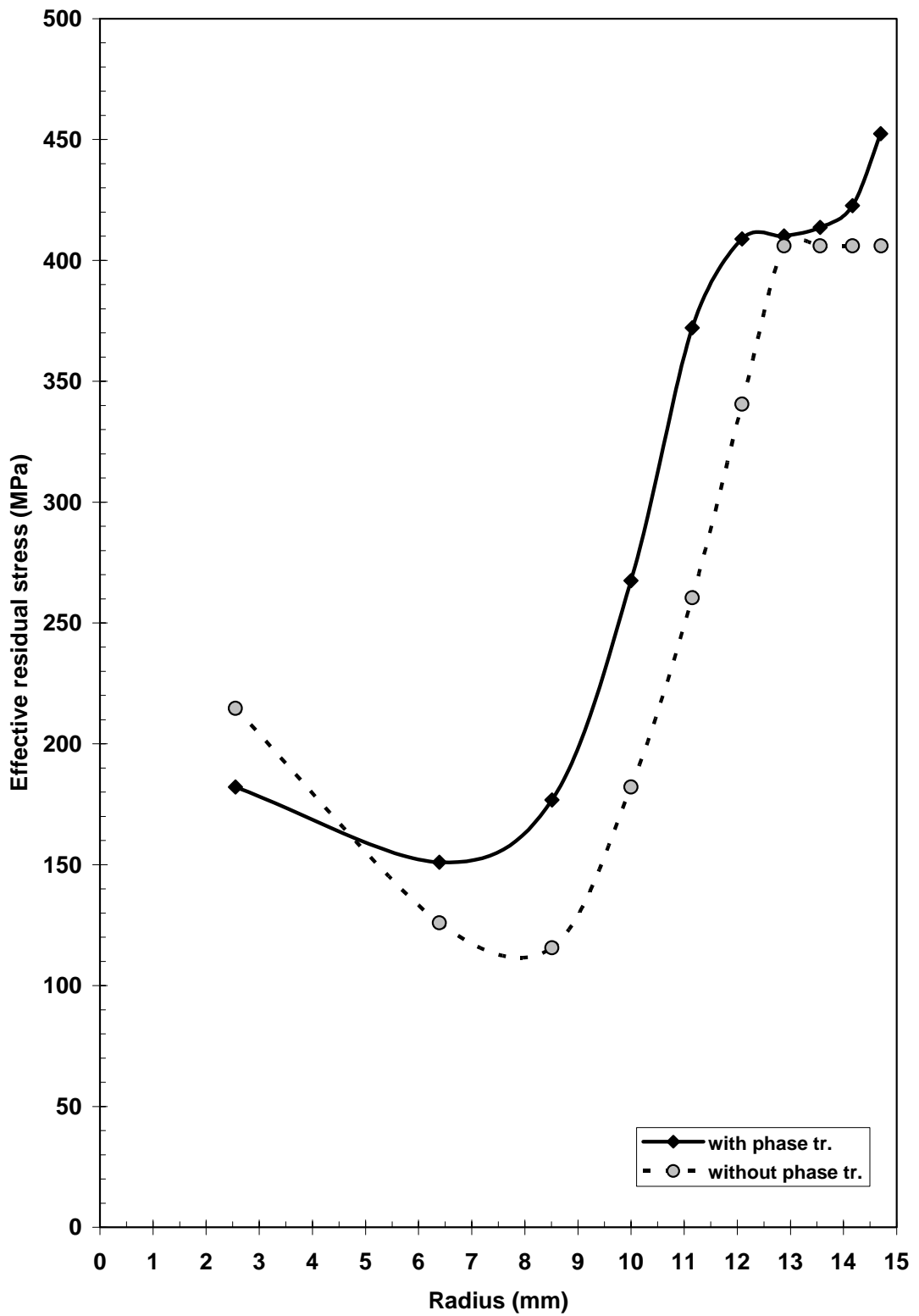


Figure 5.16. Effect of phase transformation on the effective residual stress (830°C to 60°C, C60)

5.4.3. Investigating the Evolution of Internal Stresses and Phase Transformations

The change of internal stresses during quenching of C60 steel bar with 30mm diameter was also investigated. Figure 5.17 shows the radial internal stress change during the quenching process. Initially radial stresses are compressive at the core, and tensile near the surface. After some time due to the effects of phase transformations and local plastic deformations, they become tensile at the core. The time for this transition is around 2 seconds.

Axial internal stresses are monitored in Figure 5.18. Axial stresses are tensile at the surface and compressive at the core at the initial stages of the quenching. Then, axial internal stress reverses its behavior and tends to become compressive at the surface and tensile at the core. Between 1.5 and 3 seconds some fluctuations in the axial stresses occurred between 9 and 14 mm along the radius. The reason is the transformation of austenite to pearlite. After 3 seconds these fluctuations spread on whole specimen, and the distribution of the axial stresses stabilizes after 10 seconds. At the end of the process a uniform axial residual stress distribution that is tensile at the core and compressive at the surface is achieved.

Figure 5.19 shows the change in the tangential internal stresses. Tangential internal stress shows the same behavior with the axial one. It tends to be tensile at the surface and compressive at the core at the beginning of the quench process. After 1.5 seconds the tendency reverses and the tangential stresses become compressive at the surface and tensile at the core at the end. Same fluctuations in the axial stresses are also observed in tangential stresses.

In Figure 5.20 effective internal stress change is graphically illustrated. Generally effective stresses show an increasing behavior during quench. Only between 5-8 seconds there is a decrease in effective stresses at the core because of phase transformations. Effect of fluctuations in axial and tangential internal stresses are also seen in effective internal stresses slightly. At the initial stages of quenching

effective internal stresses are almost the same at the surface and at the core. However, at the end of the process, because of the phase transformations during the process they become higher at the surface than the core.

The phase transformations were also monitored for the same run. Figure 5.21(a) shows the amount of pearlite in the specimen along the radius with respect to quench time. Pearlite formation starts at around 1 second and finishes within 8 seconds. 96% of austenite transforms into pearlite at the surface, and at the core almost all of austenite transforms into pearlite. The amount of martensite in the specimen with respect to time is shown in Figure 5.21(b). Martensite starts to form in the specimen around 10 seconds and finishes at 27.5 seconds. There forms around 4% martensite at the surface and almost no martensite transformation occurs at the core. Pearlite formation starts and ends before the martensite. The specimen is mostly pearlitic, just small amount of martensite forms at the surface.

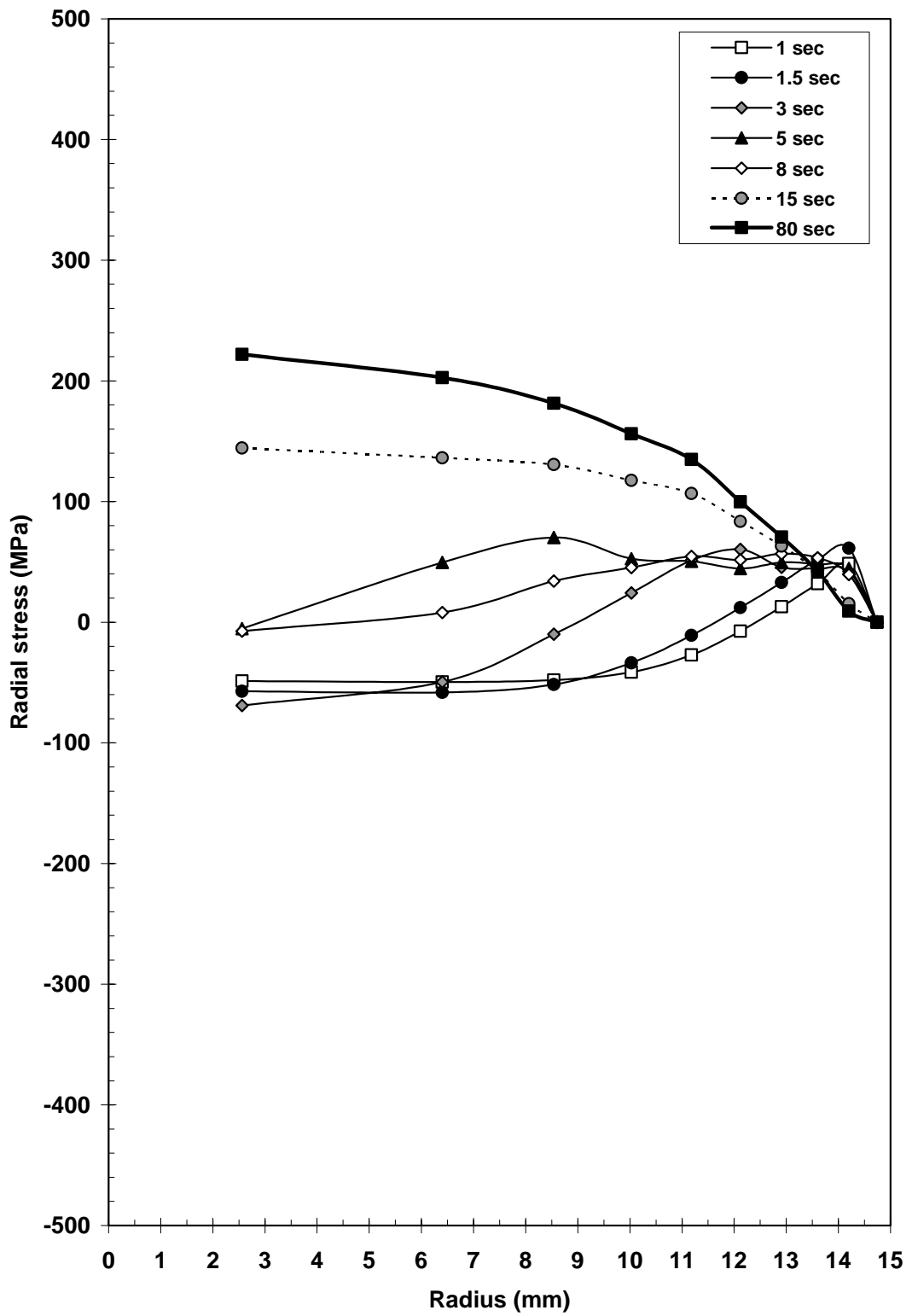


Figure 5.17. Variation of the radial component of internal stress along the radius during quenching (830°C to 60°C, C60 steel)

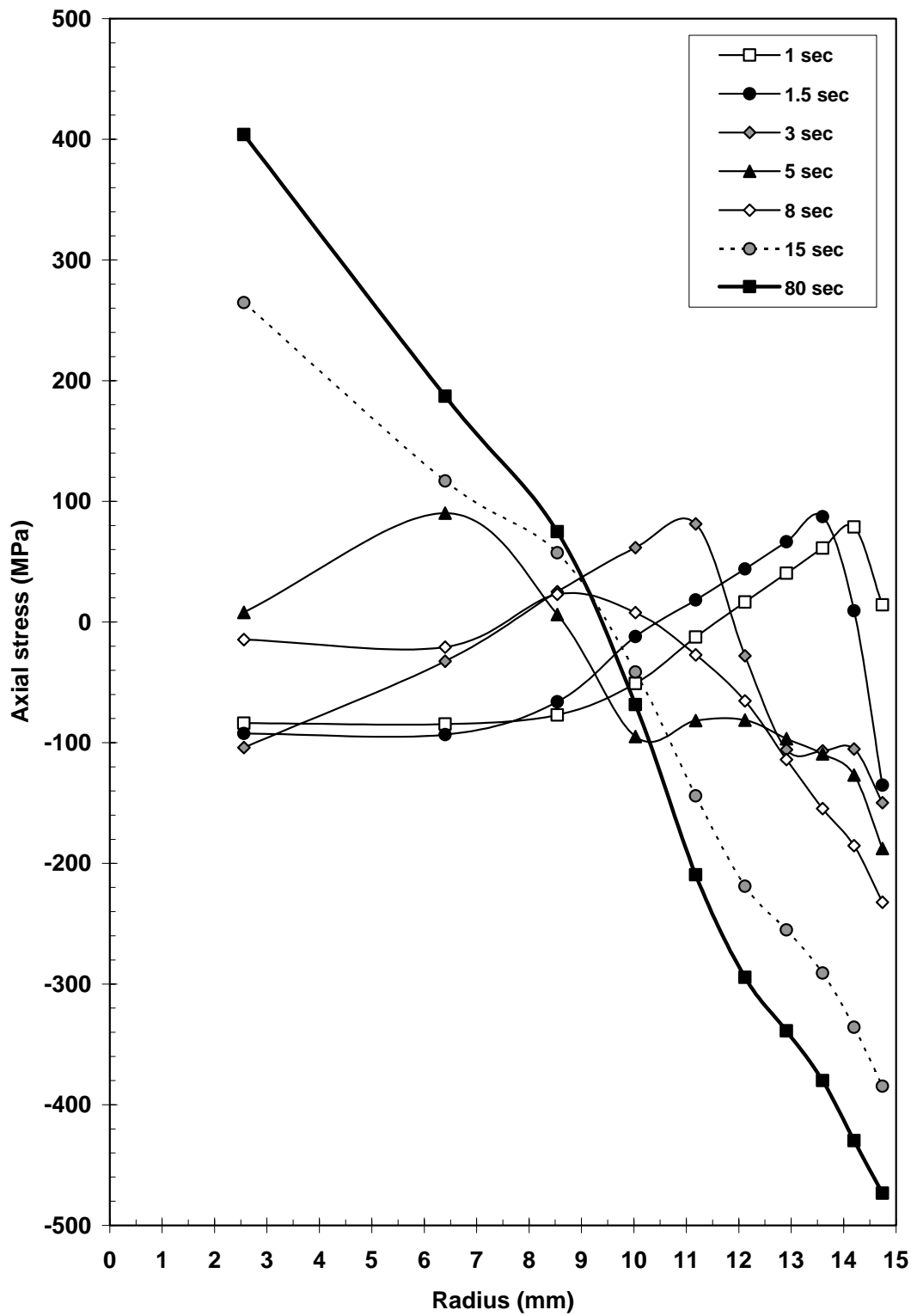


Figure 5.18. Variation of the axial component of internal stress along the radius during quenching (830°C to 60°C, C60 steel)

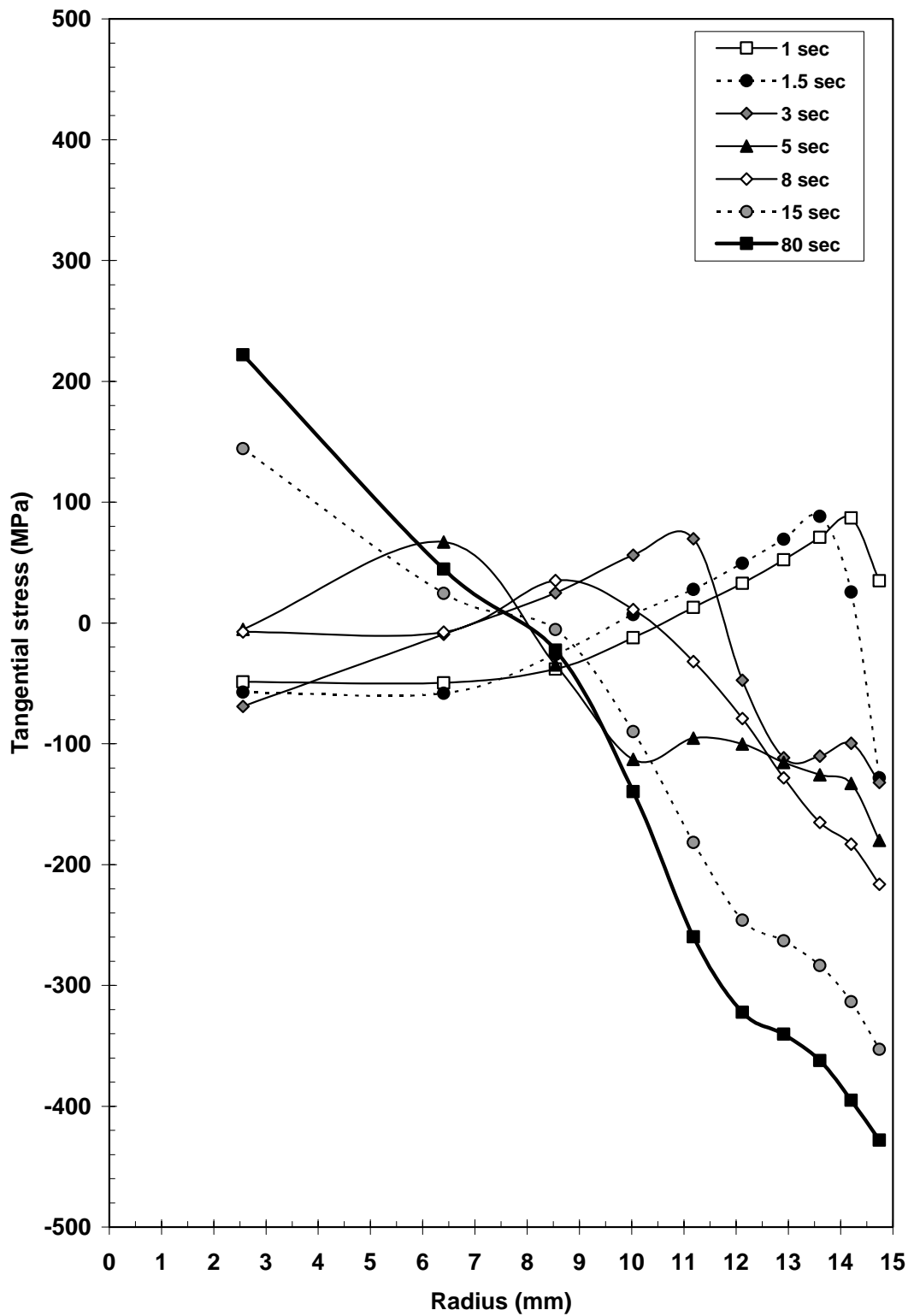


Figure 5.19. Variation of the tangential component of internal stress along the radius during quenching (830°C to 60°C, C60 steel)

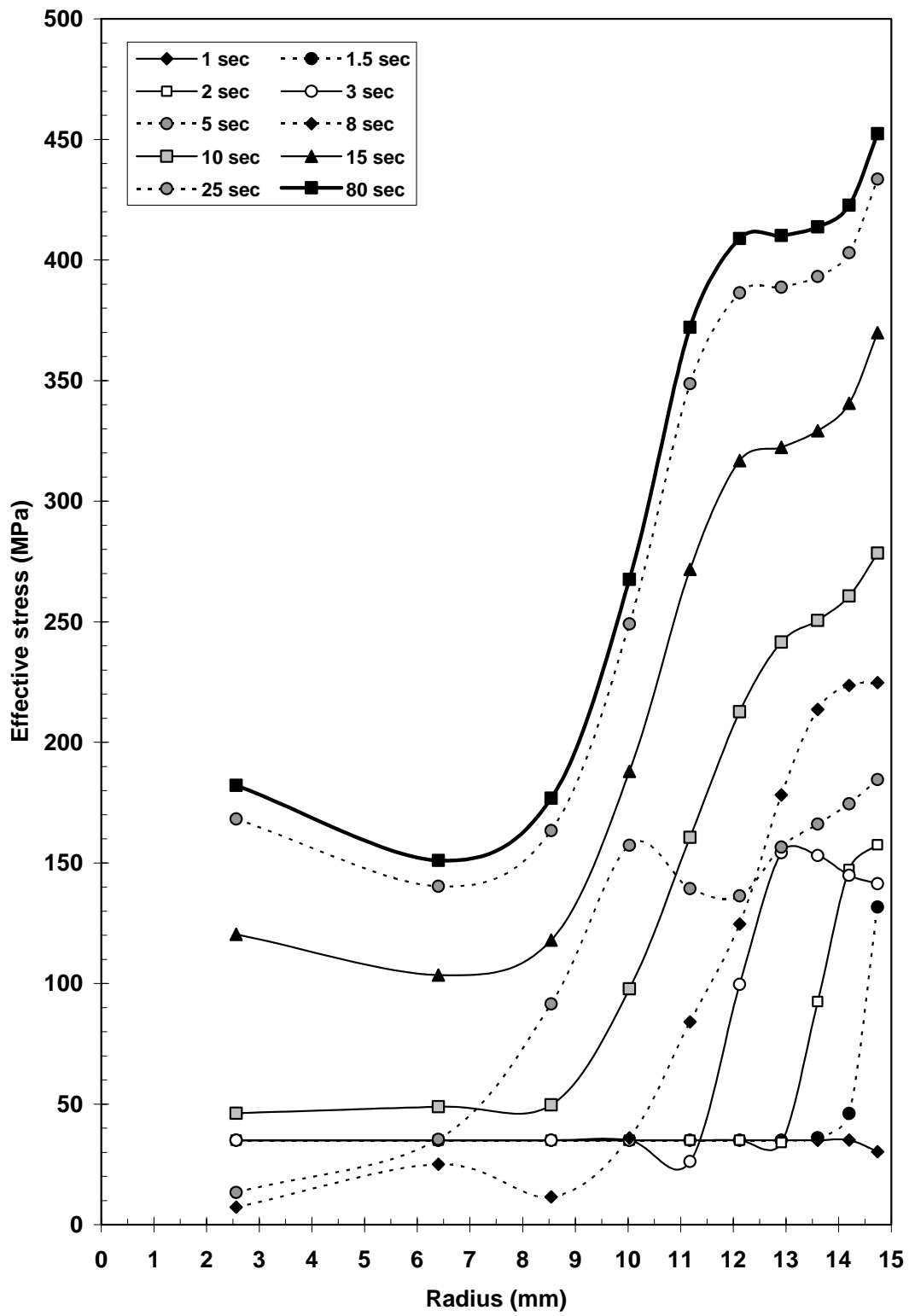
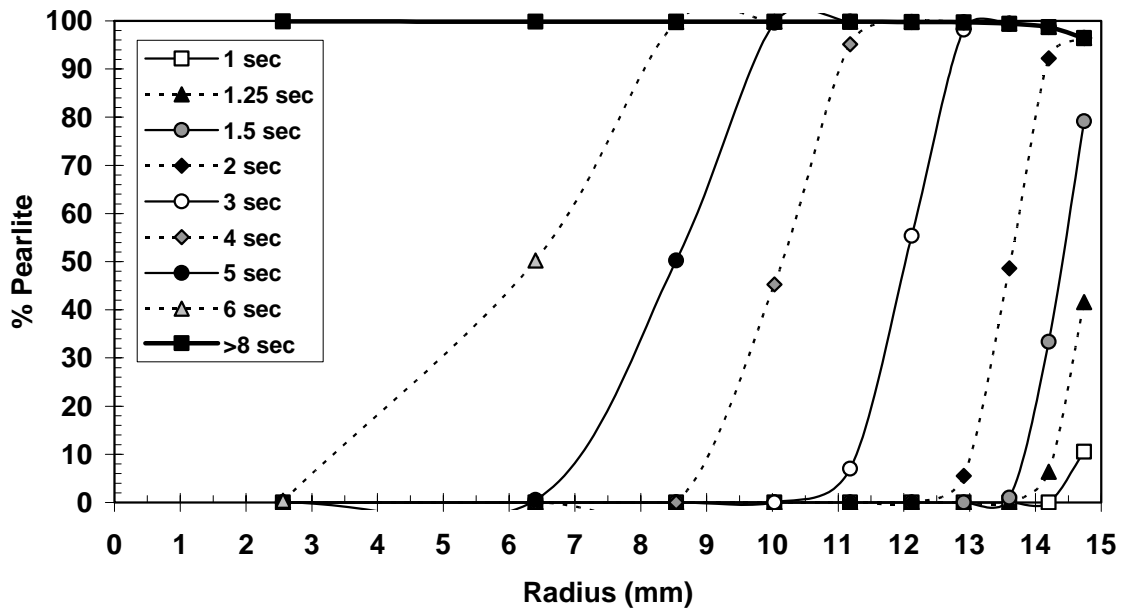
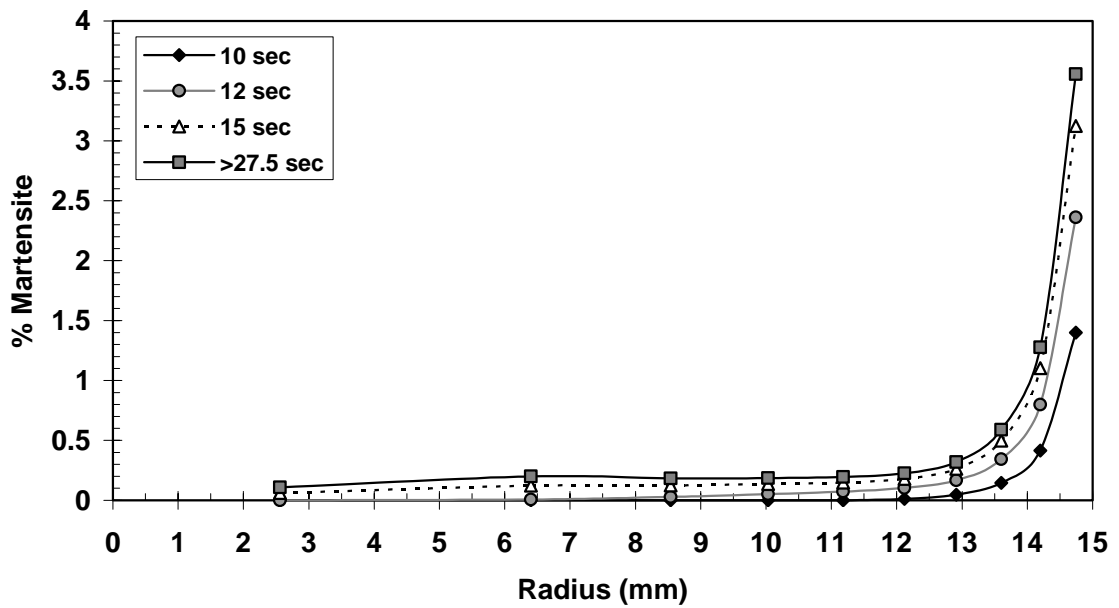


Figure 5.20. Variation of the effective internal stress along the radius during quenching (830°C to 60°C, C60 steel)



(a)



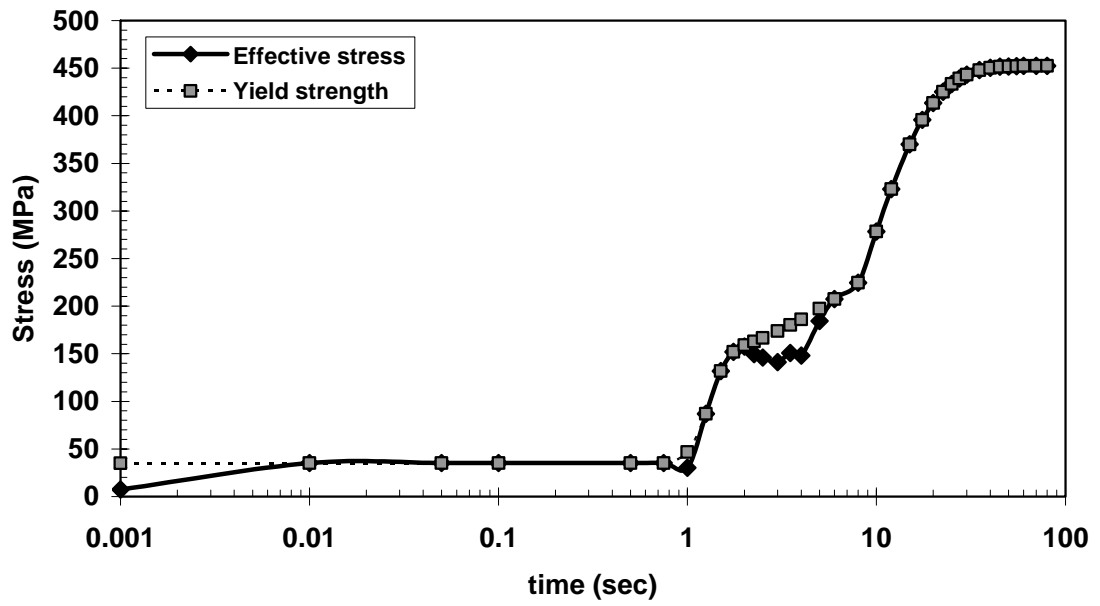
(b)

Figure 5.21. Variation of the phase content along the radius during quenching (830°C to 60°C, C60 steel)
a) Pearlite, b) Martensite

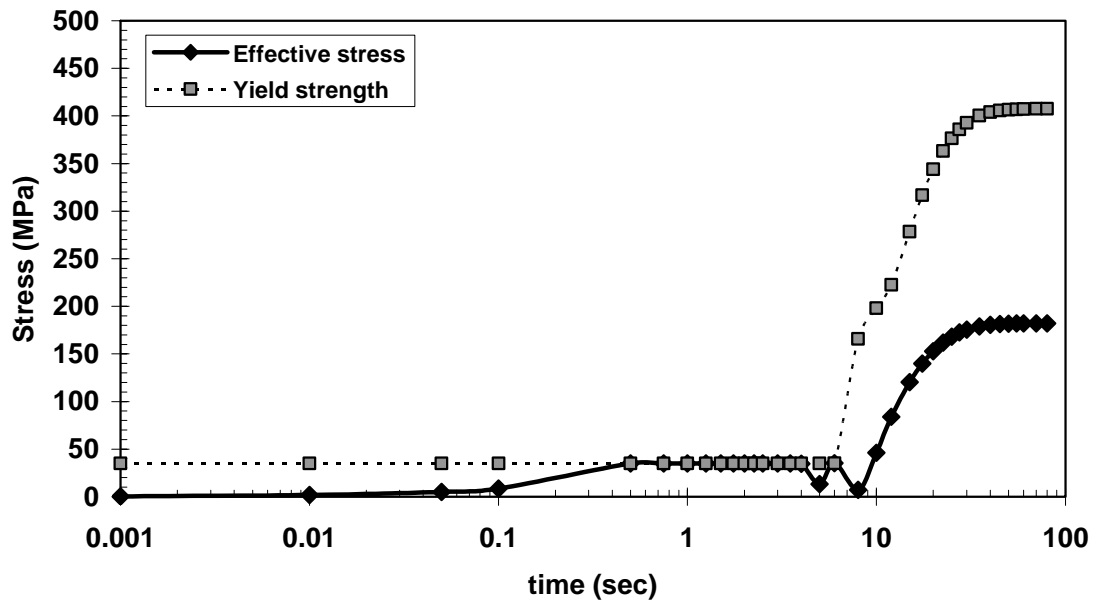
5.4.4. Monitoring the Local Plastic Deformation During Quenching

Local plastic deformations occurred during the quench process were also monitored. Figure 5.22(a) shows the comparison of effective stress and yield strength during quenching at the surface. At the surface effective stress reached the yield strength 0.01 seconds after the quenching process starts, and plastic deformation starts. At 2 seconds there is a drop in the effective stress and plastic deformation stops, but at 6th second it again reaches yield strength and from that point on it never gets lower than the yield strength, so plastic deformation occurs until the end of the process. At the center as seen in Figure 5.22(b), effective stress reaches the yield strength after 0.5 seconds, and a drop occurs at 5th second. At 6 seconds, again some plastic deformation is seen, but after that it again shows a drop and then increases to 180 MPa while yield strength increases more than the effective stress so no plastic deformation occurs from that point on at the center.

For the no phase transformation case effective stress and yield strength at the surface are shown in Figure 5.23(a). It is seen that effective stress reaches the yield strength at 0.05 seconds. Because of the plastic deformations a drop in the effective stress is seen around 2.5 seconds. At 10th second effective stress again catches the yield strength and plastic deformation continues until the end of the process. In Figure 5.23(b) effective stress and yield strength at the center are shown for the no phase transformation case. For this case effective stress at the center reaches the yield strength at around 1 second. After 5 seconds a drop in the effective stress is observed while yield strength is still increasing. After 8 seconds both effective stress and yield strength increases but effective stress never reaches the yield strength so that no plastic deformation occurs at the center after 5th second.

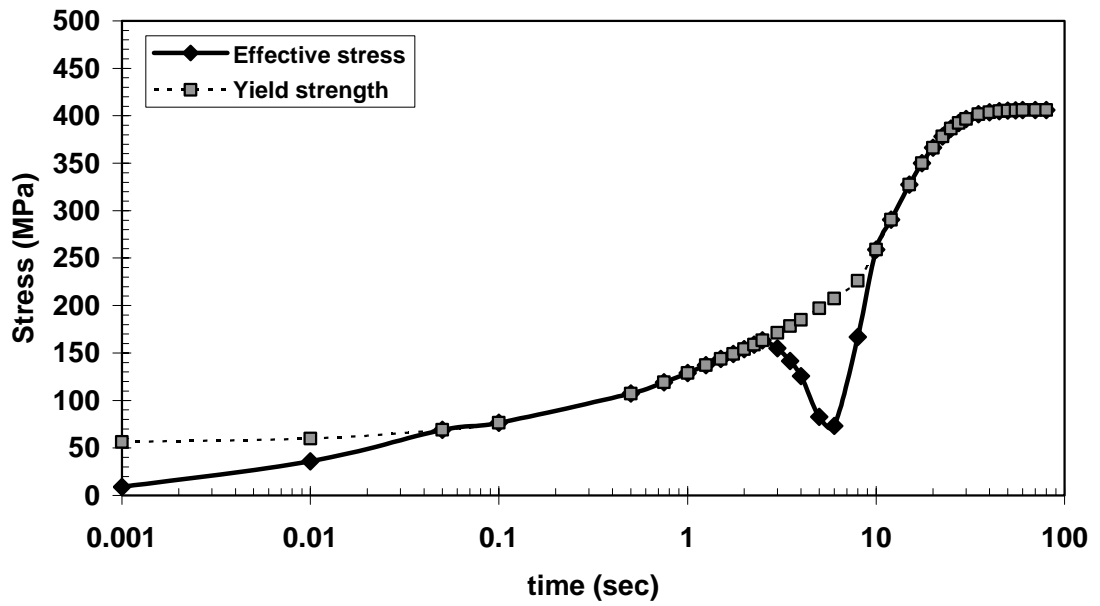


(a)

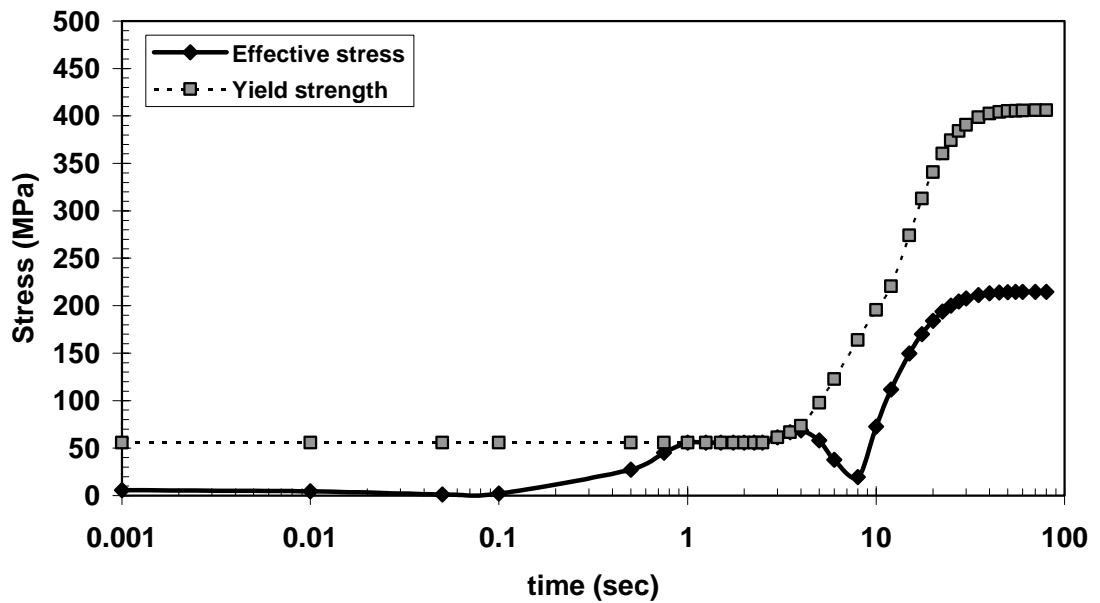


(b)

Figure 5.22. Change in effective stress and yield strength during quenching with phase transformation (830°C to 60°C, C60 steel, 30mm diameter)
a) Surface, b) Center



(a)



(b)

Figure 5.23. Change in effective stress and yield strength during quenching without phase transformation (830°C to 60°C, C60 steel, 30mm diameter)

a) Surface, b) Center

5.5. Effect of Meshing on the Results

Effect of meshing on the final thermal stresses was investigated on C60 steel with 40mm diameter, rapidly cooled from 680°C to 20°C water. Calculations were done with different number of elements, 10, 15, and 20. Input data used in the calculations is given in Table 5.4 and the results are shown in Figure 5.22.

Table 5.4. Input data for C60 steel

T(°C)	E(GPa)	ν	σ_y (MPa)	H(GPa)	α (μ /°C)	λ (J/ms °C)	C_p (MJ/m ³ °C)
0	210	0.28	360	1000	14	49.0	3.78
300	193	0.30	230	16000	14	41.7	4.46
600	165	0.31	140	10000	14	34.3	5.09
900	120	0.33	30	500	14	27.0	5.74

It is seen that changing the number of elements slightly affect the residual stresses. As number of elements increases tangential and axial stresses becomes less tensile at the center and less compressive at the surface.

Radial thermal stress, it reaches higher values at the center as number of elements decreases, they become the same at 16mm from the center and then close to the surface it decreases with decreasing number of elements. Finally they all are zero at the surface.

As the number of elements increases the results should be more accurate, since the calculation are made at more points. However, since the results are not very much affected from the change in the number of elements, less number of elements can be used in calculations to save time.

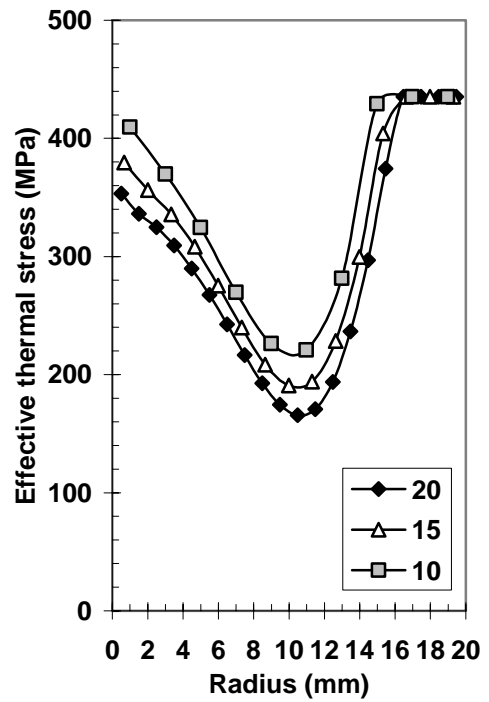
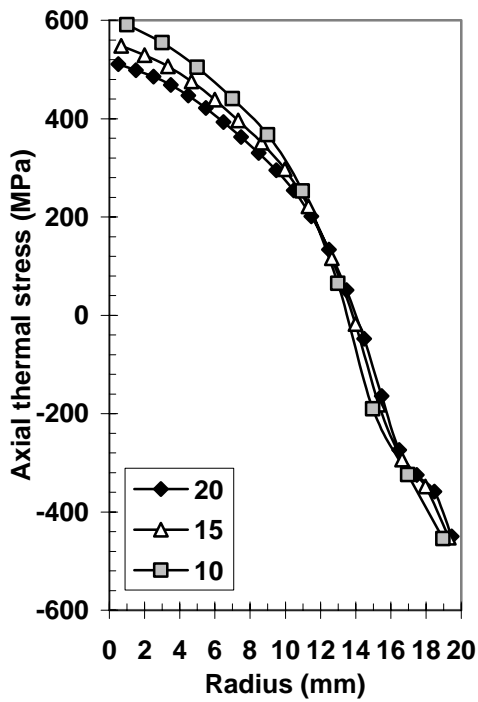
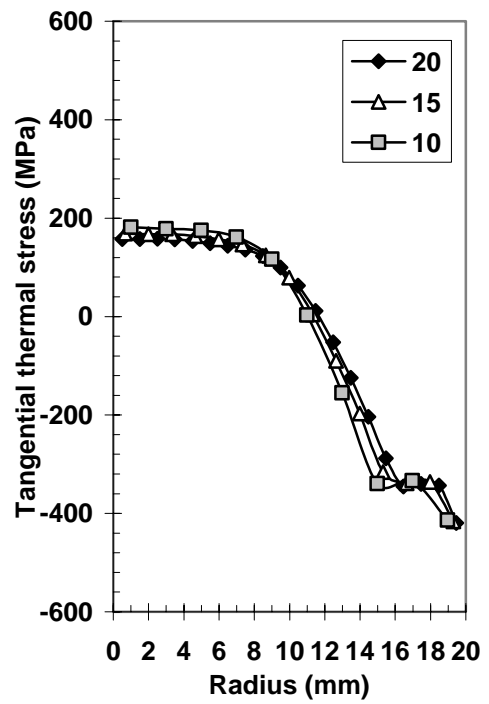
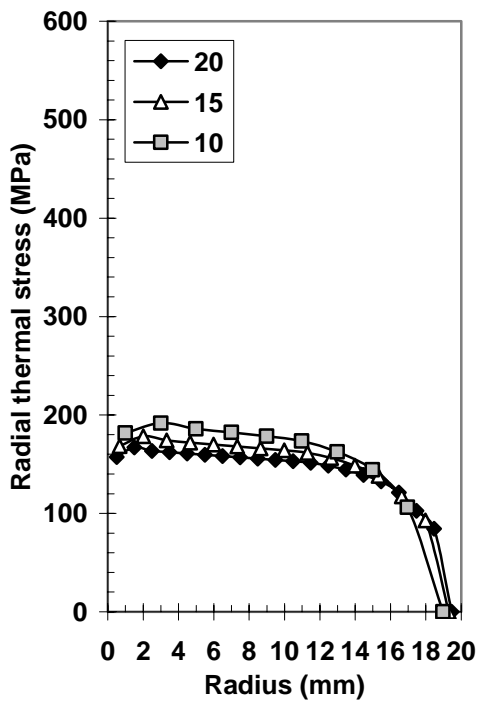


Figure 5.24. Effect of meshing on the results
(680°C to 20°C, C60)

CHAPTER 6

CONCLUSION

In this thesis, the computer program QUEANA predicting the temperature distribution, the progress of phase transformations, the evolution of internal stresses, and the residual stress state in the quenched axisymmetric parts has been improved. The model has been further verified by comparing the results with those of the commercial code MARC.

In the specimen being quenched, local plastic deformations may occur due to internal stresses originated from both the temperature gradient and volume changes during phase transformations. Phase transformations and stress distributions are highly affected by the type of the steel used and cooling conditions.

When an engineering component has cracked or heavily deformed to the outside machining tolerances during quench, it will be scrapped. The quenching of construction steels is the most critical ones, where the quench cracking risks and great deformation is often encountered. For an acceptable solution it is necessary to choose the grade of steel, and the heat treatment which result in a minimum amount of waste or machining operations to reduce the cost of manufacturing. The skill of a technician is often used to avoid the major errors in designing the part. However, this approach remains limited since there are large numbers of parameters. Although the nature of these parameters is known, little is known about the way they interact. Being able to calculate the effect of quench parameters by computer simulation would make it possible to envisage better control of residual stress distribution and avoid quench cracking.

Using the computer program, developed in the present study, it is possible

- i- to determine the temperature distribution,
- ii- to follow the evolution of the internal stresses and strains, to observe when and at which point they appear, thus to trace the quenching history, and consequently to learn about their origin,
- iii- to detect critical moments during quenching, and to have information about the risks of quench-cracking and the level of distortion,
- iv- to define rules to be applied in the choice of heat-treatment and steel grades,
- v- to estimate the residual stresses remain in the parts after quenching. These stresses are of great importance in heat treated parts regarding to the further machining, the fatigue resistance and resistance to stress corrosion cracking.

It has also been concluded that convective heat transfer coefficient is the most important parameter in quench analysis. By changing this coefficient, phase transformations and residual stresses show remarkable variations. It is dependent upon the quench medium and the specimen geometry. Exact values of this coefficient for the system considered must be used to get realistic results during quench analysis.

Mesh size is another important parameter in calculations. If the elements are taken very large the results may not be trustful. For these particular runs calculations with different number of elements on the same specimen showed similar behavior but it would be more convenient to use larger number of elements to get closer results to the actual case, although it costs a longer run time. Utilization of a finer mesh particularly in the regions near the surface is very critical when there will be martensitic transformation.

REFERENCES

- [1] H.Scott, Scientific Papers of the Bureau of Standarts, 20, 399 (1925)
- [2] Ed.Maurer, Stahl und Eisen, 47, 1323 (1927)
- [3] Ed.Maurer, Stahl und Eisen, 48, 225 (1928)
- [4] H.Treppschuh, Arch. Eishüttenwes.,13,429 (1940)
- [5] J.H.Weiner, J.V. Huddleston, ASME J.Appl.Mech., 26, 31 (1959)
- [6] H.G. Landau, Jr.E.E.Zwicky, ASME Series E, 26, 481 (1960)
- [7] R.Nickell, E. Wilson, Nucl. Engng. Des., 4,,276 (1966)
- [8] M.E. Gurtin, Quart. Appl. Math., 22, 2552 (1964)
- [9] O.C. Zienkiewicz, C.J.Parikh, Int.J. Num.Meth. in Engrn ., 2, 61, (1970)
- [10] A.Aguirre-Ramirez, J.T.Oden, ASME Paper, 69-WA-IIT-34 (1969)
- [11] I.Farhoomand, E.A.Wilson.Report SESM 71-6, Structural EngrnLab. (1971)
- [12] P.D.Richardson, Y.M. Shum, ASME Paper, 69-WA-Ht-36 (1969)
- [13] R.Yalamanchili,S.Chu, U.S.Army Weapons Comm.Tech.Rep., RE70-165 (1970)

- [14] T.Inoue, K.Tanaka, M.Aoki, Trans. Japan Soc. Mech.Eng., 38, 2490 (1972)
- [15] Y.Toshioka, M.Fukagawa, Y.Saiga, Trans. ISOJ, 12, 6 (1972)
- [16] Y.Ueda, Yakamakawa, Proc. of Int.Conf.on Mech. Behaviorof Materials SMA-Japan, 3, 10 (1972)
- [17] K.Sakai, Tetsu-thogane (J.Iron Steel Inst. Jpn.), 60, 1591, (1974)
- [18] T.Inoue, K.Tanaka, Memories Fac. Engrn., Kyoto Univ., 35, 1 (1973)
- [19] T.Inoue, K.Tanaka, J.Soc.Mat.Sci.Jap., 22,218 (1973)
- [20] T.Inoue, K.Tanaka, Int.J.Mech.Sci., 17 361 (1975)
- [21] T.Inoue, K.Haraguchi, S.Kimura, J.Soc.Mat.Sci., 25, 521 (1976)
- [22]B.Raniecki, T.Inoue, J.Soc.Mat.Sci.Japan, 26, 935 (1977)
- [23] T.Inoue, B.Raniecki, J. Mech. Phys. Solids, 2, 187 (1978)
- [24] J.A. Burnett, Evaluation of Elastic-Plastic Stresses in Quenched Carburized Cylinders by Finite Element Method, Ph.D. Thesis, Univ. Akron (1977)
- [25] J.A.Burnett, J. of Thermal Stresses, 1, 211 (1978)
- [26] H.Ishikawa, J. of Thermal Stresses, 1, 211 (1978)
- [27] H.J.Yu, Berechnung von Abkühlungs-, Umwandlungs-, Schweiß- sowie Verformungseigenstressen mit Hilfe der Methode der Finiten Elemente, Ph.D.Thesis, Univ. Of Karlsrube (1977)

- [28] I.Tzitzelkov, H.P.Houngardy, A Rose, Arch. Eisenhüttenwes., 45, 525 (1974)
- [29] H.J.Yu, U.Wolfstieg, E.Macherauch, Arch. Eisenhüttenwes., 49, 549 (1978)
- [30] H.J.Yu, U.Wolfstieg, E.Macherauch, Arch. Eisenhüttenwes., 49, 499 (1978)
- [31] H.J.Yu, U.Wolfstieg, E.Macherauch, Arch. Eisenhüttenwes., 50, 81 (1979)
- [32] H.J.Yu, U.Wolfstieg, E.Macherauch, Arch. Eisenhüttenwes., 51, 195 (1980)
- [33] F.Rammersdorfer, F.Fischer, W.mitter, Jbathe, M.D.Synder, Comp.Struct., 13, 771 (1981)
- [34]H.Fujio, T.Aida, Y.Matsumoto, Bull.ISI J, 22 504 (1982)
- [35] S.Sjöström, Calculation of Quench Stresses in Steel, Ph.D. Thesis, No.84, univ. of Linköping, (1982)
- [36] S.Denis, A.Simon, G.Beck, Trans.ISIJ, 22, 504 (1982)
- [37] S.Denis, A.Simon, G.Beck, Harterci Tech. Mitteilungen, 37, 18 (1982)
- [38] S.Denis, A.Simon, G.Beck, Proc.Int.Conf. Eigenspannung, Karlsruhe, DGM, 211 (1983)
- [39] H.Ishikawa, Y.Sugawara, K.Hata, J.of Thermal Stresses, 6, 365 (1983)
- [40] S.Sjöström, Mtas.Sci.Tech., 1, 823 (1985)
- [41] S.Denis, E.Gautier, A.Simon, G.Beck, Mater. Sci. Technol., 1, 805 (1985)
- [42] S.Denis, E.Gautier, S.Sjöström, A.Simon, Acta Metall., 35, 1621 (1987)

- [43] S.Denis, S.Sjöström, A.Simon, *Met.Trans.*, 18A, 1203 (1987)
- [44] J.-B.Lebland, G.Mottet, J.Devaux, J.-C. Devaux, *Mat.Sci. and Tech.*, 1,815 (1985)
- [45] F.M.B. Fernandes, S.Denis, A.Simon. *Mat.Sci. and Tech.*, 1, 838 (1985)
- [46] B.Raniccki, *Mat.Sci and Tech.*, 1, 857 (1985)
- [47] T.Inoue. Z.Wang, *Mats. Sci.Tech.*, 1, 845 (1985)
- [48] S.Kamamoto, T.Nishimori, S.Hinoshita, *Mats.Sci.Tech.*, 1 798 (1985)
- [49] Y.Fa-rong, W.shong-li, *Mats.Sci.Tech.*, 1, 851 (1985)
- [50] R.Schöder, *Untersuchungen zur Spannungsg- und Eigenspannungsbildung beim Abschrecken von Stahlyzylindern*, Ph.D. Thesis, Univ. of Karlsruhe, (1985)
- [51] P.Garaja, *Rechnerische und experimentelle Untersuchungen zum Einfluß kontinuierlicher und diskontinuierlicher Warmbehandlungsverfahren auf die Wärme- und Umwandlungseigenspannungen und Verzüge von un- und niedriglegierten Stählen*, Ph.D. Thesis, Univ.of Karlsruhe, (1987)
- [52] T.Inoue, D-Y.Ju, K.Arimoto, *Proc. of 1st Int. Conf. On Quenching and Control of Distortion*, Chicago, Illinois, 22-25 Sep., 205 (1992)
- [53] B.Buchmayr, J.S.Kirkaldy, *Proc.of 1st Int. Conf. On Quenching and Control of Distortion*, Chicago, Illinois, 22-25 Sep., 221 (1992)
- [54] S.Das, G.Upadhyay, U.Chandra, *Proc. of 1st Int.Conf. on Quenching and Control Distortion*, Chicago, Illinois, 22-25 Sep., 229 (1992)

- [55] A.Majorek, B.Scholtes, H.Müller, E.Macherauch, Proc.of Ist Int. Conf. On Quenching and Control of Distortion, Chicago, Illinois, 22-25 Sep., 171 (1992)
- [56] A.S.S Oddy, J.A. Goldak, J.M.J McDill, Proc. 2nd Int. Conf. On Trends in Welding Research, Gatlinburg TN, (1989)
- [57] K.Sawamiphakdi, P.K.Kropp, Proc. of ABAQUS User's Conf., 421 (1988)
- [58] D.Y.Ju, M.Sahashi, T.Omori, T.Inoue, J. Soc.Mater.Sci., 45, 643 (1996).
- [59] K.F.Wang, S.Chandrasekar, H.T.Y.Yang, J.Manuf.Sci.&Eng, 119, 257 (1997).
- [60] H.Cheng, X.Huang, H.Wang, J.Mater.Proc.Tech., 89-90, 339 (1999).
- [61] A.M.S.Hamouda, S.Sulaiman, C.K.Lau, J.Mater.Proc.Tech, 119, 354 (2001).
- [62] P.M.C.L.Pacheco, M.A.Savi, A.F.Camarao, Journal of Strain Analysis, 36, 507 (2001).
- [63] E.P.Silva, P.M.C.L.Pacheco, M.A.Savi, International Journal of Solids and Structures, 41, 1139 (2004)
- [64] S.Hossain, M.R.Daymond, C.E.Truman, D.J.Smith, Mater.Sci.Eng., 373, 339 (2004)
- [65] B.L.Ferguson, Z.Li, A.M.Freborg, Comp. Mater.Sci., 34, 274 (2005)
- [66] E.P.Silva, P.M.C.L.Pacheco, M.A.Savi, Journal of Strain Analysis, 40, 151 (2005)
- [67] T.Retzi, Z.Fried, I.Felde, Comp.Mater.Sci., 22, 261 (2001)

- [68] C.H.Gür, Finite Element Modeling and Measurement of Stress Evolution in Quenching Processes, Ph.D Thesis, Middle East Technical University (1995)
- [69] A.K.Singh, D. Mazumdar, ISIJ Int., 31, 1441 (1991).
- [70] O.C.Zienkiewicz, The Finite Elemental Method, 3rd. Edition, , Mc Graw-Hil, New York (1977).
- [71] A.J.Fletcher, Thermal Stress and Strain Generation in Heat Treatment, Elsevier Applied Sci. London (1989).
- [72] P.G.Bergan, G. Horrigmoe, B.Krakeland, T.H. Soreide, Int. J. Num. Meth. Engnrg., 12, 1677 (1978)
- [73] D.F. Watt, L.Coon, M.J.Bibby, J.A.Goldak, C.Henwood, Acta Metall., 36, 3029 (1988)
- [74] E.Scheil, Arch. EisenHüttenwes., 12, 565 (1935)
- [75] J.B.Leblood, J.Devaux, Acta meta., 32, 137 (1984)
- [76] S.Denis, S.Sjöström, A.Simon, Residual Stress in Sci. And Tech., ed. E. Macherauch, V.Hauk, Int. Conf. Of Residual Stress-1986, DGM, 2, 595 (1987).
- [77] G.K. Manning, C.H. Lorig, Trans. AIME, 167, 442 (1946)
- [78] J.S.Kirkaldy, E.A.Baganis Metall. Trans., 9A, 495 (1978).
- [79] W.C.Leslie, The Physical Metallurgy of Stells, Mc Graw-Hill, New York, 257 (1981).
- [80] K.W.Andrews, J.Iron Stell Inst., 203, 721 (1965).

[81] J.S.Kirkaldy, D.Venugopalan, Phase Transformation in Ferrous Alloys, ed. A.R.Marder, J.I.Goldstein, AIME, 125 (1984).

[82] D.A.Porter, K.E.Easterling, Phase Transformation in Metals and Alloys, 2nd edition, Chapman and Hall (1993).

[83] D.P.Koistinen, R.E. Marburger, Acta Metall., 7, 59, (1959)

[84] H.Armen, Comp.&Struct., 10, 161 (1979).

[85] D.R.J.Owen, E.Hinton, Finite Element in Plasticity, Redwood Burn Ltd. (1980)

[86] B.Hildenwall, Prediction of the Residual Stresses Created During Quenching, Ph.D. Thesis, Univ. Of Linköping (1979)